The spatial behavior of nonclassical light

Mikhail I. Kolobov

Fachbereich Physik, Universität-GH Essen, D-45117 Essen, Germany

Nonclassical effects such as squeezing, antibunching, and sub-Poissonian statistics of photons have been attracting attention in quantum optics over the last decade. Up to now most theoretical and experimental investigations have been carried out exclusively in the time domain while neglecting the spatial aspects by considering only one spatial mode of the electromagnetic field. In many situations such an approximation is well justified. There are, however, problems that do not allow *in principle* a single-mode consideration. This is the case when one wants to investigate the quantum fluctuations of light at different spatial points in the plane perpendicular to the direction of propagation of the light beam. Such an investigation requires a complete description of quantum fluctuations of light in both time and space and cannot be done within a single-mode theory. This space-time description brings about a natural generalization into the spatial domain of such notions as the standard quantum limit, squeezing, antibunching, etc. It predicts, for example, the possibility of generating a light beam with sub-Poissonian statistics of photons not only in time but also in the beam's transverse plane. Of particular relevance to the applications is a situation in which the cross section of the light beam contains several nonoverlapping areas with sub-Poissonian statistics of photons in each. Photodetection of such a beam produces several sub-shot-noise photocurrents depending on the number of independent areas with sub-Poissonian statistics. This is in marked contrast to the case of a single-mode sub-Poissonian light beam in which any attempt to collect light from only a part of the beam deteriorates the degree of shot-noise reduction. This property of multimode squeezed light opens a range of interesting new applications in optical imaging, optical parallel processing of information, parallel computing, and many other areas in which it is desirable to have a light beam with regular photon statistics across its transverse area. The aim of this review is to describe the recent development in this branch of quantum optics. [S0034-6861(99)00605-4]

CONTENTS

I. Introduction 1539
II. Single-Mode Nonclassical States of Light 1541
A. Observation of quantum fluctuations of light in time 1541
B. Bunching, antibunching, and sub-Poissonian statistics 1543
C. Single-mode squeezed states 1545
III. Quantum Fluctuations of Light in Space-Time 1548
A. Observation of quantum fluctuations of light in space-time and standard quantum limit in space-time 1548
B. Propagation and diffraction of a quantized field in free space 1550
C. Propagation and diffraction of a quantized field in a nonlinear parametric medium 1552
D. Space-time Fourier transform vs decomposition into discrete transverse modes of a resonator 1553
IV. Multimode Squeezed States of Light 1554
A. Generation of multimode squeezed states by a traveling-wave optical parametric amplifier 1554
B. Multimode squeezing as modulation of quantum fluctuations in space-time 1556
C. Homodyne detection of multimode squeezed states and reduction of the photocurrent noise in space-time below the shot-noise level 1557
D. Other schemes for generation of multimode squeezed states 1559
1. Degenerate four-wave mixing 1559
2. Subthreshold optical parametric oscillator 1561
V. Free Propagation and Diffraction of Multimode Squeezed Light 1564
A. Effects of free propagation and a thin lens on multimode squeezed light 1564
B. Assessment of physical possibilities for low-noise measurements and information transmission with multimode squeezed light 1566
VI. Noiseless Control of Multimode Squeezed Light 1567
A. Sub-shot-noise microscopy: detection of faint objects with multimode squeezed light 1567
B. Interference mixing of multimode squeezed states and noiseless optical images 1568
VII. Noiseless Amplification of Optical Images 1571
A. Optical scheme and evolution of the field 1571
B. Quantum fluctuations of the amplified image 1574
C. Spatial width of the gain and conditions for noiseless amplification 1576
D. Experimental observation of quantum noise correlations in parametric image amplification 1578
VIII. Optical Imaging with Multimode Squeezed Light 1581
A. Description of the optical scheme and observables 1581
B. Quantum fluctuations in optical imaging with multimode squeezed light 1582
C. Noise performance of an optical image processor with single-mode and multimode squeezed light 1584
IX. Conclusions and Outlook 1585
Acknowledgments 1587
References 1587

I. INTRODUCTION

Nonclassical states of electromagnetic fields have been intensively investigated in quantum optics over the last decade. Such notions as squeezing, antibunching, and sub-Poissonian photon statistics have become familiar, and many of these effects are well understood theoretically and observed experimentally (Kimble and Walls, 1987; Loudon and Knight, 1987; Teich and Saleh, 1989; Fabre and Giacobino, 1992).

Nonclassical states attract considerable attention not only because they cast a new light on some fundamental questions about quantum electrodynamics, but also be-

cause of many practical applications. Most of these applications rely on the possibility of reducing the quantum fluctuations of light below the so-called standard quantum limit. This limit is imposed by classical electrodynamics as the lowest level of light fluctuations in the optical measurement process. In many state-of-the-art technological applications the standard quantum limit has already been achieved. Therefore the possibility of overcoming this limit using nonclassical light is very attractive for high-precision optical measurements, optical communications, optical information processing, (Yamamoto *et al.*, 1990). Quantum fluctuations of light in different optical systems and the generation of coherent light fields with sub-Poissonian photon statistics were recently discussed in review articles by Davidovich (1996) and Henry and Kazarinov (1996).

In spite of the very rapid development in this area of quantum optics, at present most theoretical and experimental investigations of nonclassical light deal with quantum fluctuations in time only. In theory the spatial aspects are left aside by considering only one spatial mode of the electromagnetic field. Experimentally this is accomplished by collecting the whole light beam with a single photodetector and investigating its temporal quantum fluctuations. One may say that for the moment most of the attention has been directed toward the ''one-dimensional'' applications of nonclassical light, i.e., to phenomena evolving in time. However, there are many areas of optics that could benefit from the possibility of reducing quantum fluctuations of light not only in time, but also in space, namely, in the transverse area of the light beam. One may think, for example, about the detection of faint optical images, or applications in parallel optical computing, in which quantum fluctuations at different spatial points of the wave front would cause computing errors.

In this article we shall demonstrate that under certain physical conditions quantum fluctuations of light can be reduced below the standard quantum limit not only in time, but also at different spatial points in the transverse plane of the electromagnetic wave. Therefore one can talk about squeezing, sub-Poissonian photon statistics, and other nonclassical phenomena not only globally, with respect to the whole light beam, but also locally, i.e., at a given point in the cross section of the beam and some area around it. The size of such an area depends on the physical parameters of nonclassical light and, in particular, can be much smaller than the transverse area of the light beam. The possibility of such ''local squeezing'' was predicted and studied in detail for the first time by Kolobov and Sokolov (1989a, 1989b, 1991).

We advocate in this paper the investigation of quantum fluctuations not only globally, for the whole light beam, but also locally, for its parts, which can also manifest nonclassical effects. For such an investigation we suggest using a dense array of small photodetectors, or *pixels*, each pixel having an independent output for further analysis of photocurrents from individual pixels and of their correlations. If the size of a pixel is matched to the size of the local amplitude squeezing, for example, we can obtain as many sub-Poissonian photocurrents as the number of pixels in the array.

Another motivation for studying the spatial behavior of nonclassical light is to unify two different areas of optics: nonclassical effects and transverse nonlinear phenomena. Such a program was developed by the group of Lugiato at Milan University and has been successfully pursued in recent years (Lugiato, 1994; Gatti, Wiedemann, *et al.*, 1997; Lugiato, Gatti, and Wiedemann, 1997; Lugiato *et al.*, 1997; Gatti, Lugiato, *et al.*, 1999). Nonclassical effects and transverse nonlinear phenomena could be considered as complementary areas of optics. Indeed, while the analysis of nonclassical effects is done in the framework of quantum theory, it is almost exclusively restricted to just one mode of the electromagnetic field due to the complexity of multimode quantum treatment. On the other hand, transverse nonlinear optics, which studies instabilities, pattern formation, and similar phenomena in the transverse plane of an electromagnetic wave, is of necessity a multimode theory but only semiclassical. As often happens in physics, unification of two complementary fields brings about a wealth of interesting new phenomena. Here we only mention effects such as ''quantum images'' and the critical behavior of quantum fluctuations in space similar to the phenomena of second-order phase transitions in equilibrium systems. For descriptions of these phenomena we refer the reader to the papers of Gatti and Lugiato (1995); Lugiato and Marzoli (1995); Gatti, Wiedemann, *et al.* (1997); Lugiato, Gatti, and Wiedemann (1997); Lugiato *et al.* (1997); and Gatti, Lugiato, *et al.* (1999). In Secs. III.C and IV.D.2 we discuss some aspects of these phenomena that are connected with our treatment.

The paper is organized as follows. In Sec. II we give an overview of nonclassical phenomena for a single-mode electromagnetic field. We discuss briefly the observation of quantum fluctuations of light in time by means of photodetection, the shot-noise limit, and the possibilities of shot-noise reduction. We introduce the most important notions, such as, squeezing, antibunching, and sub-Poissonian photon statistics for a single-mode case.

In Sec. III we generalize the theory of quantum fluctuations of an electromagnetic field from the time domain into space-time. We describe the observation of quantum fluctuations in space-time using a dense array of photodetectors, or a charge-coupled device (CCD). We define the most important observables such as the space-time correlation function of the photocurrent density and its frequency and spatial-frequency noise spectrum. We define the standard quantum limit in space-time. We show that all nonclassical phenomena, such as, squeezing, antibunching, and sub-Poissonian photon statistics, discussed for a single-mode electromagnetic field, have their natural counterparts in space-time.

In Sec. IV we describe three different physical models for the generation of multimode squeezed states. These are (i) the traveling-wave optical parametric amplifier (OPA), (ii) degenerate four-wave mixing, and (iii) the ring-cavity optical parametric oscillator (OPO) below

threshold. We show that under homodyne detection of light emitted by a traveling-wave OPA with a plane-wave local oscillator, one can obtain shot-noise reduction of the photocurrent density not only for the whole light beam but also locally, at different points across the beam. We calculate the spatial resolving power and typical time scale for a sub-shot-noise photodetection and show the relation between these parameters and different types of phase matching in the nonlinear crystal serving as a medium for the OPA. Finally, we consider two other models and compare their properties.

Section V is devoted to a description of multimode squeezed light propagation in free space and in optical systems. We show that diffraction in free space deteriorates the resolving power of sub-shot-noise observation. However, this deterioration is entirely due to the phase modulation of light waves with different transverse components of wave vectors propagating in free space and is therefore reversible. We demonstrate that, using a thin lens properly inserted into the light beam, one can restore the resolving power of the sub-shot-noise observation and, furthermore, improve it to the ultimate value achievable for given physical conditions.

In Sec. VI we consider the applications of multimode squeezed light in sub-shot-noise microscopy and for the creation of noiseless optical images. We show that the employment of multimode squeezed light in microscopy for detecting faint phase objects allows us to increase the sensitivity beyond the shot-noise limit. Taking an example of the simplest phase object such as a sinusoidal phase grating, we estimate the spatial squeezing bandwidth and the size of a pixel in the photodetection array necessary for sub-shot-noise microscopy.

By noiseless optical images we mean optical images whose quantum fluctuations are reduced below the shot-noise limit and, in principle, can be suppressed completely. For the creation of such noiseless images one must find a nondestructive way to modulate multimode squeezed states. We note that not all kinds of modulation of the wave front preserve the regular photon statistics. For example, intensity modulation due to nonuniform absorption destroys the regularity of photons across the wave fronts because of the randomness of the absorption process. We show that the interference mixing of two multimode squeezed states by an interferometer with a spatially varying transmission coefficient may provide such nondestructive modulation.

In Sec. VII we describe a scheme for the amplification of faint optical images that preserves the signal-to-noise ratio of the image. The scheme consists of a ring-cavity optical parametric amplifier as an active element and two imaging lenses. This system can amplify images either "point by point," when one small region is amplified at a time, or by narrow rings. In both cases the system works as an image scanner. We evaluate the inherent noise of such an amplifier and formulate the conditions for noiseless amplification.

In Sec. VIII we discuss the noise properties of an optical image processor with multimode squeezed light. We calculate the signal-to-noise ratio of a spatially partially coherent optical processor and compare the results for illumination by three different light sources: coherent, single-mode squeezed, and multimode squeezed. We show that the signal-to-noise ratio can be improved beyond the shot-noise limit for the two last sources. Moreover, the multimode squeezed source gives better noise performance over the single-mode squeezed source for incoherent illumination.

In Sec. IX we provide an overview and formulate some open questions that might be the subjects of future research in this area.

II. SINGLE-MODE NONCLASSICAL STATES OF LIGHT

A. Observation of quantum fluctuations of light in time

Nonclassical states of light manifest their unusual properties most clearly in photodetection. Therefore, before explaining nonclassical effects, we shall give some results from quantum photodetection theory.

The theory of quantum photodetection was developed in the works of Glauber (1963, 1965). The Glauber model of photodetection is based on the absorption of photons via the photoelectric effect. A photodetector consists of a conducting photosensitive surface and the photocathode, which is normally illuminated by a light beam. The cathode contains many electrons in bound states, some of which may be emitted under the influence of the incident light. Any emitted electron is attracted by an anode, where it produces with some probability a detectable electric pulse. A detailed presentation of semiclassical and quantum photodetection theory can be found, for example, in the book of Mandel and Wolf (1995), Chapter 14.

In this section we shall study only temporal fluctuations of light and neglect any spatial effects in the transverse area of the light beam. We assume that the photodetector of area S is illuminated by a quasimonochromatic plane wave traveling along the z axis in a positive direction. Let us write the positive-frequency electric-field operator $E^{(+)}(z,t)$ as

$$E^{(+)}(z,t)=i\left(\frac{\hbar\omega_0}{2\epsilon_0 cS}\right)^{1/2}\exp[i(k_0 z-\omega_0 t)]a(t), \quad (2.1)$$

where ω_0 is the carrier frequency of the wave, k_0 is its wave number, and $a(t)$ and $a^\dagger(t)$ are the photon annihilation and creation operators in the interaction picture. These operators satisfy the commutation relations

$$[a(t),a^\dagger(t')]=\delta(t-t'),\ [a(t),a(t')]=0 \quad (2.2)$$

and are normalized so that $\langle a^\dagger(t)a(t)\rangle$ gives the mean *photon flux* in photons per second for the light beam of area S.

The quantum theory of photodetection attributes to the observed photocurrent a Hermitian operator $i(t)$. Its mean value $\langle i(t)\rangle$ describes the result of the experimental observation averaged over the statistical ensemble of identical experiments. The deviation $\delta i(t)=i(t)-\langle i(t)\rangle$ of the instant value $i(t)$ from the mean

value $\langle i(t)\rangle$ manifests the intrinsic quantum fluctuations of the photocurrent. An important characteristic of these quantum fluctuations is the correlation function $\langle \frac{1}{2}\{\delta i(t),\delta i(t')\}_+\rangle$, where $\{\ldots,\ldots\}_+$ indicates an anticommutator. The appearance of the anticommutator in the quantum theory is due to the fact that fluctuations $\delta i(t)$ at different moments of time do not commute. The mean value of the photocurrent $\langle i(t)\rangle$ and the correlation function $\langle \frac{1}{2}\{\delta i(t),\delta i(t')\}_+\rangle$ are expressed through the photon annihilation and creation operators $a(t)$ and $a^\dagger(t)$ as follows (Smirnov and Sokolov, 1976; Smirnov and Troshin, 1987):

$$\langle i(t)\rangle = \eta\langle I(t)\rangle, \tag{2.3}$$

$$\langle \tfrac{1}{2}\{\delta i(t),\delta i(t')\}_+\rangle = \langle i(t)\rangle\delta(t-t') + \eta^2\langle :I(t)I(t'):\rangle - \langle i(t)\rangle\langle i(t')\rangle, \tag{2.4}$$

where $I(t)=a^\dagger(t)a(t)$ is *the photon flux operator*. The notation :: stands for *normal and time* ordering,[1] and η is the quantum efficiency of the photodetector.

The correlation function of photocurrent fluctuations $\langle \frac{1}{2}\{\delta i(t),\delta i(t')\}_+\rangle$ contains three contributions. The first is given by the mean photocurrent multiplied by $\delta(t-t')$. This term describes completely uncorrelated photocurrent fluctuations at different moments of time. The δ-type fluctuations appear under the assumption that the photodetector has an infinitely large detection bandwidth or, in other words, an infinitely short response time. This contribution is known as *shot noise*. Shot noise is independent of the quantum statistics of light and of its spectral parameters. We shall see below that it determines the standard quantum limit of noise in time, that is, the lowest noise level of the photocurrent allowed by semiclassical theory.[2]

The informative contribution to the photocurrent correlation function that depends on spectral and statistical properties of the light is given by the normal- and time-ordered intensity correlation function

$$G^{(2)}(t;t') = \langle :I(t)I(t'):\rangle. \tag{2.5}$$

When the intensity of light is stationary in time, this correlation function depends only on the time difference $\tau=t'-t$ between two photodetections, $G^{(2)}(t;t') = G^{(2)}(\tau)$. This correlation function is proportional to the probability that a photon will be detected at time t' provided that the previous photodetection took place at t. This "non-exclusive" probability allows other photodetections between t' and t and should not be confused with the "exclusive" probability of two *successive* photodetections at t and t'. In the quantum optics literature it is more customary to deal with the normalized correlation function $g^{(2)}(\tau)$,

$$g^{(2)}(\tau) = \frac{\langle :I(t)I(t+\tau):\rangle}{\langle I(t)\rangle^2}, \tag{2.6}$$

which is called the *degree of second-order temporal coherence* (Loudon, 1983, p. 106).

Finally, the last contribution to the correlation function $\langle \frac{1}{2}\{\delta i(t),\delta i(t')\}_+\rangle$ is the product of two mean photocurrents and is time independent for light with stationary intensity.

Together with the correlation function (2.4) we shall use the photocurrent noise spectrum $(\delta i)^2_\Omega$, defined as

$$(\delta i)^2_\Omega = \int_{-\infty}^{\infty} dt\, e^{i\Omega t}\langle \tfrac{1}{2}\{\delta i(0),\delta i(t)\}_+\rangle. \tag{2.7}$$

Experimentally the photocurrent noise spectrum can be measured by performing a spectral analysis of the photocurrent fluctuations. Using the photodetection formula (2.4), we can write $(\delta i)^2_\Omega$ as

$$(\delta i)^2_\Omega = \langle i\rangle + \tilde{G}^{(2)}(\Omega) - \langle i\rangle^2\delta(\Omega). \tag{2.8}$$

The first, frequency-independent term stems from the shot noise in Eq. (2.4), the second represents the Fourier transform of the intensity correlation function $G^{(2)}(t)$,

$$\tilde{G}^{(2)}(\Omega) = \int_{-\infty}^{\infty} dt\, e^{i\Omega t}G^{(2)}(t), \tag{2.9}$$

and the last, with $\delta(\Omega)$, comes from the time-independent product of two mean photocurrents in Eq. (2.4). It is easy to show that in semiclassical theory the contribution of the last two terms is always nonnegative. Indeed, for a classical electromagnetic field, we can replace the photon annihilation and creation operators $a(t)$ and $a^\dagger(t)$ by the classical functions $\alpha(t)$ and $\alpha^\star(t)$. The correlation function of photocurrent fluctuations becomes

$$\begin{aligned}\langle \tfrac{1}{2}\{\delta i(t),\delta i(t')\}_+\rangle &= \langle i(t)\rangle\delta(t-t') + \eta^2\langle J(t)J(t')\rangle - \langle i(t)\rangle\langle i(t')\rangle \\ &= \langle i(t)\rangle\delta(t-t') + \eta^2\langle \delta J(t)\,\delta J(t')\rangle,\end{aligned} \tag{2.10}$$

where $J(t)=|\alpha(t)|^2$ is the stochastic classical intensity of light. Now the photocurrent noise spectrum reads

$$(\delta i)^2_\Omega = \langle i\rangle + (\delta J)^2_\Omega, \tag{2.11}$$

where $(\delta J)^2_\Omega$ gives the spectrum of intensity fluctuations, which is always non-negative. Therefore, in semiclassical theory, the lowest limit of the photocurrent noise spectrum is equal to

$$(\delta i)^2_\Omega = \langle i\rangle. \tag{2.12}$$

---

[1] We remind the reader that normal and time ordering means that all creation operators are placed to the left of the annihilation operator and times are increasing from the outside to the center of the correlation function. In particular,

$$\langle :I(t)I(t'):\rangle = \langle a^\dagger(t)a^\dagger(t')a(t')a(t)\rangle\theta(t'-t) + \langle a^\dagger(t')a^\dagger(t)a(t)a(t')\rangle\theta(t-t'),$$

where $\theta(t)$ is the step function.

[2] By *semiclassical theory* we understand here an approach to the photodetection process wherein light is described by classical electrodynamics while photoelectrons are treated by quantum mechanics (Mandel and Wolf, 1995, p. 439).

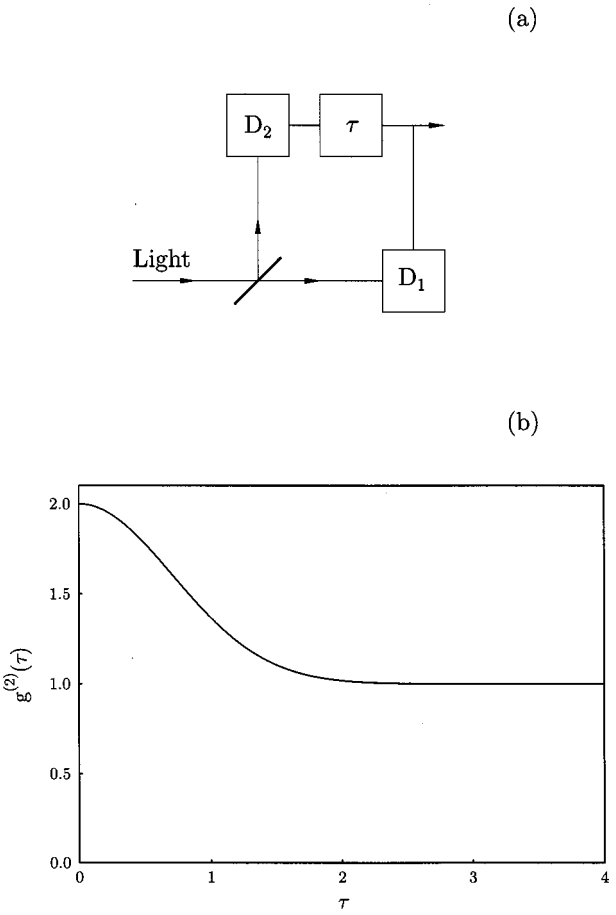

FIG. 1. Photocurrent correlation experiment. (a) A simplified outline of the apparatus. (b) The degree of second-order coherence $g^{(2)}(\tau)$ for chaotic light with Gaussian frequency distribution.

This limit is known in quantum optics as the *standard quantum limit* or the *shot-noise limit*.

B. Bunching, antibunching, and sub-Poissonian statistics

The degree of second-order coherence $g^{(2)}(\tau)$ can be measured in a photocurrent correlation experiment as shown schematically in Fig. 1(a). The primary electromagnetic wave is divided into two parts by a semitransparent mirror, and two secondary waves are detected by two independent photodetectors D_1 and D_2. The photocurrents from these photodetectors are multiplied after the introduction of a time delay τ into one of them. This kind of experiment was first performed by Hanbury Brown and Twiss (1956, 1957a, 1957b) for a thermal light from a mercury arc. Qualitatively the result of this experiment is shown in Fig. 1(b). We observe that for short time delays τ the conditional probability of detecting the second photon is higher than for large delays when these two events become independent. Nowadays this effect is known as *photon bunching* (Mandel and Wolf, 1965); it is easy to interpret in terms of classical fluctuations of light intensity. Indeed, the first photodetection occurs with higher probability during the positive fluctuation of the light intensity. Therefore the conditional probability of the second detection should be higher for short time delays τ, when the positive fluctuation has not yet disappeared. As a confirmation of this intuitive explanation, the typical time scale of bunching is given by the intensity correlation time τ_c in the thermal light source. The bunching effect disappears for light in a coherent state, i.e., without classical intensity fluctuations. Since the pioneering experiments of Hanbury Brown and Twiss, the bunching effect with thermal light has been observed by many others (Rebka and Pound, 1957; Twiss, Little, and Hanbury Brown, 1957; Arecchi, Gatti, and Sona, 1966; Morgan and Mandel, 1966; Scarl, 1966).

One may ask whether there is a phenomenon opposite to the bunching effect, that is, *antibunching*, in which the conditional probability of the second photodetection at short time delays τ is smaller than for long delays. A classical example that gives a positive answer to this question is the phenomenon of *resonance fluorescence* of a single atom driven by an external monochromatic light field. The process of photon emission takes place during the transition of the atom from its excited state $|e\rangle$ to the ground state $|g\rangle$. The probability of photon emission is proportional to the population of the excited atomic state. Since after emission of the first photon the atom is in the ground state, the probability of the second emission is zero for zero time delay τ. The second photon can be emitted only after a certain time interval needed for excitation of the atom into the upper state $|e\rangle$. In this process the probability of detecting the second photon for short time delays τ must be smaller than for long delays, thus exhibiting antibunching. This effect was theoretically predicted by Carmichael and Walls (1976a, 1976b), Kimble and Mandel (1976), and Cohen-Tannoudji (1977).

Photon antibunching was first observed in a photocurrent correlation experiment using resonance fluorescence from single sodium atoms in an atomic beam (Kimble, Dagenais, and Mandel, 1977; Dagenais and Mandel, 1978; Kimble, Dagenais, and Mandel, 1978). A diagram of the apparatus used for the two-time correlation experiment is shown in Fig. 2(a). The results of this experiment are presented in Fig. 2(b). When the Rabi frequency Ω, associated with the external driving field, is much smaller than the rate of spontaneous decay β of the atomic polarization, the typical time scale τ_c of antibunching is given by the inverse of β, $\tau_c \propto \beta^{-1}$. In a strong external field, $\Omega \gg \beta$, the antibunching time is related to the inverse of the Rabi frequency, $\tau_c \propto \Omega^{-1}$ [see Fig. 2(b)]. Since the first observation of photon antibunching in the resonance fluorescence of a single atom, this effect has also been observed in more recent experiments (Cresser *et al.*, 1982; Walker and Jakeman, 1985; Grangier, Roger, and Aspect, 1986; Grangier *et al.*, 1986).

Antibunching is a nonclassical phenomenon that cannot be explained in the framework of classical electrodynamics. Indeed, in classical electrodynamics, the photon annihilation and creation operators $a(t)$ and $a^{\dagger}(t)$

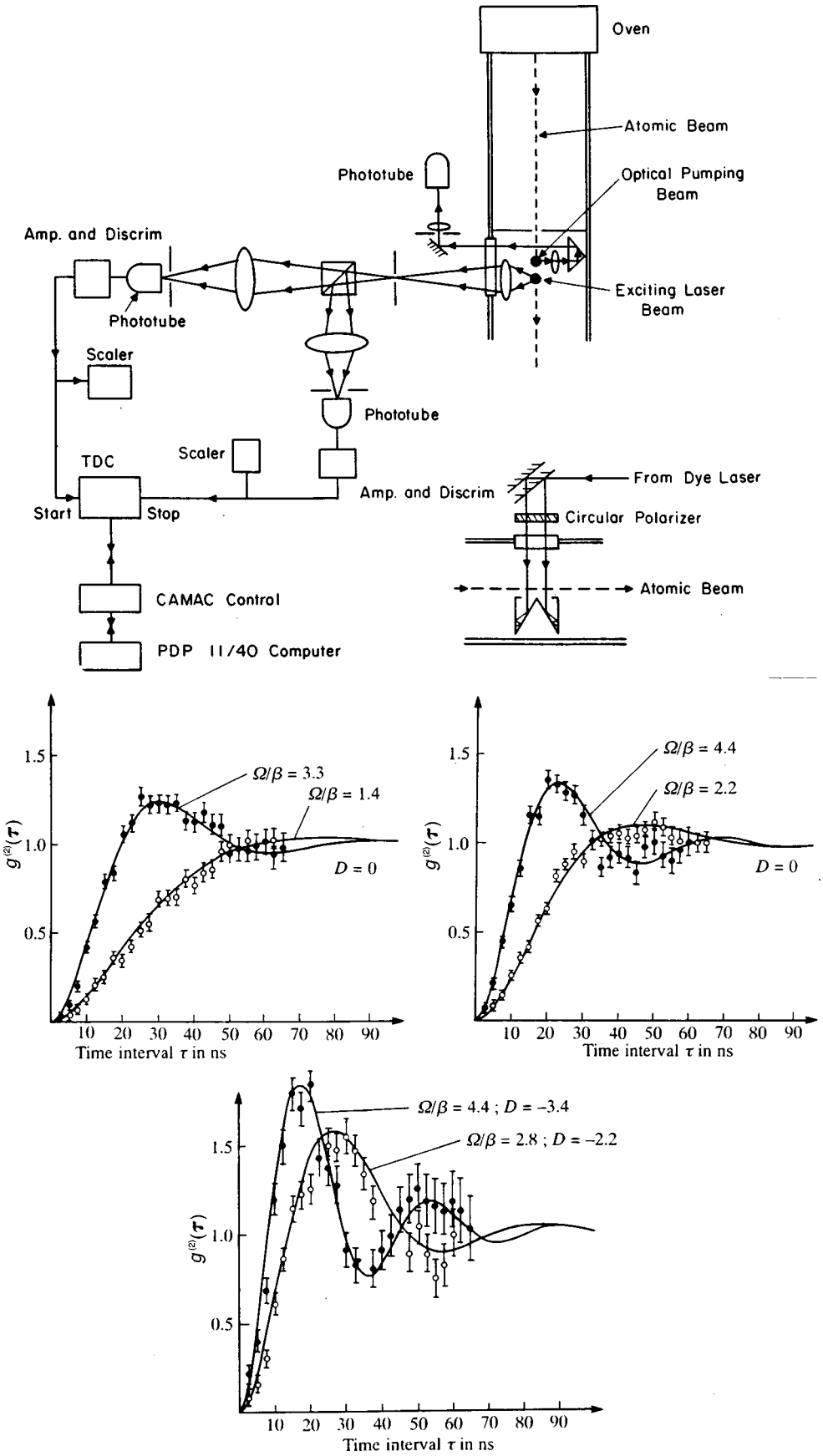

FIG. 2. Photon antibunching in resonance fluorescence of a single atom. (a) Sketch of the apparatus used for two-time correlation measurements: (b) results of correlation measurements for a single driven atom, for various exciting field strengths Ω/β and detunings D. The full curves are theoretical and exhibit antibunching. (Reproduced from Dagenais and Mandel, 1978.)

become stochastic c numbers $\alpha(t)$ and $\alpha^{\star}(t)$. The correlation function $g^{(2)}(\tau)$ from Eq. (2.6) can be written as $g^{(2)}(\tau)=\langle J(t)J(t+\tau)\rangle/\langle J(t)\rangle^2$, where $J(t)=|\alpha(t)|^2$ is the stochastic classical intensity of light. For a stationary random process $J(t)$ it follows from the Schwarz inequality that

$$g^{(2)}(\tau)\leqslant g^{(2)}(0), \tag{2.13}$$

i.e., the function $g^{(2)}(\tau)$ has its absolute maximum at zero time delay, $\tau=0$. Photon antibunching is in contradiction to inequality (2.13). Therefore light fields with antibunching cannot be described by random c numbers.

Another nonclassical effect is sub-Poissonian photon statistics. A classical monochromatic light wave with fixed complex amplitude α corresponds in quantum electrodynamics to a Glauber coherent state $|\alpha\rangle$ of a single-mode electromagnetic field (Loudon, 1983). A coherent state of light has Poissonian photon statistics, i.e., the probability $p(n)$ to find n photons in the state $|\alpha\rangle$ is given by a Poisson distribution,

$$p(n)=|\langle n|\alpha\rangle|^2=\exp(-\langle n\rangle)\frac{\langle n\rangle^n}{n!}, \tag{2.14}$$

where $\langle n\rangle=|\alpha|^2$ is the average photon number equal to the classical intensity of the light wave. For a Poisson distribution one has $\langle(\Delta n)^2\rangle=\langle n\rangle$, where $\langle(\Delta n)^2\rangle$ is the dispersion of the photon number.

A convenient quantity for characterizing the photon statistics for an arbitrary quantum state of a single-mode electromagnetic field is Mandel's Q parameter (Mandel, 1979):

$$Q=\frac{\langle(\Delta n)^2\rangle-\langle n\rangle}{\langle n\rangle}. \tag{2.15}$$

For classical states the photon statistics are always super-Poissonian, or Poissonian in the limiting case of a coherent state. Therefore, for such states, Mandel's Q parameter is always non-negative, $Q\geqslant 0$. For nonclassical states of light, the photon statistics can be sub-Poissonian and the Q parameter can become negative. The greatest possible negative value of Q, $Q=-1$, is realized for a Fock state, which has a definite number of photons, $\langle(\Delta n)^2\rangle=0$.

Sub-Poissonian statistics were first experimentally observed in photoelectric counting experiments on fluorescence from a single atom (Short and Mandel, 1983). More recently there have been reports of other processes in which sub-Poissonian statistics can be generated (Teich, Saleh, and Peřina, 1984; Saleh and Teich, 1985; Teich and Saleh, 1985; Hong and Mandel, 1986; Machida and Yamamoto, 1986; Rarity, Tapster, and Jakeman, 1987).

Strictly speaking, sub-Poissonian statistics and antibunching are two independent phenomena and do not have to accompany each other. We may note, however, the following relation between the correlation function $g^{(2)}(\tau)$ and the dispersion of the photon number:

$$g^{(2)}(0)-g^{(2)}(\infty)=\frac{\langle(\Delta n)^2\rangle-\langle n\rangle}{\langle n\rangle^2}. \tag{2.16}$$

Here we have used the fact that for an infinitely large time delay, $\tau\to\infty$, any correlations in a stationary random process disappear, and the correlation function $g^{(2)}(\tau)$ tends to unity,

$$\lim_{\tau\to\infty} g^{(2)}(\tau)=1. \tag{2.17}$$

In Fig. 3 we present three correlation functions $g^{(2)}(\tau)$ showing antibunching, i.e., $g^{(2)}(0)<g^{(2)}(\tau)$ for some values of the time delay τ. For curves (a) and (b) we also have $g^{(2)}(0)<g^{(2)}(\infty)$ and, therefore, sub-Poissonian statistics. However, for curve (c), we observe that $g^{(2)}(0)>g^{(2)}(\infty)$ and the photon statistics are super-Poissonian. We point out that, nevertheless, curve (c) cannot be attributed to a classical electromagnetic field since $g^{(2)}(0)<g^{(2)}(\tau)$ for short time delays τ.

C. Single-mode squeezed states

In this subsection we give a brief review of single-mode squeezed states of light, which will help the reader understand the multimode squeezed states to be introduced in the following sections. More detailed descriptions of squeezed states can be found in review articles by Walls (1983), Loudon and Knight (1987), Teich and Saleh (1989; 1990), Yamamoto *et al.* (1990), Reynaud *et al.* (1992), and special issues of *Journal of the Optical Society of America* (Kimble and Walls, 1987), *Journal of Modern Optics* (Loudon and Knight, 1987), and *Applied Physics B* (Fabre and Giacobino, 1992).

Single-mode squeezed states of light were first introduced by Takahashi (1965), Stoler (1970, 1971), Yuen (1976), and Caves (1981). Let us write the Heisenberg electric-field operator of a single-mode electromagnetic field as

$$\begin{aligned} E(t)&=\frac{E_0}{2}(ae^{-i\omega_0 t}+a^{\dagger}e^{i\omega_0 t})\\ &=E_0(a_1\cos\omega_0 t+a_2\sin\omega_0 t). \end{aligned} \tag{2.18}$$

Here ω_0 is the carrier frequency of the field, E_0 is the normalization constant, and a and $a^{\dagger}$ are the single-mode photon annihilation and creation operators obeying the boson commutation relation, $[a,a^{\dagger}]=1$. Hermitian operators a_1 and a_2,

$$a_1=\frac{a+a^{\dagger}}{2}, \quad a_2=\frac{a-a^{\dagger}}{2i}, \tag{2.19}$$

are called *optical quadrature components* of the electric field. From the commutation relation of a and $a^{\dagger}$ it follows that

$$[a_1,a_2]=\frac{i}{2}. \tag{2.20}$$

Since operators a_1 and a_2 do not commute, there is an uncertainty relation between their fluctuations,

$$\langle(\Delta a_1)^2\rangle\langle(\Delta a_2)^2\rangle\geqslant\tfrac{1}{4}|\langle[a_1,a_2]\rangle|^2=\tfrac{1}{16}. \tag{2.21}$$

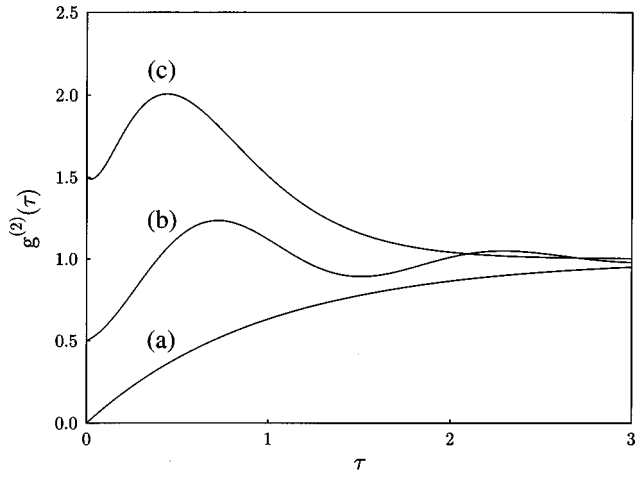

FIG. 3. Three intensity correlation functions with an antibunching effect. For curves (a) and (b) we have also sub-Poissonian photoelectron statistics, while curve (c) manifests super-Poissonian statistics.

This inequality must hold for arbitrary states of the electromagnetic field. Such states, for which Eq. (2.21) becomes an equality, are called minimum uncertainty states. One example of a minimum uncertainty state is the coherent state, including the vacuum state, for which dispersions of both quadrature components are equal:

$$\langle(\Delta a_1)^2\rangle=\langle(\Delta a_2)^2\rangle=\tfrac{1}{4}. \tag{2.22}$$

In classical electrodynamics, the complex amplitude of the electric field can be represented by a vector on the complex plane. In quantum electrodynamics, because of quantum fluctuations, this vector cannot be defined exactly. One can give only its mean value and some uncertainty region around this value in accordance with the uncertainty relation (2.21). The rigorous meaning of the uncertainty region can be defined with the help of *quasiprobability distributions*, which represent the field density matrix as a function on the complex plane (Agarwal and Wolf, 1968, 1970a, 1970b, 1970c; Cahill and Glauber, 1969a, 1969b; for a review see also Peřina, 1985, Chap. 16, and Peřina, 1991, Sec. 4.8). Using quasiprobability distributions, one can evaluate the quantum-mechanical mean values as integrals over the complex plane. For example, the mean value of the monomial $\{(a^\dagger)^n a^m\}_s$ written in a certain ordering rule indicated by the index s can be evaluated as

$$\langle\{(a^\dagger)^n a^m\}_s\rangle=\int d^2\alpha\, D_s(\alpha)(\alpha^\star)^n\alpha^m. \tag{2.23}$$

The distribution function $D_s(\alpha)$ depends on the particular ordering of operators a and $a^\dagger$. Normal ordering corresponds to the Glauber-Sudarshan P-distribution $P(\alpha)$, symmetric or Weyl ordering provides the Wigner distribution $W(\alpha)$, and antinormal ordering gives the so-called Q-distribution $Q(\alpha)$. The function $D_s(\alpha)$ is not, in general, a probability distribution and can become negative and even singular for some particular states of the field. Nevertheless, it plays a role so similar

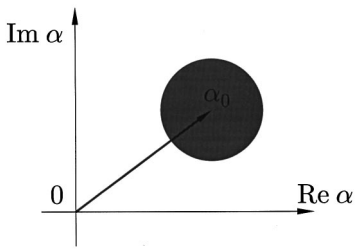

FIG. 4. Uncertainty region for a coherent state.

to that of a probability distribution that it is referred to as a "quasiprobability distribution."

Quasiprobability distributions corresponding to different ordering rules of the operators a and $a^\dagger$ are completely equivalent in the sense that they give the same mean values for the physical observables. However, for particular calculations, the choice of a particular distribution might be preferable. Here it must be noted that if the distribution $P(\alpha)$ can become singular for some nonclassical states, both $W(\alpha)$and $Q(\alpha)$ exist as regular functions for arbitrary quantum states. Moreover, while $W(\alpha)$ can take on negative values, the function $Q(\alpha)$ remains always positive.

The distribution $Q(\alpha)$ for a coherent state $|\alpha_0\rangle$ is given by a Gaussian,

$$Q(\alpha)=\frac{1}{\pi}\exp[-|\alpha-\alpha_0|^2], \tag{2.24}$$

centered at $\alpha=\alpha_0$. The circular section of this Gaussian with radius 1/2 may be used for representing the coherent state $|\alpha_0\rangle$ in the phase space. Such a visual representation is in agreement with Eq. (2.22), since $\langle(\Delta a_1)^2\rangle^{1/2}=\langle(\Delta a_2)^2\rangle^{1/2}=1/2$. This region is shown in Fig. 4.

Single-mode squeezed states can be considered as a generalization of single-mode coherent states. Let us define a new operator b as a linear combination of the photon annihilation and creation operators a and $a^\dagger$,

$$b=ua+va^\dagger. \tag{2.25}$$

Here u and v are complex coefficients satisfying the condition

$$|u|^2-|v|^2=1, \tag{2.26}$$

and therefore can be written as

$$u=\cosh[r],\quad v=\sinh[r]. \tag{2.27}$$

The parameter r is called the *squeezing parameter*. It follows from Eqs. (2.25) and (2.26) that the new operators b and $b^\dagger$ obey the same commutation relation as a and $a^\dagger$. Therefore Eq. (2.25) describes a canonical transformation and, according to the theorem of von Neuman (1931), can be represented by a unitary transformation,

$$b(a,a^\dagger)=UaU^\dagger, \tag{2.28}$$

with a unitary operator U. The structure and physical realizations of such a unitary operator, leading to the canonical transformation (2.25), were discussed by Yuen (1976). This operator can be written explicitly in terms

of the complex coefficients u and v from Eq. (2.25). Because of condition (2.26), there are only three real independent parameters in transformation (2.25). Let us rewrite this transformation as

$$b = e^{i\psi}(|u|e^{-i\phi}a + |v|e^{i\phi}a^\dagger), \tag{2.29}$$

where we have introduced two angles ψ and ϕ,

$$\psi = \tfrac{1}{2}(\arg u + \arg v), \tag{2.30a}$$

$$\phi = \tfrac{1}{2}(\arg v - \arg u). \tag{2.30b}$$

In terms of the three real parameters ψ, ϕ, and r, the unitary operator U reads

$$U = \exp[i(\psi - \phi)a^\dagger a]\exp[\tfrac{1}{2}(z^\star a^2 - z a^{\dagger 2})], \tag{2.31}$$

with

$$z = re^{2i\phi}. \tag{2.32}$$

Let us define the quadrature components of the fields a and b in their *eigencoordinate* systems determined by the angles ϕ and ψ:

$$a = e^{i\phi}(a_1 + ia_2), \tag{2.33a}$$

$$b = e^{i\psi}(b_1 + ib_2). \tag{2.33b}$$

It is easy to see from Eq. (2.29) that these quadrature components are related as

$$b_1 = (|u| + |v|)a_1 = e^r a_1, \quad b_2 = (|u| - |v|)a_2 = e^{-r}a_2. \tag{2.34}$$

Assuming that the field a is in a coherent state and taking into account that the dispersions of the quadrature components a_1 and a_2 are equal to 1/4, we can easily obtain the variances of the quadratures b_1 and b_2,

$$\langle(\Delta b_1)^2\rangle = \frac{1}{4}e^{2r}, \quad \langle(\Delta b_2)^2\rangle = \frac{1}{4}e^{-2r}. \tag{2.35}$$

Therefore the dispersion $\langle(\Delta b_2)^2\rangle$ is squeezed by the factor e^{-2r}, whereas the dispersion $\langle(\Delta b_1)^2\rangle$ is increased by the factor e^{2r}. This ensures fulfillment of the uncertainty relation (2.21). From Eq. (2.35) we can see that a squeezed state is a minimum uncertainty state.

The results of the squeezing transformation (2.25) can be summarized as follows:

(a) On input to the system, the complex field amplitude together with its uncertainty region must be decomposed into the eigen quadrature components defined by Eq. (2.33a) in the coordinate system rotated by an angle ϕ given by Eq. (2.30b); this is illustrated in Fig. 5(a) for a coherent input state with real amplitude.

(b) The quadrature component $e^{i\phi}a_1$ is rotated by an angle $-\phi$, i.e., brought to the real axis and *stretched* by the factor e^r; the quadrature component $ie^{i\phi}a_2$ is brought to the imaginary axis and *squeezed* by the factor e^{-r}, Fig. 5(b).

(c) The resulting complex field amplitude together with its uncertainty region is rotated by an angle ψ given by Eq. (2.30a), Fig. 5(c); in the chosen example the final state of the system represents a squeezed state, and its uncertainty region becomes an ellipse with unequal dispersions of quadratures.

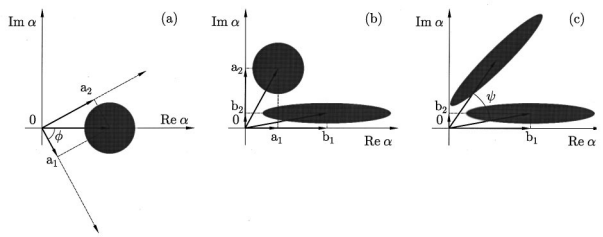

FIG. 5. Graphic illustration of squeezing for a single-mode field.

One of the reasons why squeezed states are interesting for applications is that they allow one to reduce the photocurrent fluctuations below the shot-noise level. To obtain this low-noise observation one has to use the *homodyne detection* technique (Mandel and Wolf, 1995, Chap. 21). We shall consider as an example the homodyne detection of a squeezed vacuum, i.e., a squeezed state with zero mean amplitude.

A schematic of homodyne detection is shown in Fig. 6. The incoming light wave in the squeezed vacuum is mixed by a beam splitter with a strong coherent light wave called a *local oscillator*. For simplicity we shall consider the situation in which the transmission coefficient of the beam splitter is close to unity so that the light wave in a squeezed state passes it unaffected. However, we shall assume the local oscillator to be so strong that even after reflection from the beam splitter its intensity is still large compared to the intensity of the squeezed vacuum. Under these assumptions the Heisenberg annihilation operator $e(t)$ on the photodetector surface may be written as

$$e(t) = \beta + b(t), \tag{2.36}$$

where $\beta = |\beta|e^{i\varphi_\beta}$ is the complex amplitude of the local oscillator and $b(t)$ is the annihilation operator of the field in the squeezed vacuum. Substituting Eq. (2.36) into the photodetection formulas (2.3) and (2.4) and keeping only the leading-term contributions proportional to the intensity of the local oscillator, we arrive at

$$\langle i(t)\rangle = \eta|\beta|^2, \tag{2.37}$$

$$\begin{aligned}\langle \tfrac{1}{2}\{\delta i(t), \delta i(t')\}_+\rangle &= \langle i(t)\rangle\delta(t-t') + \eta^2|\beta|^2\{\langle :b^\dagger(t)b(t'):\rangle \\ &\quad + \langle :b^\dagger(t')b(t):\rangle + e^{-2i\varphi_\beta}\langle :b(t)b(t'):\rangle \\ &\quad + e^{2i\varphi_\beta}\langle :b^\dagger(t)b^\dagger(t'):\rangle\}.\end{aligned} \tag{2.38}$$

The result becomes more transparent if instead of the photocurrent correlation function we write the photocurrent noise spectrum $(\delta i)^2_\Omega$ defined by Eq. (2.7). This requires, however, a knowledge of the temporal behavior of the quantum fluctuations of the field. To describe the temporal behavior of the field in a squeezed state, we have to generalize the single-mode squeezing transformation (2.25) to the so-called *broadband squeezing* (Mandel and Wolf, 1995, Chap. 21). Broadband squeezing can be described in terms of the Fourier components $b(\Omega)$ of the time-dependent field operator $b(t)$,

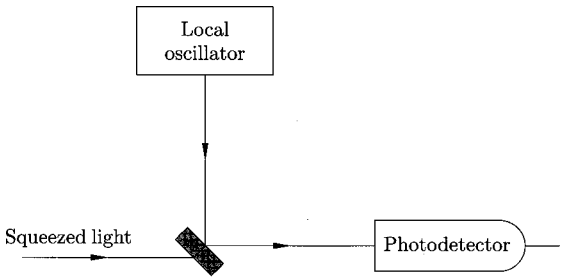

FIG. 6. Schematic of homodyne detection of squeezed light.

$$b(\Omega)=\int_{-\infty}^{\infty} dt\, e^{i\Omega t} b(t), \tag{2.39}$$

as

$$b(\Omega)=U(\Omega)a(\Omega)+V(\Omega)a^{\dagger}(-\Omega). \tag{2.40}$$

The physical meaning of this transformation will become clear in Sec. IV, where we shall discuss in detail its analog for multimode squeezing. Using Eq. (2.40) we can write the photocurrent noise spectrum as follows:

$$(\delta i)^2_{\Omega}=\langle i\rangle[1-\eta+\eta(\cos^2\theta(\Omega)e^{2r(\Omega)} +\sin^2\theta(\Omega)e^{-2r(\Omega)})], \tag{2.41}$$

where $\theta(\Omega)$ is

$$\theta(\Omega)=\psi(\Omega)-\varphi_{\beta}. \tag{2.42}$$

The angle $\psi(\Omega)$ and the squeezing parameter $r(\Omega)$ are given by Eqs. (2.30a) and (2.27), now with respect to the frequency-dependent coefficients $U(\Omega)$ and $V(\Omega)$ from Eq. (2.40).

The result (2.41) for the photocurrent noise spectrum has a simple physical explanation. The contribution $1-\eta$ in square brackets appears from partial recovery of the shot noise due to nonideal photodetection for $\eta \leqslant 1$. The terms proportional to $\cos^2\theta(\Omega)$ and $\sin^2\theta(\Omega)$ come from projections of the semimajor and semiminor axes of the squeezing ellipse at frequency Ω onto the complex amplitude of the local oscillator. Choosing $\theta(\Omega_0)=\pm\pi/2$ for some frequency Ω_0, we can obtain the shot-noise reduction according to the degree of squeezing at this frequency:

$$(\delta i)^2_{\Omega_0}=\langle i\rangle[1-\eta+\eta e^{-2r(\Omega_0)}]. \tag{2.43}$$

For high quantum efficiency $\eta\simeq 1$ and strong squeezing $r(\Omega_0)\gg 1$, one can have almost complete shot-noise reduction.

III. QUANTUM FLUCTUATIONS OF LIGHT IN SPACE-TIME

A. Observation of quantum fluctuations of light in space-time and standard quantum limit in space-time

In this subsection we shall generalize the theory of quantum fluctuations of light from a temporal domain, described in the previous section, into space-time. For this purpose we need local observation of the light fluctuations across the transverse area of the light beam. More precisely, we want to distinguish the photodetection events that take place both at different spatial points $\vec{\rho}$ across the light beam and at different time moments t. Therefore we shall assume that instead of one photodetector, as in the previous section, we have a dense array of very small photodetectors or *pixels*, which fill in the photodetection plane normally illuminated by the light wave under investigation. In practice this can be implemented by employing, for example, a charge-coupled device (CCD). A CCD is an array of metal-oxide-semiconductor capacitors designed to translate an incident pattern of photons in the light wave into an electrical charge (electrons or holes) for further electronic treatment. Nowadays CCDs are available that contain several million pixels, each just a few microns in size (Khosla, 1992).

Let us assume for the moment that the size of each pixel can be arbitrarily small (the finite size of a pixel will be taken into consideration at the end of this subsection). In reality it must be much smaller than a typical scale of change of the light intensity across the photodetection plane. In a continuum limit, when the size of a pixel goes to zero, the observed quantity is the *surface photocurrent density* $i(\vec{\rho},t)$, that is, the number of photoelectrons per unit area of the photodetection plane per second (in $\mathrm{cm}^{-2}\,\mathrm{sec}^{-1}$).

Let the photodetection plane be located at the point with longitudinal coordinate z normal to the z axis. Let us denote as $E^{(+)}(z,\vec{\rho},t)$ the positive-frequency operator of the electric field of a quasiplane and a quasimonochromatic wave traveling in the $+z$ direction, where $\vec{\rho}$ is the position vector in the transverse plane of the wave. As in Sec. II [see Eq. (2.1)], this operator can be written in terms of space- and time-dependent photon annihilation and creation operators $a(z,\vec{\rho},t)$ and $a^{\dagger}(z,\vec{\rho},t)$ as

$$E^{(+)}(z,\vec{\rho},t)=i\left(\frac{\hbar\omega_0}{2\epsilon_0 c}\right)^{1/2}\exp[i(k_0 z-i\omega_0 t)]a(z,\vec{\rho},t). \tag{3.1}$$

Here ω_0 is the carrier frequency of the wave and k_0 is its wave number. The relation of $a(z,\vec{\rho},t)$ and $a^{\dagger}(z,\vec{\rho},t)$ to the standard-modal annihilation and creation operators (Wentzel, 1949; Loudon, 1983) will be given in the next subsection, where we present the theory of quantum field propagation and diffraction in free space. These space- and time-dependent photon annihilation and creation operators obey the commutation relations

$$\begin{aligned}&[a(z,\vec{\rho},t),a^{\dagger}(z,\vec{\rho}\,',t')]=\delta(\vec{\rho}-\vec{\rho}\,')\delta(t-t'),\\ &[a(z,\vec{\rho},t),a(z,\vec{\rho}\,',t')]=0\end{aligned} \tag{3.2}$$

and are normalized so that the mean value $\langle a^{\dagger}(z,\vec{\rho},t)a(z,\vec{\rho},t)\rangle$ determines the mean *photon-flux density* in photons per cm^2 per second at point $\vec{\rho}$ and time t.

The quantum theory of photodetection provides the following expressions for the mean value of the photocurrent density $\langle i(\vec{\rho},t)\rangle$ and its space-time correlation function $\langle\frac{1}{2}\{\delta i(\vec{\rho},t),\delta i(\vec{\rho}\,',t')\}_+\rangle$:

$$\langle i(\vec{\rho},t)\rangle = \eta\langle I(\vec{\rho},t)\rangle, \tag{3.3}$$

$$\left\langle \tfrac{1}{2}\{\delta i(\vec{\rho},t),\delta i(\vec{\rho}',t')\}_+\right\rangle = \langle i(\vec{\rho},t)\rangle\,\delta(\vec{\rho}-\vec{\rho}')\,\delta(t-t') + \eta^2\langle :I(\vec{\rho},t)I(\vec{\rho}',t'):\rangle - \langle i(\vec{\rho},t)\rangle\langle i(\vec{\rho}',t')\rangle. \tag{3.4}$$

Here $I(\vec{\rho},t)=a^\dagger(z,\vec{\rho},t)a(z,\vec{\rho},t)$ is the *photon-flux density operator*.

As with the single-mode case considered in the previous section, the space-time correlation function $\langle \frac{1}{2}\{\delta i(\vec{\rho},t),\delta i(\vec{\rho}',t')\}_+\rangle$ contains three terms. The first term, $\langle i(\vec{\rho},t)\rangle\delta(\vec{\rho}-\vec{\rho}')\delta(t-t')$, describes completely uncorrelated photodetection events at different times and at different spatial points across the photodetection plane and represents the generalization of the shot noise in space-time.

The second contribution to the photocurrent density correlation function is proportional to the normal- and time-ordered space-time intensity correlation function

$$G^{(2)}(\vec{\rho},t;\vec{\rho}',t')=\langle :I(\vec{\rho},t)I(\vec{\rho}',t'):\rangle. \tag{3.5}$$

This correlation function is proportional to the probability of detecting a photon at time t' and at the spatial point $\vec{\rho}'$ under the condition that the previous detection happened at time t and point $\vec{\rho}$. When the intensity of the light is stationary in time and uniform in the transverse area of the light beam, this correlation function depends only on the time difference $\tau=t'-t$ and the spatial difference $\vec{\xi}=\vec{\rho}'-\vec{\rho}$ between two points, $G^{(2)}(\vec{\rho},t;\vec{\rho}',t')=G^{(2)}(\vec{\xi},\tau)$.

In analogy to the degree of second-order temporal coherence introduced in Sec. II, one can define the *degree of second-order spatio-temporal coherence* as

$$g^{(2)}(\vec{\xi},\tau)=\frac{\langle :I(\vec{\rho},t)I(\vec{\rho}+\vec{\xi},t+\tau):\rangle}{\langle I(\vec{\rho},t)\rangle^2}. \tag{3.6}$$

The last term in Eq. (3.4) is the product of two mean photocurrent densities and, for a light wave with intensity stationary in time and uniform in the transverse plane, is constant.

The correlation function $g^{(2)}(\vec{\xi},\tau)$ allows us to generalize the notions of photon bunching and antibunching, introduced in Sec. II.B, from the temporal domain into space-time. That is, if the correlation function $g^{(2)}(\vec{\xi},\tau)$ has its maximum at $\vec{\xi}=\vec{0}$ and at $\tau=0$, $g^{(2)}(\vec{0},0)>g^{(2)}(\vec{\xi},\tau)$, it is natural to speak about bunching in space-time. Indeed, this means that two photons are more likely to be detected when close together, both at small time intervals and at small spatial separations from one another, than when further apart. Analogously, if $g^{(2)}(\vec{0},0)<g^{(2)}(\vec{\xi},\tau)$, one may speak about antibunching in space-time, because two photodetection events are less likely to appear at close space-time points than for more distant points.

As with antibunching in time, antibunching in space-time is a purely quantum-mechanical phenomenon. Indeed, it follows from the Schwartz inequality that the correlation function $g^{(2)}(\vec{\xi},\tau)$ of a classical electromagnetic field stationary in time and uniform in space must satisfy

$$g^{(2)}(\vec{0},0)\geqslant g^{(2)}(\vec{\xi},\tau) \tag{3.7}$$

for arbitrary $\vec{\xi}$ and τ. Since antibunching in space-time means an exactly opposite inequality, it cannot be explained within the framework of semiclassical theory, i.e., when the light field is treated as a *c*-number.

At this point it is appropriate to note that the generalization of such notions as bunching and antibunching from a temporal domain into space-time is more than just writing an additional (spatial) argument in the correlation function $g^{(2)}(\vec{\xi},\tau)$. Physically, the spatial behavior of light is completely different from its temporal behavior and involves new phenomena such as diffraction. Consequently, spatial bunching and antibunching have many features different from their temporal counterparts. Spatial fluctuations of light can be investigated completely independently from temporal ones as spatial correlations of photocounts that happen simultaneously in time, i.e., for zero time delay $\tau=0$. Such a possibility clearly does not exist for a single-mode electromagnetic field.

In Sec. II we saw that, for a stationary single-mode electromagnetic field, a convenient characteristic of photocurrent fluctuations is the photocurrent noise spectrum. It was defined as a Fourier transform of the photocurrent correlation function in time. Using the photocurrent noise spectrum, we have defined the standard quantum limit as the minimum amount of noise in photodetection allowed by semiclassical theory. Now we shall generalize the notion of the photocurrent noise spectrum and standard quantum limit in space-time.

As follows from Eq. (3.4), for a light field stationary in time and uniform in the transverse plane, the correlation function of the photocurrent density $\langle \frac{1}{2}\{\delta i(\vec{\rho},t),\delta i(\vec{\rho}',t')\}_+\rangle$ depends only on the time difference $\tau=t'-t$ and the spatial difference $\vec{\xi}=\vec{\rho}'-\vec{\rho}$. Let us consider the spatiotemporal Fourier transform of this correlation function,

$$(\delta i)^2_{\vec{q},\Omega}=\int d\vec{\rho}\int dt\,\exp[i(\Omega t-\vec{q}\cdot\vec{\rho})] \times\left\langle \tfrac{1}{2}\{\delta i(\vec{0},0),\delta i(\vec{\rho},t)\}_+\right\rangle. \tag{3.8}$$

Similar to Sec. II.A, we shall call $(\delta i)^2_{\vec{q},\Omega}$ the noise spectrum of the photocurrent density and its arguments Ω and $\vec{q}$ frequency and spatial frequency.

Using the photodetection formula (3.4), we can write the noise spectrum $(\delta i)^2_{\vec{q},\Omega}$ as

$$(\delta i)^2_{\vec{q},\Omega}=\langle i\rangle+\tilde{G}^{(2)}(\vec{q},\Omega)-\langle i\rangle^2\delta(\Omega)\,\delta(\vec{q}). \tag{3.9}$$

Here the first contribution comes from the shot-noise term in Eq. (3.4), the second from the intensity correlation function,

$$\tilde{G}^{(2)}(\vec{q},\Omega)=\int d\vec{\rho}\int dt\,\exp[i(\Omega t-\vec{q}\cdot\vec{\rho})]G^{(2)}(\vec{\rho},t), \tag{3.10}$$

and the last one from the space-time independent product of two mean photocurrent densities. One can show that in semiclassical theory the sum of the second and third contributions is always non-negative. Therefore the semiclassical minimum value of the photocurrent density noise is given by the shot noise in space-time,

$$(\delta i)^2_{\vec{q},\Omega} = \langle i \rangle. \tag{3.11}$$

This formula is a generalization of the standard quantum limit (2.12) from the temporal domain into space-time. In quantum theory the sum of the second and third terms in Eq. (3.9) can be negative and compensate partially or even completely for the shot-noise contribution for some frequencies Ω and spatial frequencies $\vec{q}$. In Sec. IV we shall describe in detail the spectrum $(\delta i)^2_{\vec{q},\Omega}$ for a traveling-wave optical parametric amplifier.

The definition (3.11) of the standard quantum limit in space-time is convenient when the light intensity is stationary in time and uniform in the transverse plane of the electromagnetic wave. It is, however, not very appropriate for the case of optical images when the light intensity is a function of the transverse coordinate $\vec{\rho}$ and time t if one has a dynamic image (for example, a movie). Therefore, for imaging applications, we shall give an equivalent definition of the standard quantum limit.

We shall assume that an image is detected by a photodetection array or the CCD camera whose pixels occupy the area S_d during the observation time T_d. In the literature about optical imaging and image processing (Goodman, 1985; Yu, 1985), the noise performance of the scheme is described in terms of the signal-to-noise ratio. When the optical image is detected by a CCD camera, the observed signal of the scheme is the mean number of photoelectrons $N(\vec{\rho},t)$ collected by the pixel centered at point $\vec{\rho}$ in the photodetection plane in the time interval from $t-T_d/2$ to $t+T_d/2$:

$$\langle N(\vec{\rho},t) \rangle = \int_{S_d} d\vec{\rho}' \int_{T_d} dt' \langle i(\vec{\rho}',t') \rangle. \tag{3.12}$$

For a stationary and uniform light field this quantity is independent of $\vec{\rho}$ and t. For a real optical image it will reproduce the intensity distribution across the photodetection plane and as a function of time, if the pixel area S_d and the observation time T_d are chosen much smaller than typical spatial and temporal scales of the image.

The noise properties of the photodetection scheme are characterized by the variance in the number of collected photoelectrons $\langle \Delta N^2(\vec{\rho},t) \rangle$, which is related to the correlation function of the photocurrent density as

$$\langle \Delta N^2(\vec{\rho},t) \rangle = \int_{S_d} d\vec{\rho}' \int_{T_d} dt' \int_{S_d} d\vec{\rho}'' \times \int_{T_d} dt'' \langle 1/2\{\delta i(\vec{\rho}',t'), \delta i(\vec{\rho}'',t'')\}_+ \rangle. \tag{3.13}$$

Following the literature on optical image processing, we shall define the signal-to-noise ratio R of the scheme as (Goodman, 1985)[3]

$$R = \frac{\langle N(\vec{\rho},t) \rangle}{\langle \Delta N^2(\vec{\rho},t) \rangle^{1/2}}. \tag{3.14}$$

Using the photodetection formula (3.4) and keeping only the shot-noise contribution, we obtain the standard quantum limit for the signal-to-noise ratio as

$$R_{\mathrm{SQL}} = \langle N(\vec{\rho},t) \rangle^{1/2}. \tag{3.15}$$

In Secs. VII and VIII we shall calculate the signal-to-noise ratio R for the case of parametric image amplification and optical imaging with multimode squeezed light.

B. Propagation and diffraction of a quantized field in free space

The difficulties associated with the quantum-mechanical description of field propagation in free space or a nonlinear medium lie in the usual procedure of field quantization. The transverse component of the electromagnetic field is usually quantized at an initial time $t=0$ within a quantization volume V that is large enough to contain the spatial region of interest (Wentzel, 1949; Louisell, 1973; Loudon, 1983). After finding a set of orthogonal spatial modes for the given spatial region and corresponding canonical field variables, one introduces creation and annihilation operators for these modes that satisfy the standard commutation relations. Further evolution of the quantized field due, for example, to interaction with an atomic medium is described in terms of the Heisenberg equations for annihilation and creation operators, i.e., as purely *temporal evolution*.

Such a description of field dynamics is not well suited to the problem of field propagation in free space or a medium. For such a study, it would be more appropriate to have a quantum-mechanical analog of the classical field propagation and diffraction theory in the spirit of Huygens-Fresnel. In the next subsection we shall present such a description for transparent nonlinear media, i.e., when the field interaction with atoms can be described in terms of an effective Hamiltonian. But before taking on the problem of quantized field propagation in a nonlinear medium, we shall consider in this subsection the simpler question of quantized field propagation in free space. Our analysis here will be very similar to that of Yuen and Shapiro (1978).

Let $E^{(+)}(\vec{r},t)$, where $\vec{r}=(x,y,z)$ is the spatial coordinate, be the positive-frequency operator of the electric field in a vacuum. This field is usually quantized in a cube with linear dimensions L under periodic boundary

[3] In the literature about amplifiers it is customary to deal with the *power signal-to-noise ratio*, which is equal to R^2. Obviously both definitions are completely equivalent. We shall use the power signal-to-noise ratio in Sec. VII.A because it provides simpler final results.

conditions. In the continuum limit, i.e., when the quantization volume grows infinitely, $L\to\infty$, this operator is written in the form of the modal decomposition

$$E^{(+)}(\vec{r},t)=i\left(\frac{\hbar}{2\epsilon_0}\right)^{1/2}\int\frac{d\vec{k}}{(2\pi)^3}\omega^{1/2}(k)a(\vec{k})\times\exp[i(\vec{k}\cdot\vec{r}-\omega(k)t)]. \tag{3.16}$$

Here $a(\vec{k})$ and $a^\dagger(\vec{k})$ are the photon annihilation and creation operators of a spatial mode with wave vector $\vec{k}$; the frequency $\omega(k)$ is given by the free-space dispersion relation $\omega(k)=kc$, with $k=|\vec{k}|$. The operators $a(\vec{k})$ and $a^\dagger(\vec{k})$ obey the canonical commutation relations

$$[a(\vec{k}),a^\dagger(\vec{k}')]=(2\pi)^3\delta(\vec{k}-\vec{k}'),\quad [a(\vec{k}),a(\vec{k}')]=0. \tag{3.17}$$

Equation (3.16) determines the Heisenberg field operator $E^{(+)}(\vec{r},t)$ in all points $\vec{r}$ and t of the space-time as a solution of the initial-value problem, i.e., through the modal operators $a(\vec{k})$ and $a^\dagger(\vec{k})$ given at time $t=0$ as Schrödinger operators. For a complete quantum-mechanical description we have to specify the density matrix of the field for the continuum set of modes $\vec{k}$. In the Heisenberg representation (3.16), this density matrix remains constant as time evolves.

Though Eq. (3.16) allows us to determine the field at any point of space-time, it is illsuited for the problem of field propagation. For a solution to the propagation problem, we have to translate Eq. (3.16) from a solution of the initial-value problem into a solution of the boundary-value problem. In other words, for a wave traveling in the $+z$ direction, we would like to have a formula that determines the field operator at any point $\vec{\rho}$ in the transverse plane at coordinate z given the field operator over the plane $z=0$.

Let us introduce the slowly varying photon annihilation and creation operators $a(\vec{\rho},z,t)$ and $a^\dagger(\vec{\rho},z,t)$ according to

$$E^{(+)}(z,\vec{\rho},t)=i\left(\frac{\hbar\omega_0}{2\epsilon_0 c}\right)^{1/2}\exp[i(k_0z-\omega_0t)]a(z,\vec{\rho},t), \tag{3.18}$$

where ω_0 is the carrier frequency of a wave traveling in the $+z$ direction and $k_0=\omega_0/c$ is its wave number. The operator $a(z,\vec{\rho},t)$ is given by

$$a(z,\vec{\rho},t)=\int\frac{dk_z}{2\pi}\int\frac{d\vec{q}}{(2\pi)^2}\sqrt{\frac{\omega(k)}{k_0}}a(\vec{k})\times\exp[i(\vec{q}\cdot\vec{\rho}+(k_z-k_0)z-(\omega(k)-\omega_0)t)]. \tag{3.19}$$

Here $\vec{\rho}$ is the two-dimensional coordinate vector $\vec{\rho}=(x,y)$ in the transverse plane of the wave and $\vec{q}=(k_x,k_y)$.

Let us consider a finite spatial region of volume V. The free Hamiltonian of the electromagnetic field in this region can be written as

$$H_0=\frac{\hbar\omega_0}{c}\int_V d\vec{r}\,a^\dagger(z,\vec{\rho},t)a(z,\vec{\rho},t). \tag{3.20}$$

The factor c^{-1} appears due to the normalization of operators $a(\vec{\rho},z,t)$ and $a^\dagger(\vec{\rho},z,t)$. The temporal evolution of the slowly varying operator $a(z,\vec{\rho},t)$ is described by the following equation:

$$\dot{a}(z,\vec{\rho},t)=i\omega_0a(z,\vec{\rho},t)+\frac{i}{\hbar}[H_0,a(z,\vec{\rho},t)], \tag{3.21}$$

where the first term comes from the explicit time dependence $\exp[i\omega_0t]$ included in the definition (3.19) of the slowly varying operator $a(z,\vec{\rho},t)$. To evaluate the commutator in the right-hand side, we need to know the commutation relation of the slowly varying amplitudes $a(z,\vec{\rho},t)$ and $a^\dagger(z,\vec{\rho},t)$ at the same time, but at two different spatial points inside the medium. Using Eq. (3.19), we can write this commutation relation as

$$[a(z,\vec{\rho},t),a^\dagger(z',\vec{\rho}\,',t)]=c\int\frac{dk_z}{2\pi}\int\frac{d\vec{q}}{(2\pi)^2}\frac{\omega(k)}{\omega_0}\exp[i(k_z-k_0)(z-z')+i\vec{q}\cdot(\vec{\rho}-\vec{\rho}')]\equiv c\,\tilde{\delta}(\vec{r}-\vec{r}'). \tag{3.22}$$

Here $\tilde{\delta}(\vec{r}-\vec{r}')$ is a δ-type function that becomes the real δ function $\delta(\vec{r}-\vec{r}')$ if we neglect $\omega(k)$ dependence in the integrand.

Using this commutation relation, we obtain

$$\dot{a}(z,\vec{\rho},t)=i\omega_0a(z,\vec{\rho},t)-i\omega_0\int_V d\vec{r}'\,\tilde{\delta}(\vec{r}-\vec{r}')a(z',\vec{\rho}',t). \tag{3.23}$$

We can write this equation for operators in a form similar to a classical equation describing the diffraction of light in free space. For this we shall use quasimonochromatic and paraxial approximations, namely,

$$k=\sqrt{k_z^2+q^2}\approx k_z+\frac{q^2}{2k_0} \tag{3.24}$$

and

$$\frac{\omega(k)}{\omega_0}\approx1+\frac{k_z-k_0}{k_0}+\frac{q^2}{2k_0^2}. \tag{3.25}$$

Substituting Eq. (3.25) into Eq. (3.22) we obtain

$$\tilde{\delta}(\vec{r}-\vec{r}\,')\approx\int\frac{ds}{2\pi}\int\frac{d\vec{q}}{(2\pi)^2}\left(1+\frac{s}{k_o}+\frac{q^2}{2k_0^2}\right)\times\exp[i(s(z-z')+\vec{q}\cdot(\vec{\rho}-\vec{\rho}'))]=\left(1-\frac{i}{k_0}\frac{\partial}{\partial z}-\frac{1}{2k_0^2}\nabla_\perp^2\right)\delta(\vec{r}-\vec{r}'), \tag{3.26}$$

where $\nabla_\perp^2$ is the transverse Laplacian with respect to $\vec{\rho}$, and we have denoted $s=k_z-k_0$. Therefore, in this approximation, the equation for the slowly varying operator $a(z,\vec{\rho},t)$ reads

$$\dot{a}(z,\vec{\rho},t)=\left(-c\frac{\partial}{\partial z}+c\frac{i}{2k_0}\nabla_\perp^2\right)a(z,\vec{\rho},t). \tag{3.27}$$

In Eq. (3.27) we recognize the classical equation describing the diffraction of a light wave in free space.

C. Propagation and diffraction of a quantized field in a nonlinear parametric medium

Now we turn to derivation of the equation for propagation of a quantized field in a nonlinear parametric medium.[4] It must be noted that the problem of field quantization in a dielectric medium is very difficult one and is outside the scope of this article. For rigorous treatment we refer the reader to the book of Klyshko (1988a), the paper of Drummond (1990), and references therein. Here we present some final results following Klyshko (1988a).

The positive-frequency operator of a quantized electric field in a transparent dielectric medium can be written in a form similar to that for a vacuum (Klyshko, 1988a):

$$E^{(+)}(\vec{r},t)=i\left(\frac{\hbar}{2\epsilon_0}\right)^{1/2}\int\frac{d\vec{k}}{(2\pi)^3}\xi(k)\omega^{1/2}(k)a(\vec{k}) \times\exp[i(\vec{k}\cdot\vec{r}-\omega(k)t)]. \tag{3.28}$$

This differs from Eq. (3.16) in the factor $\xi(k)$, which describes the strength of the field in the medium as compared to that in a vacuum. This constant is given by

$$\xi^2(k)=\frac{u(k)v(k)}{c^2\cos\rho(k)}, \tag{3.29}$$

where $v(k)=c/n(k)$ is the phase velocity of light in the medium, $u(k)=\partial\omega(k)/\partial k$ is the group velocity, and $\rho(k)$ is the so-called generalized anisotropy angle, that is, the angle between the electric field and the induction.

A second difference between this equation and Eq. (3.16) is in the dispersion relation $\omega(k)$, which for the medium is different from $\omega(k)=kc$ for the vacuum. In fact, in a real crystal the ''mode'' of the field is determined not only by the wave vector $\vec{k}$, but by two additional parameters ν and μ (Klyshko, 1988a). The first corresponds to the type of polarization of the field (in the case of anisotropic material). In addition, a field with a fixed wave vector $\vec{k}$ and a polarization type ν generally contains many harmonics, which are distinguished by the index μ. For simplicity we shall neglect the polarization and anisotropy effects and assume that we are interested in a field with frequencies near one fixed branch of the dispersion law with a definite μ.

Under these assumptions we can introduce the slowly varying operator $a(z,\vec{\rho},t)$ of the quantized field in the medium,

$$E^{(+)}(z,\vec{\rho},t)=i\xi\left(\frac{\hbar\omega_0}{2\epsilon_0 c}\right)^{1/2}\exp[i(k_l z-\omega_0 t)]a(z,\vec{\rho},t). \tag{3.30}$$

[4]This derivation belongs to I. Sokolov and has not been published previously. I should like to thank him for permitting me to reproduce it in this article.

Here we have denoted by k_l the wave number of the wave in the medium, to distinguish it from the corresponding k_0 in a vacuum. The slowly varying operator $a(z,\vec{\rho},t)$ is given by an equation identical to Eq. (3.19),

$$a(z,\vec{\rho},t)=\int\frac{dk_z}{2\pi}\int\frac{d\vec{q}}{(2\pi)^2}\sqrt{\frac{\omega(k)}{k_0}}a(\vec{k}) \times\exp[i(\vec{q}\cdot\vec{\rho}+(k_z-k_0)z-(\omega(k)-\omega_0)t)], \tag{3.31}$$

but now with a dispersion relation $\omega(k)$ for the medium.

We shall describe the parametric interaction in the medium in terms of an effective Hamiltonian. Let us assume that a $\chi^{(2)}$ nonlinear parametric medium fills a volume V. This medium is illuminated by a monochromatic plane wave playing the role of the pump. The pump wave propagates in the $+z$ direction and has the frequency ω_p and wave number k_p:

$$E_p^{(+)}(z,\vec{\rho},t)=E_p\exp[i(k_p z-\omega_p t)]. \tag{3.32}$$

We choose the frequency ω_p of the pump wave to be $\omega_p=2\omega_0$. We shall consider the amplitude E_p as a c-number, i.e., we neglect the quantum fluctuations of the pump wave. We shall also assume this amplitude to be strong enough and neglect depletion of the pump wave due to parametric interaction. Under these assumptions the parametric interaction can be described by the following effective Hamiltonian (Klyshko, 1988a, p. 289):

$$H_{\rm int}=i\hbar\frac{n_0 g}{c}\int_V d\vec{r}\exp[i(k_p-2k_l)z](a^\dagger(z,\vec{\rho},t))^2+\text{H.c.} \tag{3.33}$$

Here n_0 gives the density of active atoms in the parametric medium, and g is the strength constant of the parametric interaction proportional to the amplitude E_p of the pump wave and the susceptibility constant $\chi^{(2)}$ of the medium.

The evolution of the slowly varying amplitude $a(z,\vec{\rho},t)$ in the parametric medium is described by the following equation:

$$\dot{a}(z,\vec{\rho},t)=i\omega_0 a(z,\vec{\rho},t)+\frac{i}{\hbar}[H_0+H_{\rm int},a(z,\vec{\rho},t)]. \tag{3.34}$$

Here H_0 is the free-field Hamiltonian in the medium. In terms of $a(z,\vec{\rho},t)$ and $a^\dagger(z,\vec{\rho},t)$ it is given by Eq. (3.20). We can also use Eq. (3.22) for the commutation relation of slowly varying photon operators, but now with a dispersion relation $\omega(k)$ for the medium. Thus we obtain

$$\dot{a}(z,\vec{\rho},t)=i\omega_0 a(z,\vec{\rho},t)-i\omega_0\int_V d\vec{r}'\,\tilde{\delta}(\vec{r}-\vec{r}')a(z',\vec{\rho}',t) +2n_0 g\int_V d\vec{r}'\exp[i(k_p-2k_l)z'] \times\tilde{\delta}(\vec{r}-\vec{r}')a^\dagger(z',\vec{\rho}',t). \tag{3.35}$$

To bring this equation into equation for the propagation of $a(z,\vec{\rho},t)$ along the z axis we shall perform the following Fourier transform:

$$a(s,\vec{q},\Omega)=\int dz\, e^{-isz}\int d\vec{\rho}\, e^{-i\vec{q}\cdot\vec{\rho}}\int dt\, e^{i\Omega t}a(z,\vec{\rho},t). \tag{3.36}$$

Here s is the Fourier variable corresponding to the longitudinal coordinate z. From Eq. (3.35) we obtain the following equation for the Fourier amplitude $a(s,\vec{q},\Omega)$:

$$-i\Omega a(s,\vec{q},\Omega)=-i(\omega(k)-\omega_0)a(s,\vec{q},\Omega) +2n_0 g a^{\dagger}(-s+\Delta,-\vec{q},-\Omega), \tag{3.37}$$

where $\omega(k)$ corresponds to the wave vector $\vec{k}=(\vec{q},k_l+s)$ and we have denoted $\Delta=k_p-2k_l$. We shall separate the evolution of the Fourier amplitude $a(z,\vec{q},\Omega)$ due to free propagation in the medium from the effect of the parametric interaction by introducing a new Fourier amplitude $\epsilon(z,\vec{q},\Omega)$ as

$$a(z,\vec{q},\Omega)=\epsilon(z,\vec{q},\Omega)\exp[(k_z(\vec{q},\Omega)-k_l)z], \tag{3.38}$$

where

$$k_z(\vec{q},\Omega)=\sqrt{k^2(\omega_0+\Omega)-q^2} \tag{3.39}$$

is a z component of the wave vector with frequency $\omega_0+\Omega$ and spatial frequency $\vec{q}$. From Eq. (3.38) it follows that

$$\epsilon(s,\vec{q},\Omega)=a(s+k_z(\vec{q},\Omega)-k_l,\vec{q},\Omega). \tag{3.40}$$

From Eq. (3.37) we obtain the following equation for the new Fourier amplitude $\epsilon(s,\vec{q},\Omega)$:

$$-i\Omega\epsilon(s,\vec{q},\Omega)=-i(\omega(k_+)-\omega_0)\epsilon(s,\vec{q},\Omega) +2n_0 g\epsilon^{\dagger}(-s-\Delta(\vec{q},\Omega),-\vec{q},-\Omega). \tag{3.41}$$

Here the wave vector $\vec{k}_+$ is defined as

$$\vec{k}_+=(s+k_z(\vec{q},\Omega)-k_l,\vec{q}). \tag{3.42}$$

In Eq. (3.41) we have introduced the mismatch function $\Delta(\vec{q},\Omega)$,

$$\Delta(\vec{q},\Omega)=k_z(\vec{q},\Omega)+k_z(-\vec{q},-\Omega)-k_p. \tag{3.43}$$

Now we shall use paraxial and quasimonochromatic approximations, namely,

$$\omega(k_+)\approx\omega_0+\Omega+us, \tag{3.44}$$

where $u=\partial\omega(k_l)/\partial k_l$ is the group velocity of the wave in the crystal.

Substituting Eq. (3.44) into Eq. (3.41), we arrive at

$$is\epsilon(s,\vec{q},\Omega)=\frac{2n_0 g}{u}\epsilon^{\dagger}(-s-\Delta(\vec{q},\Omega),-\vec{q},-\Omega). \tag{3.45}$$

Finally, performing the inverse Fourier transform over s, we obtain the desired equation of propagation for the Fourier amplitude $\epsilon(z,\vec{q},\Omega)$:

$$\frac{\partial}{\partial z}\epsilon(z,\vec{q},\Omega)=\sigma\epsilon^{\dagger}(z,-\vec{q},-\Omega)\exp[i\Delta(\vec{q},\Omega)z], \tag{3.46}$$

where $\sigma=2n_0 g/u$ is the coupling constant of the parametric interaction. In Sec. IV we shall use this equation to describe the generation of multimode squeezed states by a traveling-wave optical parametric amplifier.

D. Space-time Fourier transform vs decomposition into discrete transverse modes of a resonator

We shall see in Sec. IV that multimode squeezed states of light can be generated both in traveling-wave geometry without a cavity and when an active nonlinear medium is placed in a resonator. In the latter case it is more natural to describe multimode squeezing in terms of discrete transverse modes of the cavity. In this subsection we shall give an overview of such an alternative description of quantum fluctuations in space-time. More details on this approach can be found in papers by Lugiato and Gatti (1993), Gatti and Lugiato (1995), and Lugiato and Marzoli (1995).

Let $f_l(\vec{\rho})$ be a complete orthonormal set of complex functions in the transverse plane $\vec{\rho}$. Here l stands for a certain set of indices. In the case of cavity-based generation of multimode squeezed states, it is natural to choose this set as eigenmodes of the cavity. Normally, these eigenmodes depend on the longitudinal coordinate z; however, for simplicity, in this subsection we shall omit this dependence. The set of functions $f_l(\vec{\rho})$ satisfies both the condition of orthonormality,

$$\int d\vec{\rho}\, f_l^{\star}(\vec{\rho})f_{l'}(\vec{\rho})=\delta_{ll'}, \tag{3.47}$$

and completeness,

$$\sum_l f_l^{\star}(\vec{\rho})f_l(\vec{\rho}')=\delta(\vec{\rho}-\vec{\rho}'). \tag{3.48}$$

Instead of performing a space-time Fourier transform of the slowly varying field operator $a(\vec{\rho},t)$ in free space as in Eq. (3.36), we can expand it over the eigenmodes $f_l(\vec{\rho})$

$$a(\vec{\rho},t)=\sum_l f_l(\vec{\rho})a_l(t), \tag{3.49}$$

where $a_l(t)$ are operator-valued expansion coefficients that have the meaning of photon annihilation operators for the lth mode. From the commutation relations (3.2) together with Eq. (3.47) it is easy to see that $a_l(t)$ and $a_l^{\dagger}(t)$ obey

$$[a_l(t),a_{l'}^{\dagger}(t')]=\delta_{ll'}\delta(t-t'). \tag{3.50}$$

We note that these commutation relations hold for the field operators outside the cavity. To complete the analogy with the space-time Fourier transform we shall also employ the Fourier coefficients $a_l(\Omega)$, defined as

$$a_l(\Omega)=\int_{-\infty}^{\infty}dt\, e^{i\Omega t}a_l(t). \tag{3.51}$$

Using these definitions we would like to express the space-time correlation function of the photocurrent density (3.4) in terms of the noise spectrum of the individual eigenmodes similar to $(\delta i)^2_{\vec{q},\Omega}$. For this we can expand

the correlation function $\langle \frac{1}{2}\{\delta i(\vec{\rho},t),\delta i(\vec{\rho}',t')\}_+\rangle$ over the set of eigenfunctions $f_l(\vec{\rho})$,

$$\langle \tfrac{1}{2}\{\delta i(\vec{\rho},t),\delta i(\vec{\rho}',t')\}_+\rangle = \sum_{l,l'} f_l(\vec{\rho}) f_{l'}(\vec{\rho}')\langle \tfrac{1}{2}\{\delta i_l(t),\delta i_{l'}(t')\}_+\rangle = \sum_{l} f_l(\vec{\rho}) f_l(\vec{\rho}')\langle \tfrac{1}{2}\{\delta i_l(t),\delta i_l(t')\}_+\rangle. \quad (3.52)$$

Here we have assumed that the eigenfunctions $f_l(\vec{\rho})$ are real and that the photocurrent density fluctuations for different eigenmodes are uncorrelated,

$$\langle \tfrac{1}{2}\{\delta i_l(t),\delta i_{l'}(t')\}_+\rangle = \delta_{ll'}\langle \tfrac{1}{2}\{\delta i_l(t),\delta i_l(t')\}_+\rangle. \quad (3.53)$$

We shall further assume that the photocurrent density $i(\vec{\rho},t)$ is stationary in time, $\langle i(\vec{\rho},t)\rangle = \langle i(\vec{\rho})\rangle$, but not necessarily uniform in space. In this case we can introduce the noise spectrum of the photocurrent density for the lth mode as

$$(\delta i)^2_{l,\Omega} = \int_{-\infty}^{\infty} dt\, e^{i\Omega t}\langle \tfrac{1}{2}\{\delta i_l(0),\delta i_l(t)\}_+\rangle. \quad (3.54)$$

Combining Eqs. (3.52)–(3.54) we arrive at the desired expression for the space-time correlation function,

$$\langle \tfrac{1}{2}\{\delta i(\vec{\rho},t),\delta i(\vec{\rho}',t')\}_+\rangle = \sum_{l} f_l(\vec{\rho}) f_l(\vec{\rho}')\frac{1}{2\pi}\int_{-\infty}^{\infty} d\Omega\, e^{-i\Omega(t-t')}(\delta i)^2_{l,\Omega}. \quad (3.55)$$

Comparing this result with Eq. (3.8), we see that $(\delta i)^2_{l,\Omega}$ plays the role of a discrete analog for the noise spectrum of the photocurrent density $(\delta i)^2_{q,\Omega}$. An important difference between Eqs. (3.55) and (3.8) is that in arriving at Eq. (3.55) we did not assume the photocurrent density to be uniform in space, while Eq. (3.8) holds true only for spatially uniform processes. This distinction makes the method of modal decomposition more powerful and allows us to apply it to the investigation of nonuniform spatial processes. In Sec. IV.D.2 we shall illustrate the application of this method for calculating the spatial correlation function and squeezing spectra for multimode squeezed states generated by an optical parametric oscillator in a cavity with spherical mirrors.

IV. MULTIMODE SQUEEZED STATES OF LIGHT

A. Generation of multimode squeezed states by a traveling-wave optical parametric amplifier

The generation of multimode squeezed states of light by a traveling-wave optical parametric amplifier was described by Kolobov and Sokolov (1989a). In this section we shall present this model in detail and compare it with some other proposed schemes.

Let us consider a three-wave parametric interaction in a $\chi^{(2)}$ nonlinear medium having the form of a plane slab of thickness l, placed perpendicular to the z axis (see Fig. 7). A plane monochromatic pump wave of frequency $\omega_p = 2\omega_0$ is incident on this slab normal to its surface. As a result of the parametric down conversion, a pump photon ω_p splits into signal and idler photons, with frequencies $\omega_0+\Omega$ and $\omega_0-\Omega$, and wave vectors $\vec{k}(\vec{q},\Omega)$ and $\vec{k}(-\vec{q},-\Omega)$. Here we denote by $\vec{k}(\vec{q},\Omega)$ the wave vector of a photon with frequency $\omega_0+\Omega$ and transverse component $\vec{q}$. Because of stationarity in time and homogeneity in the transverse direction of the parametric process, the twin photons appear with opposite transverse components $\vec{q}$ and opposite frequencies Ω. In isotropic media the signal and idler photons have equal polarizations, determined by the polarization of the pump wave. In the case of anisotropic media, polarizations of signal and idler photons can be different and depend on the kind of nonlinear susceptibility tensor of the medium and the type of phase matching. For simplicity we do not consider here such polarization effects but refer the reader to the paper by Kolobov (1991) in which these effects were investigated in detail.

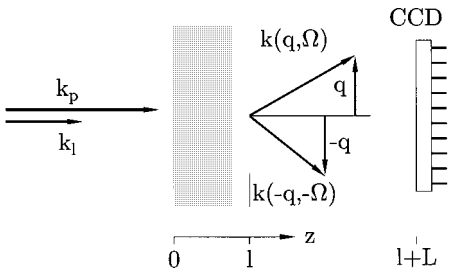

FIG. 7. Schematic of the generation of multimode squeezed light by a traveling-wave optical parametric amplifier.

In Sec. III.B we introduced the phase mismatch function $\Delta(\vec{q},\Omega)$ among three waves taking part in the parametric process [see Eq. (3.43)]. The parametric interaction is effective for such frequencies Ω and spatial frequencies $\vec{q}$ where the mismatch is small,

$$\Delta(\vec{q},\Omega)l \leqslant 1. \quad (4.1)$$

For the slowly varying Fourier amplitudes $\epsilon(z,\vec{q},\Omega)$ given by Eq. (3.38), we obtained Eq. (3.46), describing their evolution inside the crystal. Solving this equation and taking into account the relation (3.38) between the Fourier amplitudes $a(z,\vec{q},\Omega)$ and $\epsilon(z,\vec{q},\Omega)$, we arrive at the following transformation of the operators $a(z,\vec{q},\Omega)$ from the input of the crystal, $z=0$, to its output, $z=l$:

$$a(l,\vec{q},\Omega) = U(\vec{q},\Omega)a(0,\vec{q},\Omega) + V(\vec{q},\Omega)a^{\dagger}(0,-\vec{q},-\Omega), \quad (4.2)$$

with coefficients $U(\vec{q},\Omega)$ and $V(\vec{q},\Omega)$ equal to

$$U(\vec{q},\Omega) = \exp[i(k_z(\vec{q},\Omega) - k_l - \Delta(\vec{q},\Omega)/2)l] \times \left[\cosh(\Gamma l) + \frac{i\Delta(\vec{q},\Omega)}{2\Gamma}\sinh(\Gamma l)\right],$$

$$V(\vec{q},\Omega) = \exp[i(k_z(\vec{q},\Omega) - k_l - \Delta(\vec{q},\Omega)/2)l] \times \frac{\sigma}{\Gamma}\sinh(\Gamma l), \quad (4.3)$$

where

$$\Gamma=\sqrt{|\sigma|^2-\Delta(\vec{q},\Omega)^2/4}. \tag{4.4}$$

The functions $U(\vec{q},\Omega)$ and $V(\vec{q},\Omega)$ satisfy the condition

$$|U(\vec{q},\Omega)|^2-|V(\vec{q},\Omega)|^2=1, \tag{4.5}$$

necessary for conserving the commutation relations of operators $a(z,\vec{q},\Omega)$ and $a^\dagger(z,\vec{q},\Omega)$ by the transformation (4.2). At the entry to the crystal, operators $a(0,\vec{q},\Omega)$ and $a^\dagger(0,\vec{q},\Omega)$ satisfy the free-field commutation relation

$$[a(0,\vec{q},\Omega),a^\dagger(0,\vec{q}',\Omega')]=(2\pi)^3\delta(\vec{q}-\vec{q}')\delta(\Omega-\Omega'). \tag{4.6}$$

Equation (4.2) generalizes the broadband squeezing transformation (2.40) for a single-mode electromagnetic field. It should be noted that broadband squeezing (with frequency argument, but without spatial frequency) has been investigated in the literature by several authors. Spectral aspects of broadband squeezing in a three-wave interaction were discussed by Caves and Crough (1987) and Kolobov and Sokolov (1989c), and in a four-wave interaction by Levenson *et al.* (1985) in the case of parallel propagation, and by Yurke (1985) for antiparallel propagation. These and certain other publications have shown how the spectrum of the intensity fluctuations in homodyne detection of broadband squeezed states is influenced by dispersion in a parametric medium (Caves and Crough, 1987; Kolobov and Sokolov, 1989c) or in an active resonator (Yurke, 1985) and by reflection from an external cavity (Levenson *et al.*, 1985). Equation (4.2) involves the spatial frequency $\vec{q}$ in the squeezing transformation, and our major interest here is to show the physical consequences of such a generalization.

We shall assume that, together with the pump wave, a monochromatic plane wave of frequency ω_0 is incident normal to the entry surface of the crystal. This wave will serve as a local oscillator for the homodyne detection of multimode squeezed light, and, upon entering the crystal, is assumed to be in a coherent state with complex amplitude α. The quantum state of all other waves with nonzero transverse components $\vec{q}$ at the entry to the crystal is a vacuum. Therefore, if we denote the total state of the electromagnetic field at $z=0$ as $|in\rangle$, we can write

$$a(0,\vec{\rho},t)|in\rangle=\alpha|in\rangle. \tag{4.7}$$

Upon leaving the crystal, the local oscillator wave is in a coherent state with the complex amplitude β, which is found from Eq. (4.2) to be

$$\beta=|\beta|e^{i\varphi_\beta}=\alpha U(\vec{0},0)+\alpha^\star V(\vec{0},0). \tag{4.8}$$

In this section we shall assume that the photodetection plane is located directly at the output of the crystal. The effect of free propagation and diffraction of multimode squeezed states will be the subject of Sec. V. Using Eq. (4.2), we can find the mean value of the photocurrent density and its noise spectrum defined by Eqs. (3.3), (3.4), and (3.8). For the mean photocurrent density we obtain

$$\langle i\rangle=\eta|\beta|^2+\eta\int\frac{d\vec{q}}{(2\pi)^2}\frac{d\Omega}{2\pi}|V(\vec{q},\Omega)|^2\equiv\langle i\rangle_l+\langle i\rangle_s. \tag{4.9}$$

It contains two terms: the first one, $\langle i\rangle_l$, comes from the local oscillator field, and the second, $\langle i\rangle_s$, is proportional to the intensity of spontaneous parametric down conversion. It follows from Eq. (4.9) that the function

$$\delta_{\vec{q},\Omega}=|V(\vec{q},\Omega)|^2 \tag{4.10}$$

determines the frequency and spatial frequency spectrum of spontaneous parametric down conversion. We shall see below that $\delta_{\vec{q},\Omega}$ is also a convenient parameter for characterizing the degree of squeezing for a wave pair with wave vectors $\vec{k}(\vec{q},\Omega)$ and $\vec{k}(-\vec{q},-\Omega)$.

Let Ω_c and q_c be the widths of the frequency and spatial frequency spectra of spontaneous parametric down conversion, $T_c=2\pi/\Omega_c$ its coherence time, and $S_c=(2\pi/q_c)^2$ the coherence area. The mean photocurrent density $\langle i\rangle_s$ can be written as

$$\langle i\rangle_s=\eta\frac{\delta_s}{T_cS_c}, \tag{4.11}$$

where

$$\delta_s=\frac{1}{q_c^2\Omega_c}\int d\vec{q}\,d\Omega\;\delta_{\vec{q},\Omega} \tag{4.12}$$

is the degeneracy parameter for spontaneous parametric down conversion (Mandel and Wolf, 1995).

Equation (4.2) allows us to evaluate the time- and normal-ordered intensity correlation function which appears in the photocurrent correlation function (3.4). It is convenient to perform the calculations directly with Fourier amplitudes $a(z,\vec{q},\Omega)$. With the help of the commutation relations (4.6), we can bring the correlation functions of the field at the input to the crystal to the normal-ordered form and can evaluate the quantum-mechanical averages over the input state defined in Eq. (4.7). The result for the noise spectrum of the photocurrent density reads

$$\begin{aligned}(\delta i)^2_{\vec{q},\Omega}=\langle i\rangle+2\eta^2|\beta|^2(\delta_{\vec{q},\Omega}+\mathrm{Re}\{e^{-2i\varphi_\beta}g(\vec{q},\Omega)\})\\+\eta^2\int\frac{d\vec{q}'}{(2\pi)^2}\frac{d\Omega'}{2\pi}(\delta_{\vec{q}',\Omega'}\delta_{\vec{q}-\vec{q}',\Omega-\Omega'}\\+g^\star(\vec{q}',\Omega')g(\vec{q}-\vec{q}',\Omega-\Omega')),\end{aligned} \tag{4.13}$$

where

$$g(\vec{q},\Omega)=U(\vec{q},\Omega)V(-\vec{q},-\Omega). \tag{4.14}$$

The first term determines shot noise. The contribution proportional to $|\beta|^2$ comes from interference between the local oscillator wave and the waves of the spontaneous parametric down conversion. The last contribution, given by the integral term, has its origin in the self-interference of the parametric down-conversion waves. This term describes the bunching effect typical for the down-conversion process.

B. Multimode squeezing as modulation of quantum fluctuations in space-time

It was shown by Kolobov and Sokolov (1989a) that the homodyne detection of multimode squeezed states can result in sub-Poissonian statistics of photons in both time and transverse area of the light beam. Under homodyne detection the down-conversion waves $(\vec{q},\Omega)$ and $(-\vec{q},-\Omega)$ modulate the local oscillator wave in space and time. The physical picture of such modulation was briefly outlined in Kolobov and Sokolov (1989a). In this subsection we shall give a detailed description of multimode squeezing in terms of the modulation of quantum fluctuations in space-time.

The transformation (4.2) of the Heisenberg operators $a(z,\vec{q},\Omega)$ from the entry surface to the exit of the parametric crystal is valid for an arbitrary quantum state of the electromagnetic field. In the case of spontaneous parametric down conversion, the quantum state of the field $|in\rangle$ at the entry to the crystal is a vacuum for all waves with nonzero transverse components $\vec{q}$.

Let us consider the positive-frequency part of the field $\delta E^{(+)}(z,\vec{\rho},t)$ composed of a pair of down-conversion waves with Fourier components $a(z,\vec{q},\Omega)$ and $a(z,-\vec{q},-\Omega)$,

$$\delta E^{(+)}(z,\vec{\rho},t)=i\xi\left(\frac{\hbar\omega_0}{2\epsilon_0 c}\right)^{1/2}\times\exp[i(k_l z-\omega_0 t)]\delta a_{\vec{q},\Omega}(z,\vec{\rho},t), \quad (4.15)$$

where

$$\delta a_{\vec{q},\Omega}(z,\vec{\rho},t)=a(z,\vec{q},\Omega)\exp[-i(\Omega t-\vec{q}\cdot\vec{\rho})]+a(z,-\vec{q},-\Omega)\exp[-i(\Omega t-\vec{q}\cdot\vec{\rho})] \quad (4.16)$$

is the contribution of the pair of down-conversion waves to a slowly varying field amplitude with frequency Ω and spatial frequency $\vec{q}$. For illustration let us consider $\delta a_{\vec{q},\Omega}(z,\vec{\rho},t)$ as a vector in the complex plane $(\mathrm{Re}\,\delta a_{\vec{q},\Omega}(z,\vec{\rho},t),\mathrm{Im}\,\delta a_{\vec{q},\Omega}(z,\vec{\rho},t))$. We shall introduce in this complex plane the slow quadrature components $a_{\mu c}(z,\vec{q},\Omega)$ and $a_{\mu s}(z,\vec{q},\Omega)$, where $\mu=1,2$, describing the harmonic oscillations $\propto\cos(\Omega t-\vec{q}\cdot\vec{\rho})$ and $\propto\sin(\Omega t-\vec{q}\cdot\vec{\rho})$:

$$\delta a_{\vec{q},\Omega}(z,\vec{\rho},t)=\exp[i\psi(z,\vec{q},\Omega)]\{[a_{1c}(z,\vec{q},\Omega)+ia_{2c}(z,\vec{q},\Omega)]\cos(\Omega t-\vec{q}\cdot\vec{\rho})+[a_{1s}(z,\vec{q},\Omega)+ia_{2s}(z,\vec{q},\Omega)]\sin(\Omega t-\vec{q}\cdot\vec{\rho})\}. \quad (4.17)$$

Here the angle $\psi(z,\vec{q},\Omega)$ determines the orientation of the coordinate system of the quadrature components $a_{\mu c}(z,\vec{q},\Omega)$ and $a_{\mu s}(z,\vec{q},\Omega)$.

The slow quadrature components $a_{\mu\lambda}(z,\vec{q},\Omega)$, $\lambda=c,s$, are connected with the Fourier components $a(z,\vec{q},\Omega)$ and $a(z,-\vec{q},-\Omega)$ as

$$a_{1c}(z,\vec{q},\Omega)+ia_{1s}(z,\vec{q},\Omega)=e^{-i\psi}a(z,\vec{q},\Omega)+e^{i\psi}a^{\dagger}(z,-\vec{q},-\Omega),$$

$$a_{2c}(z,\vec{q},\Omega)+ia_{2s}(z,\vec{q},\Omega)=-i[e^{-i\psi}a(z,\vec{q},\Omega)-e^{i\psi}a^{\dagger}(z,-\vec{q},-\Omega)], \quad (4.18)$$

where we have written ψ instead of $\psi(z,\vec{q},\Omega)$ for brevity. Using condition (4.5) and

$$\arg[U(\vec{q},\Omega)U^{\star}(-\vec{q},-\Omega)]=\arg[V(\vec{q},\Omega)V^{\star}(-\vec{q},-\Omega)], \quad (4.19)$$

which follows from the explicit form of the functions $U(\vec{q},\Omega)$ and $V(\vec{q},\Omega)$, we find from Eq. (4.18) the transformation of the slow quadratures from the entry surface to the exit surface of the crystal,

$$a_{\mu c}(l,\vec{q},\Omega)+ia_{\mu s}(l,\vec{q},\Omega)=\exp[i\kappa(\vec{q},\Omega)]\exp[\pm r(\vec{q},\Omega)](a_{\mu c}(0,\vec{q},\Omega)+ia_{\mu s}(0,\vec{q},\Omega)), \quad (4.20)$$

where "+" corresponds to the component with $\mu=1$ and "−" to the component with $\mu=2$. The components $a_{\mu\lambda}(0,\vec{q},\Omega)$ at the entry surface to the crystal are defined in the coordinate system with $\psi(0,\vec{q},\Omega)$, and the components $a_{\mu\lambda}(l,\vec{q},\Omega)$ at the exit surface of the crystal are defined with $\psi(l,\vec{q},\Omega)$. These angles are

$$\psi(0,\vec{q},\Omega)=\tfrac{1}{2}\arg[V(\vec{q},\Omega)U^{-1}(\vec{q},\Omega)],\qquad \psi(l,\vec{q},\Omega)=\tfrac{1}{2}\arg[U(\vec{q},\Omega)V(-\vec{q},-\Omega)]. \quad (4.21)$$

Two other squeezing parameters, $r(\vec{q},\Omega)$ and $\kappa(\vec{q},\Omega)$, are given by

$$\exp[\pm r(\vec{q},\Omega)]=|U(\vec{q},\Omega)|\pm|V(\vec{q},\Omega)|,\qquad \kappa(\vec{q},\Omega)=\tfrac{1}{2}\arg[U(\vec{q},\Omega)U^{-1}(-\vec{q},-\Omega)]. \quad (4.22)$$

Equations (4.20)–(4.22) describe the multimode squeezing of the slow quadrature components. Let us consider the transformation of the vector $a(z,\vec{\rho},t)$ of the sum of the local oscillator wave and the pair of down-conversion waves $(\vec{q},\Omega)$ and $(-\vec{q},-\Omega)$. In the complex plane of quadrature components, the vector $a(z,\vec{\rho},t)$ is given by the sum of the fixed vector of the local oscillator and the vector $\delta a_{\vec{q},\Omega}(z,\vec{\rho},t)$ of two down-conversion waves, which oscillates in time with frequency Ω and in space with spatial frequency $\vec{q}$.

At the entry surface to the crystal, the plane of the quadrature components is defined by the angle $\psi(0,\vec{q},\Omega)$. In this plane the average value of vector $a(0,\vec{\rho},t)$ is determined by the complex amplitude α of the local oscillator. The down-conversion waves at the entry surface to the crystal are in a vacuum state. Therefore the noise modulation of the vector $a(0,\vec{\rho},t)$ has equal mean square uncertainties of both quadrature components, i.e., neither phase nor amplitude modulation predominates.

The results of the squeezing transformation are as follows:

(1) The plane of slow quadrature components $a_{\mu\lambda}(l,\vec{q},\Omega)$ at the exit surface of the crystal is defined by the angle $\psi(l,\vec{q},\Omega)$. In this coordinate system the slow quadrature components $a_{1\lambda}(l,\vec{q},\Omega)$ increase by the factor $\exp[r(\vec{q},\Omega)]$, whereas the components $a_{2\lambda}(l,\vec{q},\Omega)$ de-

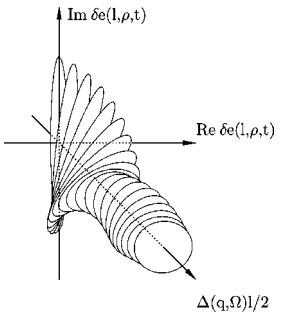

FIG. 8. Dependence on $\vec{q}$ and Ω of the squeezing ellipse at the exit from the parametric crystal for $\exp[2r_m]=10$. The dimensionless phase mismatch $\Delta(\vec{q},\Omega)l/2$ is taken in steps of 0.32; the squeezing ellipse for a pair of conjugate down-conversion waves $(\vec{q},\Omega)$ and $(-\vec{q},-\Omega)$ is shown as a function of dimensionless phase mismatch.

crease by the factor $\exp[-r(\vec{q},\Omega)]$. Therefore at the exit surface of the crystal the noise modulation of the vector $a(l,\vec{\rho},t)$ takes place on average inside the uncertainty ellipse, whose semimajor axis is oriented at the angle $\psi(l,\vec{q},\Omega)$. Because squeezing parameters $r(\vec{q},\Omega)$ and $\psi(z,\vec{q},\Omega)$ depend on frequency and spatial frequency, the uncertainty ellipses for every pair of down-conversion waves have different degrees of squeezing and different orientations. This effect is illustrated in Fig. 8.

(2) The local oscillator wave at the exit surface of the crystal has the complex amplitude β. The type of noise modulation of the resultant field in space-time is determined by the angle

$$\theta(\vec{q},\Omega)=\psi(l,\vec{q},\Omega)-\varphi_\beta. \tag{4.23}$$

Phase modulation predominates for $\theta(\vec{q},\Omega)\simeq\pm\pi/2$ and amplitude modulation for $\theta(\vec{q},\Omega)\simeq 0,\pi$.

(3) Because of the factor $\exp[i\kappa(\vec{q},\Omega)]$ in Eq. (4.20), there is a phase delay in the slow oscillations at frequencies $\vec{q},\Omega$ at the exit surface of the crystal,

$$\begin{aligned} &a_{\mu c}(l,\vec{q},\Omega)\cos(\Omega t-\vec{q}\cdot\vec{\rho})+a_{\mu s}(l,\vec{q},\Omega)\sin(\Omega t-\vec{q}\cdot\vec{\rho})\\ &\quad=\exp[\pm r(\vec{q},\Omega)]\{a_{\mu c}(0,\vec{q},\Omega)\cos(\Omega t-\vec{q}\cdot\vec{\rho}-\kappa(\vec{q},\Omega))\\ &\qquad+a_{\mu s}(0,\vec{q},\Omega)\sin(\Omega t-\vec{q}\cdot\vec{\rho}-\kappa(\vec{q},\Omega))\}. \end{aligned} \tag{4.24}$$

We want to point out that the squeezing transformation (4.2) is characterized by *four* real parameters $\psi(0,\vec{q},\Omega)$, $\psi(l,\vec{q},\Omega)$, $r(\vec{q},\Omega)$, and $\kappa(\vec{q},\Omega)$, given by Eqs. (4.21) and (4.22). For the vacuum input state of the wave pair $(\vec{q},\Omega)$ and $(-\vec{q},-\Omega)$ considered above, their output state depends on only two parameters, namely, $\psi(l,\vec{q},\Omega)$ and $r(\vec{q},\Omega)$. We shall see in the next subsection that this is also true for the noise spectrum of the photocurrent density. In the literature about squeezed states one usually finds only these two parameters (see, for example, Caves and Schumaker, 1985). However, the squeezing transformation (4.2) is applicable not only for the vacuum input state but for the arbitrary quantum state of the wave pair $(\vec{q},\Omega)$ and $(-\vec{q},-\Omega)$ at the input to the crystal. Dependence on $\psi(0,\vec{q},\Omega)$ in the observation should manifest itself when the quadrature components of the field at the input have different uncertainties. We would expect to see dependence on $\kappa(\vec{q},\Omega)$ if different Fourier amplitudes at the input become coupled due to parametric interaction. This would happen, for instance, in pulsed down conversion or in down conversion with a nonplanar pump wave.

C. Homodyne detection of multimode squeezed states and reduction of the photocurrent noise in space-time below the shot-noise level

As we have already said, in the literature devoted to squeezed states more attention has been paid to their behavior in time. We would like to mention, however, some early works attempting to bring spatial dependence into consideration. Kilin (1989) generalized the notion of the squeezing spectrum to include spatial dependence in connection with anomalous field correlations. He pointed out that the presence of such anomalous correlations can lead to the appearance of a narrow spectral component in the spectrum of a second-harmonic generation. This narrow component was registered experimentally by Piskarskas, Stabinis, and Yankauskas (1989).

Spatial correlations of twin photons emitted in spontaneous parametric down conversion have been studied both theoretically and experimentally (Malygin, Penin, and Sergienko, 1985; Rubin *et al.*, 1994; Shih and Sergienko, 1994; Strekalov *et al.*, 1995). However, these investigations were performed for direct correlation-type measurements and not for the homodyne detection scheme. We shall see below that homodyne detection drastically changes the noise spectrum of the photocurrent density and makes it possible to reduce shot noise in both space and time.

As has now become clear the phenomenon of nonlinear resonance diffraction is closely associated with squeezed states. Quantum correlations in space have been studied in relation to the placement of photodetectors for the separation of different elementary processes in an active volume. To our knowledge, only Le Berre-Rousseau, Ressayre, and Tallet (1979) have pointed out that there could be nonclassical correlations in the cross section of a light beam.

Squeezed states of light can be created in a medium whose dielectric and magnetic susceptibility changes in space-time. Spatial aspects of nonclassical fluctuations in such a process were studied by Bialynicka-Birula and Bialynicka-Birula (1987).

The question of the spatial behavior of squeezed states was addressed by Yuen and Shapiro (1978), and Akhmanov, Belinskii, and Chirkin (1988). Yuen and Shapiro considered the diffraction of squeezed light in free space. They assumed that squeezed light was emitted by a single-mode source with a finite aperture. In contrast, here we consider multimode squeezed states. We shall see below that this difference leads to qualitatively different physical conclusions about the possibilities of noise reduction in the photodetection of squeezed

light. Akhmanov, Belinskii, and Chirkin investigated the diffraction of squeezed light with emphasis on phase matching.

The role of phase matching in parametric interactions has been investigated from various points of view. The spectral, angular, and power characteristics of parametric down conversion (Klyshko, 1988a), photon correlations in the absence of the local oscillator (so-called *biphotons*), and squeezing efficiency (Akhmanov, Belinskii, and Chirkin, 1988) have been examined in the literature.

In this subsection we take a different approach to the role of phase matching in parametric interactions. We shall show that different types of phase matching in a nonlinear medium correspond to different types of observation of spatial squeezing with the photocurrent noise reduced below shot noise in space-time. We shall give the criteria for choosing the type of phase matching for a particular measurement. We shall also determine the typical spectral and spatio-temporal scales that govern the resolving power of sub-shot-noise measurements with multimode squeezed states.

Let us assume that the intensity of the local oscillator wave is high, so that we can neglect the contribution from the self-interference term in Eq. (4.13). At the end of this subsection we shall formulate this condition quantitatively. Discarding the integral term in the noise spectrum of the photocurrent density (4.13), we can rewrite it as follows:

$$(\delta i)^2_{\vec{q},\Omega}=\langle i\rangle[1-\eta+\eta(\cos^2\theta(\vec{q},\Omega)e^{2r(\vec{q},\Omega)} +\sin^2\theta(\vec{q},\Omega)e^{-2r(\vec{q},\Omega)})], \tag{4.25}$$

where $r(\vec{q},\Omega)$ and $\theta(\vec{q},\Omega)$ are the squeezing parameter and the orientation angle from Eqs. (4.22) and (4.23). The squeezing parameter is related to the spectral power of spontaneous parametric down conversion $\delta_{\vec{q},\Omega}$ from Eq. (4.10) as

$$\exp[r(\vec{q},\Omega)]=(1+\delta_{\vec{q},\Omega})^{1/2}+\delta^{1/2}_{\vec{q},\Omega}. \tag{4.26}$$

We observe from Eq. (4.25) that the spectral power density of fluctuations at frequencies $\vec{q},\Omega$ is determined by projecting the noise motion of the field inside the uncertainty ellipse onto the amplitude of the local oscillator. The phase modulation of the local oscillator at frequencies $\vec{q},\Omega$ predominates for $\theta(\vec{q},\Omega)\simeq\pm\pi/2$. In this case we have a reduction of shot noise in the photocurrent density spectrum (4.25) at these frequencies and spatial frequencies.

Maximum squeezing occurs at frequencies $\vec{q}_m,\Omega_m$, which belong to the phase-matching surface in the $(\vec{q},\Omega)$ space defined by the condition $\Delta(\vec{q}_m,\Omega_m)=0$. For these frequencies the squeezing parameter $r(\vec{q},\Omega)$ reaches its maximum value, $r(\vec{q}_m,\Omega_m)\equiv r_m=l/l_{\rm amp}$, where $l_{\rm amp}=|\sigma|^{-1}$ is the amplification length. Tuning the local oscillator so that $\theta(\vec{q}_m,\Omega_m)=\pm\pi/2$, we reduce shot noise to the highest extent,

$$(\delta i)^2_{\vec{q}_m,\Omega_m}=\langle i\rangle[1-\eta+\eta e^{-2r_m}]_{\eta\to1}\to\langle i\rangle e^{-2r_m}. \tag{4.27}$$

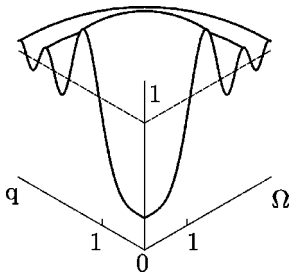

FIG. 9. Noise spectrum of the photocurrent density for degenerate phase matching, $\Delta(\vec{0},0)=0$ and $k''_\Omega<0$. The spectrum is normalized to the shot-noise level; the frequency Ω is given in units of $(|k''_\Omega|l/2)^{-1/2}$, the spatial frequency in $(2k_l/l)^{1/2}$; the squeezing parameter is equal to $\exp[r_m]=2$, $\eta=1$.

Let us determine the frequency and spatial frequency range of shot-noise reduction. In paraxial approximation for $\vec{q}$ and quadratic approximation for Ω we can write the phase mismatch function $\Delta(\vec{q},\Omega)$ as

$$\Delta(\vec{q},\Omega)\approx\Delta(\vec{0},0)+k''_\Omega\Omega^2-q^2/k_l, \tag{4.28}$$

where

$$\Delta(\vec{0},0)=2k_l-k_p \tag{4.29}$$

is the phase mismatch for zero frequency and spatial frequency, and $k''_\Omega=\partial^2k/\partial\Omega^2$ for $\Omega=0$. Using the explicit expressions for the functions $U(\vec{q},\Omega)$ and $V(\vec{q},\Omega)$, it is easy to verify that for large squeezing, $r_m\gg1$, parameters $r(\vec{q},\Omega)$ and $\theta(\vec{q},\Omega)$ near the phase-matching surface have the form

$$r(\vec{q},\Omega)\approx r_m,\quad \theta(\vec{q},\Omega)\approx\theta(\vec{q}_m,\Omega_m)+\Delta(\vec{q},\Omega)l_{\rm amp}/4. \tag{4.30}$$

This approximation is valid for $\vec{q}$ and Ω where $|\Delta(\vec{q},\Omega)l_{\rm amp}|\ll1$. From Eq. (4.30) we conclude that as we depart from the phase-matching surface, the squeezing ellipse starts to rotate, initially retaining its dimensions. Therefore a projection of the stretched "noisy" component of the ellipse appears on the vector of the local oscillator, which leads to increased noise of the photocurrent.

Let us consider the frequency and angle-degenerate phase matching, $\Delta(\vec{0},0)=0$. In this case the signal and idler photons, generated in parametric down conversion, have close frequencies and are mostly emitted in the forward direction. Using Eqs. (4.28) and (4.30), we can write approximately the spectrum of the photocurrent density in the vicinity of the phase-matching surface as

$$(\delta i)^2_{\vec{q},\Omega}\approx\langle i\rangle\left[1-\eta+\eta\left\{\left(\operatorname{sign}k''_\Omega\frac{\Omega^2}{\Omega_m^2}-\frac{q^2}{q_m^2}\right)^2+e^{-2r_m}\right\}\right], \tag{4.31}$$

where

$$\Omega_m=2(|k''_\Omega|l_{\rm amp}\exp r_m)^{-1/2},\qquad q_m=2(k_l^{-1}l_{\rm amp}\exp r_m)^{-1/2} \tag{4.32}$$

are the characteristic frequency and spatial frequency.

Figure 9 shows the typical noise spectrum (4.25), for

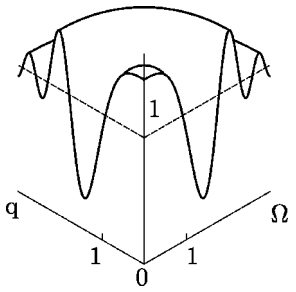

FIG. 10. Noise spectrum of the photocurrent density for the case of nondegenerate phase matching, $\Delta(\vec{0},0)>0$, $k''_\Omega < 0$. The spectrum is normalized to the shot-noise level; the frequency Ω is given in units of $(|k''_\Omega| l/2)^{-1/2}$, the spatial frequency in $(2k_l/l)^{1/2}$; the squeezing parameter is equal to $\exp[r_m]=2$, $\eta=1$.

the case of degenerate phase matching and $k''_\Omega<0$. From this figure and Eq. (4.25), we conclude that in the region of frequencies $\Omega<\Omega_m$ and spatial frequencies $q<q_m$ the noise of the photocurrent density is reduced below the shot-noise level. In space-time language this can be interpreted as follows. Suppose that the photocurrent is collected by a photodetector of area $\Delta S \geqslant S_m=(\pi/q_m)^2$ and during the time $\Delta T \geqslant T_m=\pi/\Omega_m$. Fluctuations in the number of collected photoelectrons are determined by the low-frequency harmonics of the photocurrent density noise such that $q \leqslant q_m$ and $\Omega \leqslant \Omega_m$. The high-frequency harmonics do not contribute because of averaging over the surface of the photodetector and the acquisition time. Since the low-frequency noise components of the photocurrent density are reduced below the shot-noise level, the fluctuation of the number of collected photoelectrons is less than the Poissonian value. Therefore the frequencies Ω_m and q_m determine the minimum time T_m and the minimum area of photodetector S_m, which are necessary for reducing fluctuations in the observed number of photoelectrons below the Poissonian limit. Note that the factor $(l_{\rm amp}/k_l)^{1/2}$ in the linear size of the photodetection area S_m is due to wave propagation inside the crystal. That is, the diffractive spreading of a light spot of this size is about the size itself.

Often it is necessary to perform low-noise measurements when (i) the useful information in the dynamical image is ''concentrated'' near nonzero carrier frequencies $\vec{q}$ and Ω, i.e., a space-time spectral analysis must be carried out near such frequencies and spatial frequencies; (ii) a spectral analysis of the image is required only for the spatial variable near the carrier spatial frequency $\vec{q}$, and there is no need for spectral analysis in the time variable; and (iii) a spectral analysis is required in the time domain but not in the spatial domain.

These kinds of measurements can be performed for the case of nondegenerate phase matching in a crystal, for example, when $\Delta(\vec{0},0)>0, k''_\Omega<0$. The typical example of the noise spectrum for this case is shown in Fig. 10. For the three types of measurement just mentioned, one has to choose a nonlinear crystal and observation geometry that will ensure that the phase-matching surface crosses the surface with the noise reduction region where (i) $\vec{q}\neq\vec{0},\Omega\neq 0$, (ii) $\vec{q}\neq\vec{0},\Omega=0$, and (iii) $\vec{q}=\vec{0},\Omega\neq 0$. Other varieties of phase matching can be described in a similar way.

For the observation of spatial squeezing, we have to make sure that the last contribution from the self-interference of the down-conversion waves is negligible compared with the shot noise and the interference term in Eq. (4.13). To conclude this subsection, let us estimate the intensity of a local oscillator wave that would guarantee such a possibility. Suppose that the local oscillator is turned off, $\beta\to 0$. The spectrum (4.13) then contains the shot noise and self-interference of parametric down-conversion. At low frequencies and spatial frequencies we can assess the noise spectrum as

$$(\delta i)^2_{\vec{0},0}=\langle i\rangle_s+2\eta^2\int\frac{d\vec{q}}{(2\pi)^2}\frac{d\Omega}{2\pi}\delta^2_{\vec{q},\Omega}, \tag{4.33}$$

where we have used the fact that $|U(\vec{q},\Omega)|^2-|V(\vec{q},\Omega)|^2=1$ and that $\delta_{\vec{q},\Omega}$ and $g(\vec{q},\Omega)$ are even functions of $\vec{q}$ and Ω. In the first approximation we replace one factor $\delta_{\vec{q},\Omega}$ by $\delta_{\vec{0},0}$ and use the definition (4.9) of $\langle i\rangle_s$. This gives

$$(\delta i)^2_{\vec{0},0}\approx\langle i\rangle_s(1+\eta+2\eta\delta_{\vec{0},0}). \tag{4.34}$$

The contribution $\langle i\rangle_s(1+\eta)$ is of a corpuscular nature and represents the noise in the detection of pairs of simultaneously emitted twin photons or *biphotons* (Klyshko, 1988a). If squeezing is effective, i.e., the degeneracy parameter δ_s is much larger than unity, the noise spectrum (4.34) is dominated by the wave noise proportional to $\delta_{\vec{0},0}$. The spectral power of self-interference and the shot-noise component of spontaneous parametric down conversion are negligible compared to the shot-noise term in the local oscillator and the interference of the local oscillator with the down-conversion waves if the following inequality is fulfilled:

$$\langle i\rangle_l(1-\eta+\eta e^{-2r_m})\gg\langle i\rangle_s(1+\eta+2\eta\delta_{\vec{0},0}). \tag{4.35}$$

D. Other schemes for generation of multimode squeezed states

1. Degenerate four-wave mixing

A degenerate four-wave mixing process as a possible source for squeezed light was first suggested by Yuen and Shapiro (1979). Since that work, many publications have appeared with more elaborate theories of squeezed-state generation via degenerate mixing (Bondurant *et al.*, 1984; Kumar and Shapiro, 1984; Reid and Walls, 1985a, 1985b; Ho, Kumar, and Shapiro, 1986) and nondegenerate mixing with (Yurke and Denker, 1984) and without (Levenson *et al.*, 1985; Yurke, 1985; Ho, Kumar, and Shapiro, 1991) the use of optical cavities. Several groups have also reported successful experimental observations of squeezing by means of intracavity backward four-wave mixing in an atomic beam (Slusher *et al.*, 1987), forward four-wave mixing in an optical fiber

(Shelby *et al.* 1986; Bergman and Haus, 1991; Rosenbluh and Shelby, 1991) and forward four-wave mixing in sodium vapor (Maeda, Kumar, and Shapiro, 1987; Ho, Kumar, and Shapiro, 1991). In all of these theoretical and experimental investigations, squeezing was predicted and observed in the temporal domain, i.e., for signal and noise of the measurement scheme evolving in time.

That multimode squeezed states of light can be generated in a four-wave mixing process was shown for the first time by Kumar and Kolobov (1994). A four-wave mixer can be configured either in a backward geometry, as proposed by Yuen and Shapiro (1979) or in a forward geometry, according to Kumar and Shapiro (1984). Here we present the results of Kumar and Kolobov. In particular, we calculate the spatial bandwidth of multimode squeezing obtainable with backward four-wave mixing (BFWM) and forward four-wave mixing (FFWM) and compare them with that obtainable with an optical parametric amplifier, considered in the previous subsection. Our analysis aims to show that the BFWM scheme can produce multimode squeezed light with a much larger spatial bandwidth than the other two schemes because it is not restricted by the phase-matching condition. This result makes the BFWM scheme very attractive for applications in optical imaging with reduced quantum noise (Kolobov and Kumar, 1993).

For simplicity, in what follows we restrict ourselves to the BFWM geometry. Our description can be readily adapted to FFWM geometry (Kumar and Shapiro, 1984). A schematic of the backward geometry for producing multimode squeezed light by means of four-wave mixing in a transparent $\chi^{(3)}$ nonlinear medium is shown in Fig. 11. The medium is supposed to be in the form of a plane slab of thickness l oriented perpendicular to the z direction. Two counterpropagating plane monochromatic pump waves E_1 and E_2 of angular frequency ω_0 and wave vectors $\vec{k}_1$ and $\vec{k}_2$, respectively, intersect the slab at a small angle to the z axis. A quasiplane and quasimonochromatic probe wave of carrier frequency ω_0 enters the medium from the left and propagates in the $+z$ direction. As a result of the nonlinear interaction between the two pump waves and the probe wave, a phase conjugate wave is generated in the medium that propagates in the opposite direction to the probe wave. We describe the probe and conjugate waves by two corresponding operator-valued slowly varying amplitudes $\epsilon_p(z,\vec{\rho},t)$ and $\epsilon_c(z,\vec{\rho},t)$, where $\vec{\rho}=(x,y)$ is the two-dimensional coordinate in the plane transverse to the z axis.

Let $k_\mu(\vec{q},\Omega)$, $\mu = p,c$, be the wave vectors of the probe and conjugate waves, respectively, with transverse components $\vec{q}$ and angular frequencies $\omega_0+\Omega$. As a result of the four-wave mixing interaction, the spatio-temporal Fourier amplitudes $\epsilon_\mu(z,\vec{q},\Omega)$,

$$\epsilon_\mu(z,\vec{q},\Omega)=\int d\vec{\rho}\int dt\,\epsilon_\mu(z,\vec{\rho},t)\exp[i(\Omega t-\vec{q}\cdot\vec{\rho})], \tag{4.36}$$

corresponding to $\vec{k}_p(\vec{q},\Omega)$ and $\vec{k}_c(-\vec{q},-\Omega)$, become coupled. In the undepleted pump approximation, the pump amplitudes can be considered classical and described by c-number quantities. As in the derivation performed in Sec. III.B for three-wave interactions, it can be shown that the operator-valued amplitudes of probe and conjugate waves evolve in the nonlinear medium according to (Fisher, 1983)

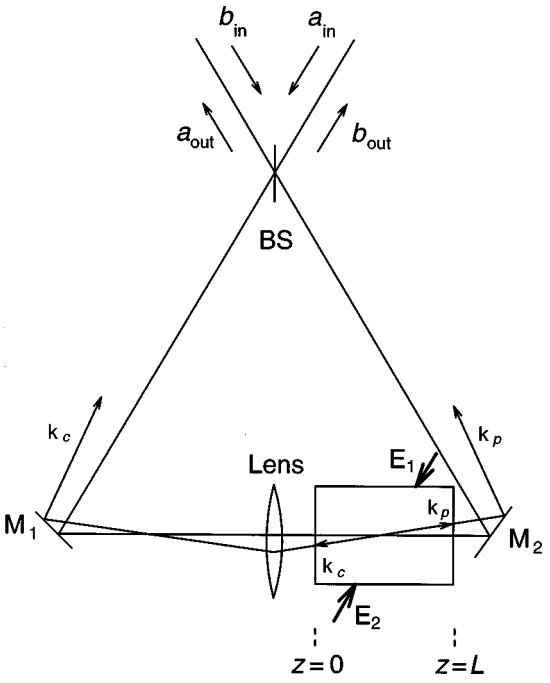

FIG. 11. Schematic of the backward four-wave mixing (BFWM) scheme for the generation of multimode squeezed light. Multimode squeezed light described by the operators $a_{\rm out}$ and $b_{\rm out}$ emerges from both ports of the beam splitter BS. E_1 and E_2 are the pump waves; M_1 and M_2 are plane mirrors; and the lens serves to match the paths of the probe and conjugate waves from the input to the output ports of BS.

$$\frac{d}{dz}\epsilon_p(z,\vec{q},\Omega)=-i\kappa\epsilon_c^\dagger(z,-\vec{q},-\Omega)\exp[-i\Delta(\vec{q},\Omega)z], \tag{4.37a}$$

$$\frac{d}{dz}\epsilon_c(z,\vec{q},\Omega)=i\kappa\epsilon_p^\dagger(z,-\vec{q},-\Omega)\exp[-i\Delta(\vec{q},\Omega)z]. \tag{4.37b}$$

Here κ is a coupling constant proportional to the product of the two pump wave amplitudes and to the nonlinear susceptibility $\chi^{(3)}$ of the medium; $\Delta(\vec{q},\Omega)$ is a phase-mismatch function for the four interacting waves given by [cf. Eq. (3.43)]

$$\Delta(\vec{q},\Omega)=k_p^z(\vec{q},\Omega)+k_c^z(-\vec{q},-\Omega)-k_1^z-k_2^z, \tag{4.38}$$

with $k_{p,c}^z(\vec{q},\Omega)$ being the projections of the probe and conjugate wave vectors onto the positive z direction, and $k_{1,2}^z$ the corresponding projections for the pump waves. As in the case of three-wave interaction, the four-wave interaction occurs effectively only for those probe and conjugate Fourier harmonics for which the spatial frequencies $\vec{q}$ and the frequencies Ω satisfy the phase-matching condition $|\Delta(\vec{q},\Omega)l|\leqslant 1$.

The solution of Eqs. (4.37a) and (4.37b) with the

boundary conditions $\epsilon_p(z=0,\vec{q},\Omega)=\epsilon_p(0,\vec{q},\Omega)$ and $\epsilon_c(z=l,\vec{q},\Omega)=\epsilon_c(l,\vec{q},\Omega)$ is well known in the literature (Fisher, 1983), and in our case can be written as

$$\epsilon_p(l,\vec{q},\Omega)\propto U(\vec{q},\Omega)\epsilon_p(0,\vec{q},\Omega)+V(\vec{q},\Omega)\epsilon_c^{\dagger}(l,-\vec{q},-\Omega), \tag{4.39a}$$

$$\epsilon_c(0,\vec{q},\Omega)\propto U(\vec{q},\Omega)\epsilon_c(l,\vec{q},\Omega)+V(\vec{q},\Omega)\epsilon_p^{\dagger}(0,-\vec{q},-\Omega). \tag{4.39b}$$

The coefficients $U(\vec{q},\Omega)$ and $V(\vec{q},\Omega)$ depend on the coupling constant κ and the phase-mismatch function $\Delta(\vec{q},\Omega)$ and can be found, for example, in Fisher (1983). We write "$\propto$" in Eqs. (4.39a) and (4.39b) instead of "=" because of the different phase factors for the probe and conjugate waves, which depend on $\vec{q}$ and Ω but nevertheless can be easily compensated for.

To obtain the input-output transformations for the operators corresponding to the waves entering and leaving the medium in the scheme of Fig. 11, we use the scattering properties of the outcoupling beam splitter. We arrive at the following input-output transformations:

$$a_{\rm out}(\vec{q},\Omega)\propto U(\vec{q},\Omega)a_{\rm in}(\vec{q},\Omega)+V(\vec{q},\Omega)a_{\rm in}^{\dagger}(-\vec{q},-\Omega), \tag{4.40a}$$

$$b_{\rm out}(\vec{q},\Omega)\propto U(\vec{q},\Omega)b_{\rm in}(\vec{q},\Omega)+V(q,\Omega)b_{\rm in}^{\dagger}(-\vec{q},-\Omega). \tag{4.40b}$$

Equations (4.40a) and (4.40b) look exactly like the squeezing transformation (4.2) for the case of three-wave interactions in a traveling-wave OPA. Therefore all the spatio-temporal features described in Sec. IV.A should be manifested by Eqs. (4.40a) and (4.40b). However, there is an important difference between the multimode squeezing obtained with an OPA and that obtained by means of the four-wave mixing process. To investigate this difference, let us consider explicitly the frequency and spatial frequency dependence of the phase-mismatch functions for BFWM and FFWM and compare them with that of the OPA. We have seen in Sec. IV.A that in the quadratic approximation for the spatial frequency $\vec{q}$ and the frequency Ω, the phase-mismatch function $\Delta(\vec{q},\Omega)$ for the OPA is [see Eq. (4.28)]

$$\Delta(\vec{q},\Omega)=k_{\Omega}''\Omega^2-q^2/k_l. \tag{4.41}$$

Here we have assumed degenerate matching, $\Delta(\vec{0},0)=0$; k_l is the wave number of the local oscillator and $k_{\Omega}''=\partial^2 k/\partial\Omega^2$ for $\Omega=0$. Using quadratic approximation and, for simplicity, considering the wave vectors for the probe and conjugate waves to be the same functions of $\vec{q}$ and Ω, $\vec{k}_p(\vec{q},\Omega)=\vec{k}_c(\vec{q},\Omega)=\vec{k}(\vec{q},\Omega)$, we can write

$$k_p^z(\vec{q},\Omega)=k_p+k_{\Omega}'\Omega+k_{\Omega}''\Omega^2/2-q^2/2k_l, \tag{4.42a}$$

$$k_c^z(-\vec{q},-\Omega)=k_c-k_{\Omega}'\Omega+k_{\Omega}''\Omega^2/2-q^2/2k_l, \tag{4.42b}$$

where $k_{\Omega}'=\partial k/\partial\Omega$ for $\Omega=0$. Therefore we arrive at

$$\Delta(\vec{q},\Omega)=k_{\Omega}''\Omega^2-q^2/k_l \tag{4.43}$$

for the FFWM process, and

$$\Delta(\vec{q},\Omega)=2k_{\Omega}'\Omega \tag{4.44}$$

for the BFWM process (the probe and conjugate waves propagate in opposite directions). Thus, in the quadratic approximation, the phase-mismatch function for BFWM does not depend on spatial frequency. Hence the spatial bandwidth of squeezing obtainable with BFWM is not limited by the phase-matching condition. It must therefore be much larger for BFWM than for an OPA and for FFWM.

Since our interest here is in spatial squeezing, let us explicitly compare the bandwidths for degenerate OPA, FFWM, and BFWM. From Eqs. (4.41), (4.43), and (4.44), we obtain $\Delta_{\rm OPA}=\Delta_{\rm FFWM}=-q^2/k_l$ and $\Delta_{\rm BFWM}=0$. For the case of an OPA (or FFWM), therefore, $\Delta_{\rm OPA}l=1$ gives a spatial squeezing bandwidth of $q=(k_l/l)^{1/2}$. However, for the BFWM case, $\Delta_{\rm BFWM}l=0$, which implies an infinite spatial bandwidth. (In reality, however, the spatial bandwidth will not be infinite. Our results are valid in the paraxial approximation, which will break down when $q\sim k_l$.) In a typical OPA experiment at $\lambda\simeq 1\ \mu$m (Aytür and Kumar, 1992), $l\simeq 5$ mm; therefore the spatial squeezing bandwidth is $\simeq(4\pi)^{1/2}\times 10^2\ {\rm cm}^{-1}$, corresponding to a spatial resolution of $\simeq 6$ line pairs/mm. In contrast, for the case of BFWM a spatial resolution of 400 line pairs/mm has been demonstrated (Levenson *et al.*, 1981).

We conclude with a few words about the frequency dependence of the phase-mismatch function for BFWM in Eq. (4.44). It is well known (Fisher, 1983) that this frequency dependence can be used to filter the probe signal. The bandwidth of such a filter rapidly decreases with increasing $|\kappa|l$, which determines the gain of the four-wave mixer. Therefore one can expect that the frequency bandwidth will decrease as the $|\kappa|l$ parameter grows. Also, in the multimode theory of four-wave mixing presented above, we assumed that the nonlinear medium is ideal so that its response could be described classically. When the realistic microscopic nature of the medium is taken into account, the spectrum of temporal squeezing is known[5] to be modified due to various factors such as propagation loss, spontaneous emission, self-focusing, etc. Therefore we expect that the spectrum of spatial squeezing will also be modified when the quantum nature of the medium is taken into account.

2. Subthreshold optical parametric oscillator

In previous subsections we have been concerned with traveling-wave generation schemes of multimode squeezed states. Traveling-wave geometry is the most natural one because it automatically produces a broad spectrum of spatial frequencies. However, the picture would be incomplete without mentioning the cavity-based configurations for multimode squeezed-state generation.

[5]See, for example, Yurke and Denker, 1984; Levenson *et al.*, 1985; Reid and Walls, 1985a, 1985b, 1986; Yurke, 1985; Holm, Sargent, and Capron, 1986; Ho, Kumar, and Shapiro, 1986, 1987, 1991.

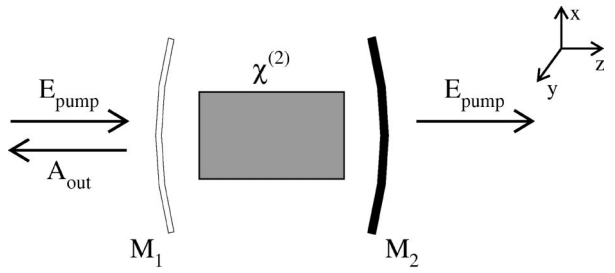

FIG. 12. Schematic of an optical parametric oscillator. A cavity with spherical mirrors containing a $\chi^{(2)}$ nonlinear medium is illuminated by a pump wave $E_{\rm pump}$ with frequency ω_p; cavity mirrors are assumed to be completely transparent for this wave; squeezed light is generated at the frequency $\omega_s=\omega_p/2$ and is described by a signal wave $A_{\rm out}$.

To our knowledge, the first cavity-based scheme was proposed by Belinskii and Rosanov (1992), who considered a wide-aperture nonlinear interferometer with a $\chi^{(3)}$ nonlinear medium. It is well known that such a device can exhibit bistable behavior. In recent years it has also been learned that in the vicinity of the turning points on the bistability curve one can achieve a strong squeezing effect. Belinskii and Rosanov generalized the theory of optical bistability and quantum fluctuations in such an interferometer to take spatial degrees of freedom into consideration.

Another scheme for the generation of multimode squeezed states in a cavity-based configuration is a subthreshold optical parametric oscillator (OPO). This scheme was considered by Gatti and Lugiato (Lugiato and Gatti, 1993; Gatti and Lugiato, 1995) for a cavity with plane mirrors and by Lugiato and Marzoli (1995) for a cavity with spherical mirrors. Here we give an outline of the last model and the results for the space-time correlation function and fluctuation spectra. More details can be found in the references cited.

A schematic of the OPO for the generation of multimode squeezed states is shown in Fig. 12. A medium with $\chi^{(2)}$ nonlinearity is contained in a single-ended cavity with spherical mirrors. The driving pump wave with frequency $\omega_p=2\omega_s$ is injected into the cavity. Due to nonlinear interaction in the $\chi^{(2)}$ medium, pump photons are converted into pairs of signal photons with frequency ω_s. To simplify the analysis the following assumptions are made: (i) the Rayleigh range of the cavity is much larger than its length, and (ii) the cavity mirrors are completely transparent for the pump wave, which is assumed to be a plane wave. Moreover, both the mean-field limit and the paraxial and slowly varying approximation for the fields taking part in the nonlinear interaction are assumed to be valid. The slowly varying amplitude approximation guarantees that the pump and the signal waves are uniform along the sample in the longitudinal direction z.

As mentioned in Sec. III.C, for a cavity-based geometry a more natural language for the description of multimode squeezing is that of discrete eigenmodes of the resonator. In the case of the cavity with spherical mirrors, such a discrete eigenset is given by the Gauss-Laguerre modes

$$f_{pli}(r,\phi)=\tilde{f}_{pl}(r)\times\begin{cases}\cos(l\phi), & \text{for } i=1,\\ \sin(l\phi), & \text{for } i=2,\end{cases} \tag{4.45a}$$

with

$$\tilde{f}_{pl}(r)=\frac{2}{(2^{\delta_{l,0}}\pi w^2)^{1/2}}\left[\frac{p!}{(p+l)!}\right]^{1/2}\times\left(2\frac{r^2}{w^2}\right)^{l/2}L_p^l\left(2\frac{r^2}{w^2}\right)e^{-r^2/w^2}, \tag{4.45b}$$

where w is the waist of the beam and $p,l=0,1,2,\ldots$, are the radial and angular indices, respectively; $r=(x^2+y^2)^{1/2}$ is the radial and ϕ is the angular variable. The functions L_p^l are the Laguerre polynomials (Abramowitz and Stegun, 1965). The functions $f_{pli}(r,\phi)$ obey the following condition of orthonormality:

$$\int_0^{2\pi}d\phi\int_0^{\infty}r\,dr\,f_{pli}(r,\phi)f_{p'l'i'}(r,\phi)=\delta_{pp'}\delta_{ll'}\delta_{ii'}. \tag{4.46}$$

The eigenfrequencies of these modes are given by

$$\omega_{pl}=\omega_{00}+(2p+l)\zeta, \tag{4.47}$$

where the parameter ζ depends on the mirrors' curvature and the distance between them (Yariv, 1989). One can see from Eq. (4.47) that modes gather in degenerate groups characterized by an integer $q=2p+l$. The modal expansion of the field operator $A(r,\phi)$ inside the cavity reads

$$A(r,\phi)=\sum_{i=1,2}\sum_{p,l}f_{pli}(r,\phi)a_{pli}, \tag{4.48}$$

with the corresponding expression for its Hermitian conjugate; a_{pli} and $a_{pli}^{\dagger}$ are the photon annihilation and creation operators obeying the standard commutation relations: $[a_{pli},a_{p'l'i'}^{\dagger}]=\delta_{pp'}\delta_{ll'}\delta_{ii'}$.

The quantum model of the subthreshold OPO considered by Lugiato and Marzoli is formulated in terms of the master equation for the density matrix ρ of the cavity eigenmodes f_{lpi}. The pump wave is treated as a classical c-number, i.e., its depletion and the quantum fluctuations are neglected. The master equation in the interaction picture reads

$$\dot{\rho}=\frac{1}{i\hbar}[H_{\rm int},\rho]+\sum_{i=1,2}\sum_{p,l}\Lambda_{pli}\rho, \tag{4.49}$$

where the generator $\Lambda_{pli}\rho$,

$$\Lambda_{pli}\rho=\gamma(2a_{pli}\rho a_{pli}^{\dagger}-a_{pli}^{\dagger}a_{pli}\rho-\rho a_{pli}^{\dagger}a_{pli}), \tag{4.50}$$

describes the damping of the mode *pli* due to cavity decay through the outcoupling mirror with the rate γ. The interaction Hamiltonian $H_{\rm int}$ is given by (Lugiato and Marzoli, 1995)

$$H_{\rm int}=i\hbar\frac{\gamma}{2}A_p\int_0^{2\pi}d\phi\int_0^{\infty}r\,dr[(A^{\dagger}(r,\phi))^2-A^2(r,\phi)], \tag{4.51}$$

where A_p is the coupling constant proportional to the nonlinear susceptibility $\chi^{(2)}$ of the medium and the amplitude of the pump wave. Inserting the modal expansion (4.48) into Eq. (4.51) and using the orthonormality relation (4.46), we can rewrite this interaction Hamiltonian as

$$H_{\rm int}=i\hbar\frac{\gamma}{2}A_p\sum_{i=1,2}\sum_{p,l}[(a_{pli}^{\dagger})^2-a_{pli}^2]. \tag{4.52}$$

From this expression we see the advantage of the eigenmodes method. That is, the master equation (4.49) with the interaction Hamiltonian (4.52) describes the evolution of an infinite set of independent, single-mode, degenerate parametric oscillators. Instead of solving the master equation (4.49), we can write a set of independent Langevin equations (Walls and Milburn, 1994) for the annihilation and creation operators a_{pli} and $a_{pli}^{\dagger}$ inside the cavity,

$$\dot{a}_{pli}(t)=-\gamma[(1+i\Delta_{pl})a_{pli}(t)-A_p a_{pli}^{\dagger}(t)]+\sqrt{2\gamma}c_{pli}(t), \tag{4.53}$$

where

$$\Delta_{pl}=\frac{\omega_{pl}-\omega_s}{\gamma}, \tag{4.54}$$

with ω_{pl} given by Eq. (4.47). The operators $c_{pli}(t)$ and $c_{pli}^{\dagger}(t)$ correspond to the operator-valued Langevin forces and describe the vacuum fluctuations entering the cavity through the outcoupling mirror. These operators obey the commutation relations

$$[c_{pli}(t),c_{p'l'i'}^{\dagger}(t')]=\delta_{pp'}\delta_{ll'}\delta_{ii'}\delta(t-t'). \tag{4.55}$$

Equations (4.53) are easy to solve by performing the Fourier transform,

$$a_{pli}(\Omega)=\int_{-\infty}^{\infty}dt\,e^{i\Omega t}a_{pli}(t). \tag{4.56}$$

Using the input-output relation (Collet and Gardiner, 1984) for the field operators $b_{pli}(t)$ in the wave outgoing from the cavity, $c_{pli}(t)$ of the vacuum fluctuation entering it, and $a_{pli}(t)$ inside the cavity,

$$b_{pli}(t)=\sqrt{2\gamma}a_{pli}(t)-c_{pli}(t), \tag{4.57}$$

we obtain the following squeezing transformation between the Fourier amplitudes of the incoming and outgoing waves:

$$b_{pli}(\Omega)=U_{pl}(\Omega)c_{pli}(\Omega)+V_{pl}(\Omega)c_{pli}^{\dagger}(-\Omega), \tag{4.58}$$

which constitutes a discrete equivalent of the multimode squeezing transformation (4.2). The functions $U_{pl}(\Omega)$ and $V_{pl}(\Omega)$ read as follows:

$$U_{pl}(\Omega)=\frac{[1-i\Delta_{pl}(-\Omega)][1-i\Delta_{pl}(\Omega)]+A_p^2}{[1+i\Delta_{pl}(\Omega)][1-i\Delta_{pl}(-\Omega)]-A_p^2},$$

$$V_{pl}(\Omega)=\frac{2A_p}{[1+i\Delta_{pl}(\Omega)][1-i\Delta_{pl}(-\Omega)]-A_p^2}, \tag{4.59}$$

where $\Delta_{pl}(\pm\Omega)=\Delta_{pl}\mp\Omega/\gamma$. Since Eq. (4.58) is exactly equivalent to Eq. (4.2), the calculation of the photocurrent noise spectrum proceeds similarly to the case of the continuous Fourier transform considered in Sec. IV [cf. Eqs. (4.13) and (4.25)]. We omit repetition of this procedure and go directly to the results (Lugiato and Marzoli, 1995). The space-time correlation function of the photocurrent density in homodyne detection of multimode squeezed light at the output of the cavity with spherical mirrors can be written as [cf. Eq. (3.55)]

$$\left\langle\tfrac{1}{2}\{\delta i(\vec{\rho},t),\delta i(\vec{\rho}',t')\}_+\right\rangle$$

$$=\sum_{p,l}\tilde{f}_{pl}(r)\tilde{f}_{pl}(r')\cos[l(\phi-\phi')]$$

$$\times\frac{1}{2\pi}\int_{-\infty}^{\infty}d\Omega\,e^{-i\Omega(t-t')}(\delta i)_{pl,\Omega}^2. \tag{4.60}$$

The dependence of the space-time correlation function on the phase difference $\phi-\phi'$ is a consequence of rotational symmetry $\phi\to\phi+\theta$ of the cavity with spherical mirrors. The fluctuation spectrum of the photocurrent density $(\delta i)_{pl,\Omega}^2$ is that for a single-mode degenerate OPO, which was calculated previously by several authors (Collet and Walls, 1985; Savage and Walls, 1987):

$$(\delta i)_{pl,\Omega}^2=\langle i\rangle\Bigg[1+\frac{4A_p}{(1+\Delta_{pl}^2-A_p^2-\tilde{\Omega}^2)^2+4\tilde{\Omega}^2}\times(2A_p+{\rm Re}\{e^{-2i\varphi_\beta}(1-\Delta_{pl}^2+A_p^2+\tilde{\Omega}^2-2i\Delta_{pl})\})\Bigg], \tag{4.61}$$

where φ_β is the phase of the local oscillator and $\tilde{\Omega}=\Omega/\gamma$ is the dimensionless frequency. We assume that $\eta=1$.

As an illustration of this result let us consider this spectrum at zero frequency, $\Omega=0$, which would correspond to the pure spatial frequency fluctuation spectrum in the continuous Fourier transform case. For an optimal choice of the local oscillator phase at $\Delta_{pl}=0$, $\varphi_\beta=\pm\pi/2$, the spectrum (4.61) for $\Omega=0$ simplifies to

$$(\delta i)_{pl,0}^2=\langle i\rangle\left[1+\frac{4A_p}{(1+\Delta_{pl}^2-A_p^2)^2}(\Delta_{pl}^2-(1-A_p)^2)\right]. \tag{4.62}$$

This spectrum is shown in Fig. 13 as a function of the detuning Δ_{pl} (which one can view as a normalized spatial frequency in this case) for two different values of the coupling constant A_p: (a) $A_p=0.5$ and (b): $A_p=0.9$. One sees from Fig. 13 that squeezing persists for small values of detunings Δ_{pl}, i.e., small "spatial frequencies." This spatial bandwidth of squeezing shrinks when the OPO approaches threshold, $A_p\to1$. Moreover, the maximum of the curve, corresponding to the excess noise of photodetection, increases and moves closer to $\Delta_{pl}=0$, which should make squeezing hard to observe when the OPO operates too close to threshold.

In concluding this section we should like to add that several papers (Gatti and Lugiato, 1995; Lugiato and

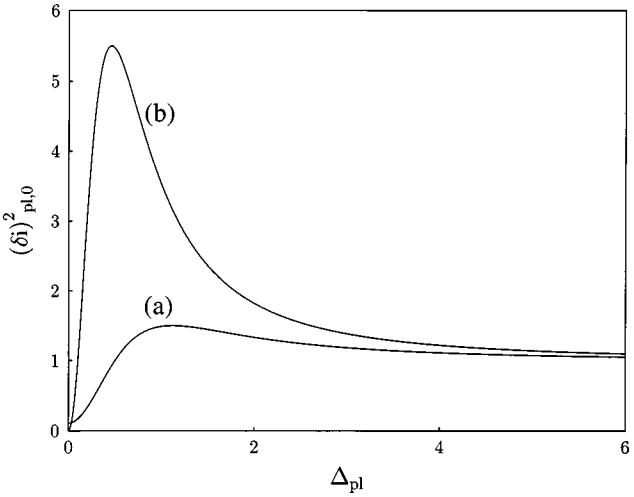

FIG. 13. Zero-frequency photocurrent noise spectrum $(\delta i)^2_{pl,0}$ vs the detuning Δ_{pl} for different values of the coupling constant A_p: (a) $A_p=0.5$; (b) $A_p=0.9$; the spectrum is normalized to the shot-noise level.

Marzoli, 1995; Lugiato, Gatti, and Wiedemann, 1997; Lugiato *et al.*, 1997) discuss spatial correlation functions extensively, as well as the concept of quantum image; the reader is referred to the literature for these issues.

V. FREE PROPAGATION AND DIFFRACTION OF MULTIMODE SQUEEZED LIGHT

A. Effects of free propagation and a thin lens on multimode squeezed light

In this subsection we shall extend the above conclusion about the possibilities of low-noise measurements in space-time with multimode squeezed light by taking into account light propagation in free space and the simplest optical system, such as a thin lens. We shall see that propagation in free space in general deteriorates the resolving power of low-noise measurements with squeezed light. However, we shall also show that a lens allows us to compensate for this deterioration and even further improve the resolving power by a proper choice of geometry. We shall establish the following important property of lens systems and systems similar to them: they can compensate for the spatial frequency and frequency dependence of multimode squeezed light, which appears due to the diffraction and dispersion of light in the crystal during the generation process and in free space on the way to the photodetection plane.

We shall assume that the plane of photodetection lies at a distance L from the exit plane of the nonlinear crystal and is parallel to it. In the case of wave propagation in free space, the slowly varying operators $a(l,\vec{q},\Omega)$ at the exit plane of the crystal and $a(l+L,\vec{q},\Omega)$ at the photodetection plane are related as [cf. Eq. (3.38)]

$$a(l+L,\vec{q},\Omega)=\exp[i(k_z^{(0)}(\vec{q},\Omega)-k_0)L]a(l,\vec{q},\Omega). \quad (5.1)$$

Here we have denoted by $k_z^{(0)}(\vec{q},\Omega)$ the z component of the wave vector in free space, to distinguish it from $k_z(\vec{q},\Omega)$ in the crystal. We can relate the field operator at the plane of photodetection with that at the entry to a nonlinear crystal by the squeezing transformation, similar to Eq. (4.2),

$$a(l+L,\vec{q},\Omega)=\tilde{U}(\vec{q},\Omega)a(0,\vec{q},\Omega)+\tilde{V}(\vec{q},\Omega)a^{\dagger}(0,-\vec{q},-\Omega), \quad (5.2)$$

where

$$\tilde{U}(\vec{q},\Omega)=\exp[i(k_z^{(0)}(\vec{q},\Omega)-k_0)L]U(\vec{q},\Omega), \quad (5.3)$$

and likewise for coefficients $\tilde{V}(\vec{q},\Omega)$ and $V(\vec{q},\Omega)$. Let us introduce the new squeezing parameter $\tilde{r}(\vec{q},\Omega)$ and the orientation angle $\tilde{\theta}(\vec{q},\Omega)$ analogous to $r(\vec{q},\Omega)$ and $\theta(\vec{q},\Omega)$ given by Eqs. (4.22) and (4.23). It can readily be seen from Eqs. (5.2) and (5.3) that in the case of free propagation from $z=l$ to $z=l+L$ the degree of squeezing remains unchanged, $\tilde{r}(\vec{q},\Omega)=r(\vec{q},\Omega)$, and the new orientation angle $\tilde{\theta}(\vec{q},\Omega)$ becomes

$$\tilde{\theta}(\vec{q},\Omega)=\theta(\vec{q},\Omega)+[k_z^{(0)}(\vec{q},\Omega)+k_z^{(0)}(-\vec{q},-\Omega)-2k_0]\times L/2\approx\theta(\vec{q},\Omega)-\frac{q^2L}{2k_0}, \quad (5.4)$$

where we have assumed a paraxial and quasimonochromatic approximation. From Eq. (5.4) we observe that free propagation enhances the dependence of the angle $\tilde{\theta}(\vec{q},\Omega)$ on spatial frequency $\vec{q}$. In a figure analogous to Fig. 8 this would appear as rapid rotation of the squeezing ellipse with increasing values of q. Using the language of noise modulation, we can say that the conjugate down-conversion waves traveling at the angle q/k_0 and the local oscillator wave that they modulate have different phase shifts, so that the phase and amplitude modulation of the resultant field rapidly change each other in space. These oscillations appear in the noise spectrum of the photocurrent density as shown in Fig. 14 for its spatial frequency component, i.e., $\Omega=0$.

Let us estimate the area of low-noise detection in the case in which a photodetection plane is located at a distance L from the output plane of the nonlinear crystal. Near the phase-matching surface we can use approximation (4.30) for the orientation angle $\theta(\vec{q},\Omega)$, which gives for $\tilde{\theta}(\vec{q},\Omega)$

$$\tilde{\theta}(\vec{q},\Omega)\approx\theta(\vec{q}_m,\Omega_m)+[\Delta(\vec{0},0)+k''_{\Omega}\Omega^2]\times l_{\mathrm{amp}}/4-q^2\left(\frac{l_{\mathrm{amp}}}{4k_l}+\frac{L}{2k_0}\right), \quad (5.5)$$

where the amplification length l_{amp} has been combined with the free-propagation length L. In Sec. IV.C we estimated the minimum area S_m of low-noise detection [see Eq. (4.32) and the paragraph after it]. To obtain an analogous estimate of such an area at a distance L from the crystal, we can use Eq. (4.32) with l_{amp}/k_l replaced by $l_{\mathrm{amp}}/k_l+2L/k_0$. For the case $L\gg l_{\mathrm{amp}}$ this low-noise area is entirely determined by diffraction over the free-propagation length L. It should be noted that we assume the size of the spot illuminated by the pump wave

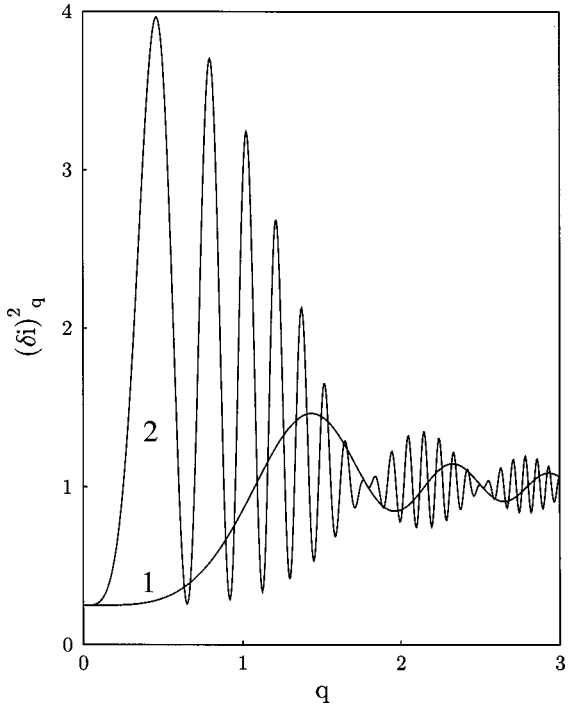

FIG. 14. Spatial-frequency noise spectrum of the photocurrent density observed at the exit from the crystal (curve 1) and at distance $L=7l_{\rm amp}k_0/(2k_l)$ from it (curve 2). The phase matching is degenerate in frequency and angle, $\theta(\vec{0},0)=\pm\pi/2$, $\exp[r_m]=2$, $\eta=1$; the spectrum is normalized to the shot noise, and spatial frequency q is in units of $(2k_l/l)^{1/2}$.

at the input surface of the crystal to be large and confine ourselves to the near-field diffraction zone of this spot.

Thus we conclude that free propagation deteriorates the resolving power of a low-noise observation. However, this deterioration is entirely due to the phase shifts experienced by light waves with different transverse components of the wave vector during propagation in free space, and is therefore reversible. Furthermore, as we shall now show, the phase shifts produced during wave propagation inside the nonlinear crystal can be compensated for, as well, and this allows us to achieve the ultimate value of the resolving power.

Let as assume that a lens of focal length f is inserted into the light beam with its center at the axis of the beam. The thin lens "multiplies" the complex amplitude of the monochromatic wave by the factor $\exp[-ik_0\rho^2/(2f)]$, i.e., it introduces a phase shift. We do not consider here the effects of the finite aperture of the lens. If the lens is inserted at the plane $z+2f$, the transformation of the field operator $a(z,\vec{\rho},t)$ from plane z to plane $z+4f$ reads as follows:

$$a(z+4f,\vec{\rho},t)=\exp[-ik_0\rho^2/(2f)]\times a\left(z,-\vec{\rho},t-\left[4f+\frac{\rho^2}{2f}\right]\Big/c\right). \quad (5.6)$$

From Eq. (5.6) it is easy to see that the noise spectrum $(\delta i)^2_{\vec{q},\Omega}$ observed in the plane located at $z+4f$ is identical to that at z. Indeed, this conclusion follows from the following considerations: (i) the phase factor $\exp[-ik_0\rho^2/(2f)]$ has no effect on the light intensity and cancels out in the photodetection formulas given by Eqs. (3.3) and (3.4); (ii) the time delay is constant for $f\gg\rho$ in the region of photodetection and therefore has no effect on the spectrum of the stationary photocurrent density $i(\vec{\rho},t)$; and (iii) inversion of the transverse coordinate $\vec{\rho}\to-\vec{\rho}$ in Eq. (5.6) has no effect on the photocurrent density noise spectrum, since the latter is an even function of $\vec{\rho}$.

If the lens and the plane of photodetection are arranged as described above and we choose $z=l$, i.e., the exit plane of the crystal, the noise spectrum observed in the plane $l+4f$ is identical with the spectrum recorded at the exit surface from the crystal. This result is not surprising, because such a geometry corresponds to geometrical imaging with unit magnification of the low-noise detection area from the exit plane of the crystal into the photodetection plane located at $z+4f$. It can be shown that such imaging can be performed with arbitrary magnification as well.

Less obvious, but more advantageous is a geometry that images onto the detection plane some plane inside the crystal. Let us consider $z=l+L$ and keep L arbitrary for the moment. The total transformation of the field from the exit plane $z=l$ to the observation plane $z=l+L+4f$ now consists of free propagation over the distance L and transformation (5.6) performed by the lens. The latter transformation does not change the spectrum. Therefore the spectrum at $z=l+L+4f$ will be identical to that at $z=l+L$, where L can be both positive and negative. In the case $L\leqslant 0$, transformation (5.1) is valid as well and describes free propagation in a backward direction. From Eq. (5.5) we observe that if we choose L as

$$L=-l_{\rm amp}\frac{k_0}{2k_l}, \quad (5.7)$$

the orientation angle $\tilde{\theta}(\vec{q},\Omega)$ in the vicinity of the matching surface becomes independent of spatial frequency. Thus geometrical imaging of the plane inside the crystal at the distance L given by Eq. (5.7) onto the photodetection plane broadens the range of spatial frequencies at which one has a noise reduction below the shot-noise level. In a figure analogous to Fig. 8, the squeezing ellipses would have appeared with equal orientation practically over the whole range of spatial frequencies where the parametric interaction is effective.

Figure 15 shows the spatial frequency spectrum for observation at the exit from the crystal and in the optimal case with the lens correcting for the dispersion of the squeezing ellipses as described above. We can see that in the latter case shot-noise reduction takes place over a much greater region of spatial frequencies. This improves the resolving power of a low-noise observation to its ultimate value.

In the literature it has been noticed that the squeezing efficiency becomes greater when the light is focused on a nonlinear medium (Akhmanov, Belinskii, and Chirkin, 1988). The consequences of energy concentration

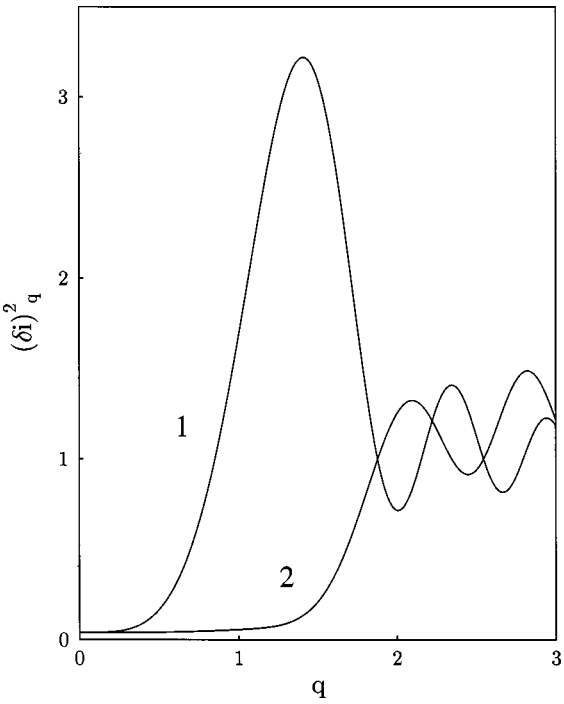

FIG. 15. The effect of a thin lens on the spatial-frequency noise spectrum of the photocurrent density: curve 1, observation at the exit from the crystal; curve 2, observation with compensation of the dispersion of the squeezing angle by the lens; $\exp[r_m]=5$, $\eta=1$; the spectrum is normalized to the shot noise, and spatial frequency q is in units of $(2k_l/l)^{1/2}$.

(Sokolov, 1977) and separation of the waves in space by focusing (Klyshko, 1988c) have been discussed as well. In our case, focusing means controlling the phase modulation of the resultant field independent of the nonlinear medium; it is therefore irrelevant to energy concentration or spatial separation of twin photons.

To improve the frequency behavior of the noise spectrum, we can introduce additional frequency-dependent phase shifts into the down-conversion waves with nonzero Ω. This can be done, for example, by inserting into the light beam a slab of a dispersive medium with wave number $k^{(1)}(\Omega)$. If the length of the slab is $L^{(1)}$ and we choose the sign of $k_\Omega^{(1)''}$ properly, then it is easy to see that, for

$$L^{(1)}=-l_{\rm amp}\frac{k''_\Omega}{2k_\Omega^{(1)''}}, \tag{5.8}$$

the frequency dependence of $\tilde{\theta}(\vec{q},\Omega)$ in Eq. (5.5) in the vicinity of the phase-matching surface also disappears.

Thus in this subsection we have shown that multimode squeezed light retains and sometimes even improves its capacity for low-noise measurement in optical systems such as lenses and in dispersive media.

B. Assessment of physical possibilities for low-noise measurements and information transmission with multimode squeezed light

In this subsection we shall make some simple assessments of physical possibilities for employing multimode squeezed light in low-noise optical measurements and information transmission. More precisely, we shall give some estimates for the spectral, spatio-temporal, and power characteristics of measurements with multimode squeezed light.

From the discussion in the previous subsection we see that with the help of a lens and an additional slab of dispersive medium we can eliminate the $\vec{q}$ and Ω dependence in the orientation angle $\theta(\vec{q},\Omega)$ of the squeezing ellipse over the whole bandwidth of spontaneous parametric down conversion. Then the photodetection noise is effectively suppressed below the shot-noise limit over the entire region of frequencies $\Omega\leqslant\Omega_c/2$ and spatial frequencies $q\leqslant q_c/2$, where Ω_c and q_c are the widths of frequency and spatial frequency spectra of spontaneous parametric down conversion [see Eqs. (4.11), (4.12), and the paragraph before them]. Let us estimate the dispersion $\langle\Delta N^2\rangle$ of the photoelectron number collected by a pixel with the area S_d during the time interval T_d according to Eqs. (3.12) and (3.13). Expressing the space-time correlation function of photocurrent density via its noise spectrum $(\delta i)^2_{\vec{q},\Omega}$ we arrive at

$$\langle\Delta N^2\rangle=\langle N\rangle\int_{-\infty}^{\infty}dq_x\int_{-\infty}^{\infty}dq_y\int_{-\infty}^{\infty}d\Omega\,\tilde{\delta}_{1/T_d}(\Omega)\times\tilde{\delta}_{1/L_d}(q_x)\tilde{\delta}_{1/L_d}(q_y)\frac{(\delta i)^2_{\vec{q},\Omega}}{\langle i\rangle}, \tag{5.9}$$

where the δ-like function $\tilde{\delta}_{1/a}(x)$ is defined as

$$\tilde{\delta}_{1/a}(x)=\frac{a}{2\pi}\frac{\sin^2(ax/2)}{(ax/2)^2}. \tag{5.10}$$

We have assumed that a pixel has the shape of a square with the side of length L_d. From Eqs. (5.9) and (5.10) we can conclude that, provided $L_d\geqslant 2\pi/q_c$ and $T_d\geqslant 2\pi/\Omega_c$, the dispersion of the photoelectron number is determined by the noise spectral density at low frequencies $\Omega\leqslant\Omega_c$ and spatial frequencies $q_x,q_y\leqslant q_c$, i.e., is equal to

$$\langle\Delta N^2\rangle=\langle N\rangle(1-\eta+\eta e^{-2r_m}). \tag{5.11}$$

For high quantum efficiency, $\eta\simeq 1$, and effective squeezing, $e^{-r_m}\ll 1$, the statistics of photoelectrons are sub-Poissonian. The minimum area of a pixel and the minimum collection time are determined by the coherence area S_c and coherence time T_c of spontaneous parametric down conversion.

The average number of down-conversion photons necessary for a single low-noise measurement is therefore given by $\langle i\rangle_s S_c T_c$, i.e., for $\eta=1$ is equal to the degeneracy parameter of spontaneous parametric down conversion δ_s defined by Eq. (4.12). The average number of local-oscillator photons is equal to $\langle i\rangle_l S_c T_c$.

If the pump and the local oscillator waves illuminate a spot of area $S\gg S_c$ at the entry to the nonlinear crystal, the total number of low-noise measurements that can be performed with multimode squeezed light in a time interval $T\gg T_c$ is given by $ST/S_cT_c\gg 1$. If one employs the multimode squeezed light for transmission of informa-

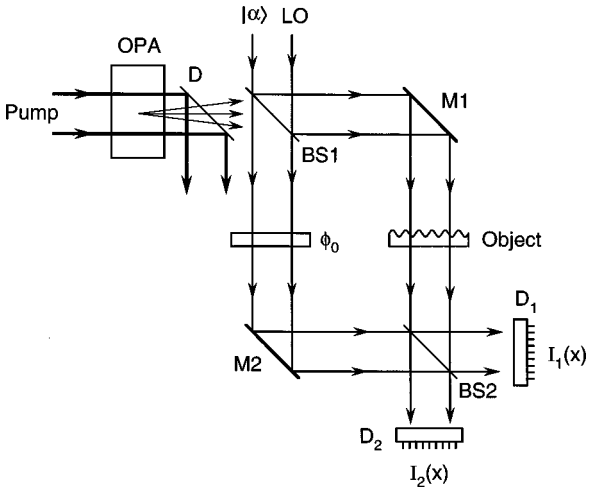

FIG. 16. Schematic of the sub-shot-noise microscopy with multimode squeezed light. This scheme allows us to detect faint phase objects with a sensitivity better than the shot-noise limit.

tion this is equivalent to the transmission of $T/T_c \gg 1$ images, each image containing $S/S_c \gg 1$ elements. In other words, one can say that the source of multimode squeezed light under investigation contains $S/S_c \gg 1$ spatial modes of radiation. This is the most important distinction of multimode squeezed light from single-mode squeezed light, where the ratio S/S_c is of the order of unity.

We should also note that the scheme of homodyne detection of multimode squeezed light is very closely related to holographic measurements. Indeed, one may consider photodetection of the interference pattern created by the local oscillator wave and the waves of parametric down conversion as the writing of a hologram. The local oscillator wave in this case plays the role of the reference wave and the down-conversion waves play the role of the subject waves. The result of writing such a hologram is paradoxical from the point of view of classical electrodynamics. The modulation of "blackening" in space, which is produced by a hologram of this type, is not superimposed, as is usual, on the Poisson or shot noise of photons in the photodetection plane, but is subtracted from it. This analogy has not yet been explored in detail.

VI. NOISELESS CONTROL OF MULTIMODE SQUEEZED LIGHT

A. Sub-shot-noise microscopy: detection of faint objects with multimode squeezed light

In this subsection we shall describe the application of multimode squeezed light for the detection of faint phase objects with a sensitivity better than the shot-noise limit, as proposed by Kolobov and Kumar (1993). Conceptually, the scheme of sub-shot-noise microscopy parallels in the spatial domain what was experimentally demonstrated in the time domain by Xiao, Wu, and Kimble (1987). Figure 16 shows a schematic of the sub-shot-noise microscopy. A Mach-Zehnder interferometer is formed by two 50-50 beam splitters, BS1 and BS2, and two highly reflective mirrors, M1 and M2. A plane wave is injected into one port of BS1, which serves as the local oscillator. The other port is illuminated by the squeezed vacuum produced by means of a traveling-wave OPA, for example, an OPA pumped by the second harmonic of a mode-locked and Q-switched laser (Aytür and Kumar, 1992). The dichroic mirror D prevents the pump wave of the OPA from entering the interferometer.

The outgoing light from the two ports of BS2 is detected by two photodetector arrays, D_1 and D_2. The size and number of elements in each array must be chosen to resolve the details of the phase object that is inserted in one arm of the interferometer (see the estimation below). The difference between the two photocurrent densities, $i_o(\vec{\rho}) \equiv i_1(\vec{\rho}) - i_2(\vec{\rho})$, is observed as a function of the spatial coordinate $\vec{\rho} = (x,y)$ on the arrays. Following the work of Caves (1981) and Yurke (1988), we shall calculate the sensitivity to the local oscillator phase and the enhancement of the minimum detectable spatially varying phase change in the object when multimode squeezed light is used.

For simplicity and notational convenience, in what follows we explicitly consider only the spatial dependence of the fields. Let $a_1(\vec{\rho})$ and $a_2(\vec{\rho})$ be the photon annihilation operators for the light waves at the two input ports of the interferometer. From an analysis of a Mach-Zehnder interferometer (Caves, 1981) we obtain the following expression for the mean difference in photocurrent density:

$$\langle i_o(\vec{\rho})\rangle = \eta[\cos\phi\langle a_1^\dagger(\vec{\rho})a_1(\vec{\rho}) - a_2^\dagger(\vec{\rho})a_2(\vec{\rho})\rangle - \sin\phi\langle a_1^\dagger(\vec{\rho})a_2(\vec{\rho}) + a_2^\dagger(\vec{\rho})a_1(\vec{\rho})\rangle], \quad (6.1)$$

where η is the quantum efficiency of the photodetector elements in the array (we assume η to be the same for all the elements) and ϕ is the phase difference for wave propagation along the two arms of the interferometer. In arriving at Eq. (6.1) we have implicitly assumed that the beam sizes are such that there is negligible diffraction from the input to the output of the interferometer. We consider the local oscillator field $a_1(\vec{\rho})$ to be in a coherent state with the complex amplitude α. If we denote the quantum state of the system by $|\Psi\rangle$, then

$$a_1(\vec{\rho})|\Psi\rangle = \alpha|\Psi\rangle. \quad (6.2)$$

We assume that the field $a_2(\vec{\rho})$ entering the second port of the interferometer is generated by the traveling-wave OPA. As we know from Sec. IV.A, a traveling-wave OPA generates a multimode squeezed vacuum at its output surface. The spatial Fourier amplitudes $a(z,\vec{q})$ of the annihilation operators transform from the input of the OPA ($z=0$) to the output ($z=l$) as

$$a(l,\vec{q}) = U(\vec{q})a(0,\vec{q}) + V(\vec{q})a^\dagger(0,-\vec{q}), \quad (6.3)$$

where $U(\vec{q})$ and $V(\vec{q})$ are the functions from Eq. (4.3) for $\Omega = 0$. We assume that the input port of the interferometer coincides with the output plane of the OPA so that $a_2(\vec{\rho}) = a(l,\vec{\rho})$.

Here we recall the expression for the spatial noise spectrum $(\delta i)_q^2(\theta)$ of the photocurrent density, calculated in Sec. IV.C. It depends on the spatial frequency $\vec{q}$ and the relative phase θ between the local oscillator field and the semimajor axis of the squeezing ellipse. Because squeezing ellipses with different $\vec{q}$ have different orientations, the angle θ is a function of $\vec{q}$, $\theta=\theta(\vec{q})$. If we neglect the anisotropy of the crystal, the spatial noise spectrum depends only on the absolute value of $|\vec{q}|=q$. As shown in Sec. IV.C [see Eq. (4.25)], this spectrum has the form

$$(\delta i)_q^2(\theta)=\langle i\rangle[1-\eta+\eta(\cos^2\theta(q)e^{2r(q)}+\sin^2\theta(q)e^{-2r(q)})], \tag{6.4}$$

where $\theta(q)$ and $r(q)$ are defined in Eqs. (4.23) and (4.22).

Going back to the Mach-Zehnder interferometer and using Eqs. (6.1)–(6.3), we can calculate the mean value of the difference in photocurrent density $\langle i_o(\vec{\rho})\rangle$ and its noise spectrum $(\delta i_o)_q^2(\theta,\phi)$ as a function of the phase difference ϕ in the interferometer. When the local oscillator field is strong compared to the mean intensity of the squeezed-vacuum field, the result is

$$\langle i_o(\vec{\rho})\rangle=\eta|\alpha|^2\cos\phi, \tag{6.5}$$

$$(\delta i_o)_q^2(\theta,\phi)=\eta|\alpha|^2[1-\eta+\eta(e^{2r(q)}\cos^2\theta(q)+e^{-2r(q)}\sin^2\theta(q))\sin^2\phi+\eta\cos^2\phi]. \tag{6.6}$$

If we define the phase sensitivity of the interferometer by $S(\phi)\equiv|\partial\langle i_o\rangle/\partial\phi|$ and the minimum detectable phase change by $\Delta\phi_{\min}^2=\Delta i_o^2/S_{\max}^2$, then we can see that the interferometer reaches its maximum sensitivity $S_{\max}=\eta|\alpha|^2$ near the operating points $\phi_o=(2n+1)\pi/2$, $n=0,1,2,\ldots$. The minimum detectable phase change at these operating points is

$$\Delta\phi_{\min}^2(q,\theta)=[1-\eta+\eta(\cos^2\theta(q)e^{2r(q)}+\sin^2\theta(q)e^{-2r(q)})]/\eta|\alpha|^2. \tag{6.7}$$

Comparing Eq. (6.7) with Eq. (6.4) we conclude that for spatial frequencies inside the squeezing bandwidth, $q\leqslant q_c$, the angle $\theta(q_m)=\pm\pi/2$, and the quantum efficiency $\eta\simeq 1$, the minimum detectable phase change is

$$\Delta\phi_{\min}^2(q_m)=e^{-2r_m}/|\alpha|^2. \tag{6.8}$$

If the squeezed-vacuum port of the interferometer is blocked, then one would get $\Delta\phi_{\min}^2(q_m)=1/|\alpha|^2$. Therefore illumination of the normally unused port of the interferometer by a multimode squeezed vacuum with maximum squeezing in a region of spatial frequencies $q\leqslant q_c$ reduces the minimum detectable phase change of this spatial frequency by a factor of e^{-2r_m}. This result is the spatial analog of the time domain result derived by Caves (1981).

Note that in general the spectra (6.4) and (6.6) also depend upon the frequency Ω at which the photocurrent noise is analyzed. We know from the analysis in Sec. IV that for a given spatial frequency q there is a range of frequencies Ω over which squeezing occurs. To obtain the maximum sensitivity enhancement predicted by Eq. (6.8), the postdetection electronics that processes the array photocurrents must be arranged to sense only this band of frequencies.

To explore the practical implications of this prediction in the experiment of Fig. 16, we insert in one arm of the interferometer an object with a faint phase modulation. The simplest object to use is a sinusoidal phase grating with spatial modulation across a chosen direction, say x. Such a grating will impart phase modulation onto the plane wave passing through it. The phase ϕ becomes $\phi=\phi_0+\delta\cos(ax)$ with $\delta\ll 1$, where $2\pi/a$ is the period of the sinusoidal modulation. The constant phase ϕ_0 can be canceled by inserting a flat piece of glass in the reference arm of the interferometer as shown in Fig. 16. To achieve enhancement of the phase sensitivity, we choose the spatial frequency a of the grating to be less than the squeezing bandwidth $(k_l/l)^{1/2}$ of the OPA.

Expanding Eq. (6.5) for small δ around one of the operating points, we obtain for the signal $\langle i_o(x)\rangle=\eta|\alpha|^2\delta\cos(ax)$. Now we estimate the number of elements in the photodetector arrays and their required size for the detection of this signal. The Whittaker-Shannon sampling theorem (Goodman, 1968) states that the maximum spacing Δx of the sample lattice for an exact recovery of the original function with finite spectral bandwidth B is $\Delta x=2\pi/B$. Because the spatial spectrum of our signal is proportional to the sum of two δ functions, $\delta(q\pm a)$, we have $\Delta x=\pi/a$. The size of each element, however, must be larger than the inverse of the spatial squeezing bandwidth; otherwise the photodetector elements will be sensitive to the stretched-noise component outside the squeezing bandwidth. Therefore, for the chosen example, the size of each element must be at least $2\pi\sqrt{l/k_l}$.

B. Interference mixing of multimode squeezed states and noiseless optical images

To create an optical image one has to modulate a wave front of an electromagnetic wave in space. However, not every modulation preserves the regular (sub-Poissonian) photon statistics across the wave front that can be obtained with multimode squeezed states. For example, the amplitude modulation in space due to nonuniform absorption would destroy this regularity, because photons would be absorbed randomly at different spatial points on the wave front. Therefore, for the creation of optical images with regular photon statistics, we have to learn how to modulate multimode squeezed light without destroying the regularity of photons in space.

One example of such nondestructive modulation in space is binary modulation by means of an opaque screen with apertures. The area of an aperture must be chosen to be larger than the coherence area of squeezed light, S_c, estimated in Sec. IV. Then under homodyne detection, the light collected from each aperture will

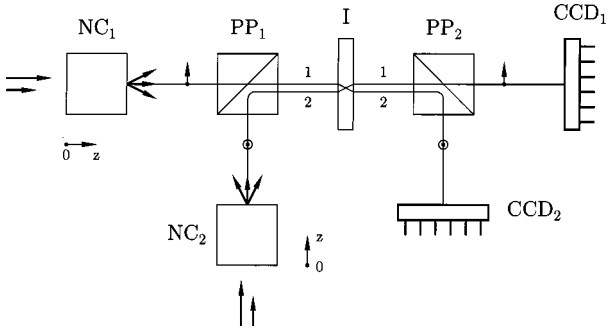

FIG. 17. Optical scheme for creation of noiseless optical images. Two orthogonally polarized multimode light beams are produced by nonlinear parametric crystals NC_1 and NC_2. Two polarization prisms, PP_1 and PP_2, combine and separate these light beams on the interferometer I. The image is created by spatial modulation of the Faraday rotation or birefringence of the interferometer. Two dense arrays of photodetectors CCD_1 and CCD_2 serve to detect the images at two outputs of the polarization prism PP_2 and investigate their quantum fluctuation in a balanced homodyne detection scheme.

have sub-Poissonian photon statistics. The opaque areas of the screen, obviously, do not introduce shot-noise having no photons. Therefore such a binary modulation with properly chosen aperture size preserves regular photon statistics in space. This kind of modulation might be of interest for digital two-dimensional optical computing. However, binary modulation does not allow us to create optical images with halftones. For the creation of a noiseless optical image with halftones we need nondestructive modulation of the wave front in space with an arbitrary degree of modulation.

It has been shown theoretically by many authors (Caves, 1981; Bondurant and Shapiro, 1984; Heidmann, Reynaud, and Cohen-Tannoudji, 1984; Kolobov and Sokolov, 1986; Yurke and Whittaker, 1987; Yurke, McCall, and Klauder, 1988) and also confirmed experimentally (Grangier *et al.*, 1987; Xiao, Wu, and Kimble, 1987) that interference mixing of two single-mode light waves provides such nondestructive modulation in time with the arbitrary degree of modulation. Recently the scheme of interference mixing was generalized (Sokolov, 1991, 1992; Sokolov and Fofanov, 1993) for multimode squeezed light and was shown to serve for the creation of optical images with regular photon statistics. In this subsection we shall describe this scheme.

Figure 17 shows a possible optical scheme for creation of noiseless optical images (Sokolov, 1991). Two nonlinear parametric crystals, NC_1 and NC_2, produce two beams of multimode squeezed light with orthogonal polarizations. In principle, this can also be done by a single crystal with type-II matching condition (Kolobov, 1991). Two polarization prisms, PP_1 and PP_2, serve to combine and separate the light beams in the interferometer, I, in such a way that the wave fronts of both light waves coincide at its surface. The image is created by spatial modulation of Faraday rotation or birefringence of the interferometer. This image is detected by two dense arrays of photodetectors, D_1 and D_2, and quantum fluctuations of these images are investigated by a balanced homodyne detection technique.

Let $a_m(\vec{\rho},t)$, $b_m(\vec{\rho},t)$, and $e_m(\vec{\rho},t)$ with $m=1,2$ be the photon annihilation operators at the inputs of nonlinear crystals at their outputs, and at the outputs of the interference mixer, respectively. For simplicity we shall neglect diffraction effects, assuming the distances between the components of the optical scheme to be small. We shall further assume that the interference mixer does not introduce any losses and therefore can be described by the following unitary scattering matrix:

$$R(\vec{\rho},t)=\begin{pmatrix}\exp(i\varphi_1) & 0\\ 0 & \exp(i\varphi_2)\end{pmatrix}\begin{pmatrix}c & s\\ -s & c\end{pmatrix}\times\begin{pmatrix}\exp(-i\kappa_1) & 0\\ 0 & \exp(-i\kappa_2)\end{pmatrix}. \tag{6.9}$$

The real parameters φ_m, κ_m, c, and s, with $c^2+s^2=1$, which describe the transformation of the amplitudes and phases of the scattered waves, depend upon the time and the spatial coordinates. We assume that this dependence is controlled from outside, and as a result of such control an optical image is formed in the scattered waves. The second prism PP_2 serves as an analyzer, which directs the scattered waves into the photodetection arrays D_1 and D_2, where the image is detected and its fluctuations analyzed. For the field operators $e_n(\vec{\rho},t)$ on the nth photodetection array we have

$$e_n(\vec{\rho},t)=\sum_{m=1}^{2} R_{nm}(\vec{\rho},t)b_m(\vec{\rho},t), \tag{6.10}$$

with $R_{nm}(\vec{\rho},t)$ given by Eq. (6.9).

We assume that the fields $b_m(\vec{\rho},t)$ are created by two independent optical parametric amplifiers. Therefore we can write the following relations between the operators of the slowly varying Fourier amplitudes at the inputs and outputs of the crystals:

$$b_m(\vec{q},\Omega)=U_m(\vec{q},\Omega)a_m(\vec{q},\Omega)+V_m(\vec{q},\Omega)a_m^{\dagger}(-\vec{q},-\Omega), \tag{6.11}$$

where the coefficients $U_m(\vec{q},\Omega)$ and $V_m(\vec{q},\Omega)$ for both crystals are defined by Eq. (4.3). As in Sec. IV, we shall assume that two strong monochromatic plane waves, which play the role of the local oscillators, enter both crystals. At the entries to the crystals these waves are in coherent states with complex amplitudes α_m. Their complex amplitudes β_m at the exit surface of the crystals are given by

$$\beta_m=U_m(0,0)\alpha_m+V_m(0,0)\alpha_m^{\star}. \tag{6.12}$$

We denote the complex amplitudes of the local oscillator waves at the photodetection planes as ϵ_m. These amplitudes are found from Eq. (6.10) as

$$\epsilon_n=\sum_{m=1}^{2} R_{nm}(\vec{\rho},t)\beta_m. \tag{6.13}$$

A particular image, generated by the transformation (6.10), is localized in space and in time, in the case of a dynamical image. Hence the parameters of the quantum

fluctuations also depend on the spatial point and the time. In order to draw more general conclusions we shall study a statistical ensemble of images that is homogeneous in space and time (Sokolov, 1991). As in Sec. IV, we can calculate the noise spectrum of the photocurrent density in both photodetection planes using the photodetection formulas (3.3) and (3.4) and the transformation of the field amplitudes (6.10) and (6.11). Keeping only the contributions proportional to the intensity of the local oscillator, we arrive at the following result:

$$(\delta i_n)^2_{\vec{q},\Omega}=\overline{\langle i_n(\vec{\rho},t)\rangle}(1-\eta)+\eta^2\sum_{m=1}^{2}\frac{1}{(2\pi)^3}\times\int d\vec{q}\,'d\Omega'(G^{(1)}_{nm}(\vec{q}-\vec{q}\,',\Omega-\Omega')\times[\cos^2\theta_{nm}(\vec{q},\vec{q}\,',\Omega,\Omega')e^{2r_m(\vec{q}\,',\Omega')}+\sin^2\theta_{nm}(\vec{q},\vec{q}\,',\Omega,\Omega')e^{-2r_m(\vec{q}\,',\Omega')}])+(G^{(1)}\leftrightarrow G^{(2)},\cos\leftrightarrow\sin). \tag{6.14}$$

Here the overbar denotes statistical averaging over the ensemble of images so that the mean value $\overline{\langle i_n(\vec{\rho},t)\rangle}$ is independent of the spatial coordinate $\vec{\rho}$ and time t.

The intensity distribution in the photodetection plane is determined by the interference of the squeezed vacuum waves produced by nonlinear crystals with the following combination of amplitudes of the local oscillator waves with transmission coefficients $R_{nm}(\vec{\rho},t)$:

$$B_{nm}(\vec{\rho},t)=\sum_{l=1}^{2}R^{\star}_{nm}(\vec{\rho},t)R_{ml}(\vec{\rho},t)\beta_l. \tag{6.15}$$

For a stationary and spatially uniform ensemble of images, the space-time correlation functions of $B_{nm}(\vec{\rho},t)$ at two different space-time points depend only on the interval between them. We can, therefore, introduce the cross-spectral density of these complex amplitudes as follows:

$$(B_{nm}B_{kl})_{\vec{q},\Omega}=\int d\vec{\rho}\,dt\overline{B_{nm}(\vec{0},0)B_{kl}(\vec{\rho},t)}\times\exp[i(\Omega t-\vec{q}\cdot\vec{\rho})]. \tag{6.16}$$

The quantities $G^{(p)}_{nm}(\vec{q},\Omega)$, $p=1,2$, appearing in Eq. (6.14), are defined as

$$G^{(p)}_{nm}(\vec{q},\Omega)=\tfrac{1}{2}[G_{nm}(\vec{q},\Omega)-(-1)^p|(B^2_{nm})_{\vec{q},\Omega}|], \tag{6.17}$$

where

$$G_{nm}(\vec{q},\Omega)=\tfrac{1}{2}[(B^{\star}_{nm}B_{nm})_{\vec{q},\Omega}+(B_{nm}B^{\star}_{nm})_{\vec{q},\Omega}]. \tag{6.18}$$

As shown by Sokolov (1991), the coefficients $G^{(p)}_{nm}(\vec{q},\Omega)$ arise when the complex amplitudes $B_{nm}(\vec{\rho},t)$ are expanded in the quadrature components. The orientation of the coordinate system in which this expansion is performed is given by the angle

$$\Phi_{nm}(\vec{q},\Omega)=\tfrac{1}{2}\arg(B^2_{nm})_{\vec{q},\Omega}. \tag{6.19}$$

Finally, the angles $\theta_{nm}(\vec{q},\vec{q}\,',\Omega,\Omega')$, which appear in Eq. (6.14), are given by the following expressions:

$$\theta_{nm}(\vec{q},\vec{q}\,',\Omega,\Omega')=\tfrac{1}{2}\arg[U_m(\vec{q}\,',\Omega')V_m(-\vec{q}\,',-\Omega')]-\Phi_{nm}(\vec{q}-\vec{q}\,',\Omega-\Omega'). \tag{6.20}$$

We can see from Eqs. (6.14) and (6.20) that the spectral components $\vec{q}$ and Ω of the photocurrent density fluctuations are created by interference of the harmonics $\vec{q}\,'$ and Ω' of the squeezed vacuum with the harmonics $\vec{q}-\vec{q}\,'$ and $\Omega-\Omega'$ of the effective image field, given by the complex amplitude $B_{nm}(\vec{\rho},t)$. In order to suppress the quantum fluctuations of the photocurrent density, it is necessary to have a source of squeezed vacuum with a wide range of frequencies Ω and spatial frequencies $\vec{q}$ and also to take into account the spectral properties of the effective field of the image.

Following Sokolov (1991), we shall discuss the arbitrary degree of spatial and temporal modulation of the scattering coefficients of the interferometer. Our goal is to formulate conditions that will guarantee nondestructive modulation of the incoming light waves. These conditions will pertain not only to noiseless optical images but also to a high degree of temporal modulation, i.e., the single-mode case.

In order to achieve nondestructive modulation of multimode squeezed waves and create a noiseless image at the output n of the interferometer, it is sufficient to satisfy simultaneously the conditions

$$G^{(2)}_{nm}(\vec{q},\Omega)=0, \tag{6.21}$$

for $m=1,2$ in the required range of frequencies Ω and spatial frequencies $\vec{q}$ [see Eq. (6.14)]. In this case the effective field of the image for both $m=1$ and $m=2$ will be concentrated in the quadrature 1. By proper choice of the phase of squeezed light at both entrance surfaces to the interferometer, one can ensure that the beats of the effective field of the image cancel with the noisy quadrature of the fluctuations.

The complex amplitude $B_{nm}(\vec{\rho},t)$ in Eq. (6.15) contains the contribution $p=m$, with a constant phase equal to $\arg(\beta_m)$, and the contribution $p\neq m$, with the phase depending on $\vec{\rho}$ and t. A sufficient condition for both contributions to have the same phase, independent of spatial and temporal modulation, reads

$$\arg\beta_1-\kappa_1(\vec{\rho},t)=\arg\beta_2-\kappa_2(\vec{\rho},t). \tag{6.22}$$

For an interferometer described by Eq. (6.9), this condition means that the output phase increments $\varphi_1(\vec{\rho},t)$ and $\varphi_2(\vec{\rho},t)$ are arbitrary, while the constraint

$$\kappa_1(\vec{\rho},t)-\kappa_2(\vec{\rho},t)=\text{const} \tag{6.23}$$

is imposed on the phase increments at the input. The latter condition is satisfied only for some particular methods of interference mixing. If condition (6.23) is met and the phases of the local oscillator waves are chosen according to Eq. (6.22), then from the definition of the quadrature components of the effective field of the image (Sokolov, 1991) it follows that

$$\Phi_{nm}=\arg\beta_m \tag{6.24a}$$

and

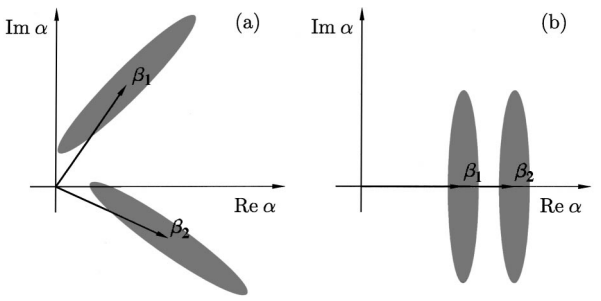

FIG. 18. Matching of the phases of the local oscillator and squeezed vacuum arriving from two inputs on one of the photodetectors of the optical image: (a) general case without phase matching; (b) phase matching that guarantees reduction of the amplitude fluctuations in the image below the shot-noise level.

$$G_{nm}^{(1)}(\vec{q},\Omega)=(|B_{nm}|^2)_{\vec{q},\Omega}, \quad G_{nm}^{(2)}(\vec{q},\Omega)=0. \tag{6.24b}$$

In the spectrum (6.14) the contribution of beats with the quadrature component 2 disappears. The quantum fluctuations in the resulting optical image are reduced below the shot-noise limit to the same degree as in incoming squeezed light waves with the proper choice of phases θ_{nm}, for $m=1,2$:

$$\theta_{nm}(\vec{q},\vec{q}',\Omega,\Omega')=\pm\pi/2. \tag{6.25}$$

These results are easy to illustrate graphically. Figure 18 shows the quadrature components of the output amplitude $e_n(\vec{\rho},t)$ and the complex vectors of the local oscillator waves together with the uncertainty regions of the squeezed light. Figure 18(a) pertains to the general case when no care is taken to match the phases of the waves according to Eqs. (6.22) and (6.23). Figure 18(b) displays the case when such phase matching is achieved. In the latter case the spatial and temporal modulation of the scattering coefficients does not destroy the orientation of the squeezing ellipses relative to the vectors of the local oscillator waves. Therefore, at the output of the interference mixer, we have reduced the amplitude fluctuations of the resulting field and correspondingly, reduced the photocurrent density fluctuations below the shot-noise limit.

In concluding this subsection we present a possible physical mechanism for the nondestructive control of multimode squeezed states. For a more detailed description we refer the reader to the paper by Sokolov and Fofanov (1993). As mentioned above, not all methods of interference mixing satisfy condition (6.23) for the creation of noiseless optical images. Two examples that do satisfy this condition are Faraday rotation and birefringence. Let the input light waves be polarized linearly and orthogonally to one another. The analyzer PP_2 separates outgoing waves with the same states of polarization. The interference mixer contributes the externally controlled phase increments $\chi_1(\vec{\rho},t)$ and $\chi_2(\vec{\rho},t)$ to waves with orthogonal circular polarization (Faraday rotation). The matrix $R(\vec{\rho},t)$ from Eq. (6.9) takes the form

$$R(\vec{\rho},t)=\exp[i\chi'(\vec{\rho},t)]\begin{pmatrix} e^{i\Delta_1} & 0 \\ 0 & e^{i\Delta_2}\end{pmatrix} \times\begin{pmatrix} \cos\chi''(\vec{\rho},t) & \sin\chi''(\vec{\rho},t) \\ -\sin\chi''(\vec{\rho},t) & \cos\chi''(\vec{\rho},t)\end{pmatrix}\begin{pmatrix} e^{-i\Delta_1} & 0 \\ 0 & e^{-i\Delta_2}\end{pmatrix}, \tag{6.26}$$

where

$$\chi'(\vec{\rho},t)=[\chi_1(\vec{\rho},t)+\chi_2(\vec{\rho},t)]/2, \quad \chi''(\vec{\rho},t)=[\chi_1(\vec{\rho},t)-\chi_2(\vec{\rho},t)]/2. \tag{6.27}$$

Here Δ_1 and Δ_2 are the constant phase shifts. If orthogonal circular polarizations are separated at the input and output, and the interferometer induces controllable phase increments in orthogonal linear polarizations (birefringence), then we have a transformation similar to Eq. (6.26).

It is obvious that condition (6.23) is satisfied for transformation (6.26). Therefore we conclude that Faraday rotation and birefringence are suitable physical mechanisms for the nondestructive control of multimode squeezed states with an arbitrary degree of modulation, and thus for the creation of noiseless optical images.

VII. NOISELESS AMPLIFICATION OF OPTICAL IMAGES

A. Optical scheme and evolution of the field

It has been shown by many authors that phase-insensitive optical amplifiers introduce at least 3 dB of extra noise in the output, whereas phase-sensitive amplifiers may preserve the input signal-to-noise ratio and in this sense are "noiseless."[6] Investigations of the noise properties of optical amplifiers are usually carried out in the time domain and neglect spatial aspects pertaining to a single mode of electromagnetic field.

However, the spatial domain is by no means to be cast out from the scope of noiseless amplification. Indeed, many areas of physics would benefit from the possibility of *noiseless amplification of faint optical images*. Those that come to mind immediately are astronomy and microscopy, which in this case would be able to widen the range of the faintest detectable galaxies and microscopic objects.

The first step towards realization of a noiseless amplifier of optical images was taken by Kolobov and Lugiato (1995). In this section we shall describe the results of their analysis and mention some experiments relevant to the practical implementation of the proposed scheme.

A possible realization of a parametric image amplifier and its equivalent linear scheme are shown in Fig. 19. A faint image that is to be amplified is located in the object

[6]See, for example, Caves, 1982; Yurke and Denker, 1984; Gilson, Barnett, and Stenholm, 1987; Milburn, Steyn-Ross, and Walls, 1987; Mander, Loudon, and Shepherd, 1988; Yamamoto *et al.*, 1990; Kimble, 1992; Protsenko and Lugiato, 1994; Protsenko, Lugiato, and Fabre, 1994.

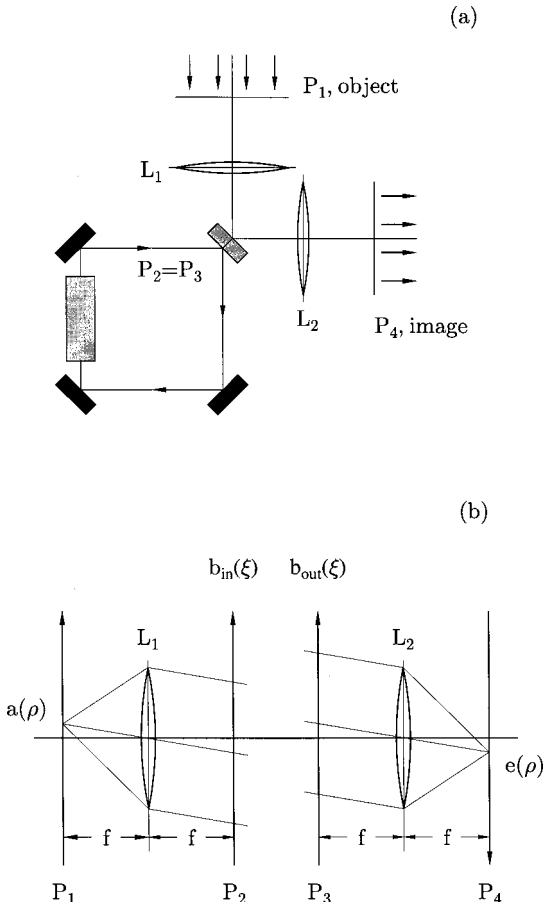

FIG. 19. A possible realization of the parametric image amplifier (a) and its equivalent linear scheme (b). A faint optical image located in the object plane P_1 is projected onto the image plane P_4 by lenses L_1 and L_2. P_2 and P_3 are the input and output planes of a ring-cavity optical parametric amplifier (OPA).

plane P_1. This image is projected by the lens L_1 in the input plane P_2 of a ring-cavity degenerate OPA. We consider the case of a cavity with plane mirrors. The amplified image from the output plane P_3 is projected onto the image plane P_4 by the lens L_2. We shall assume that in the output plane P_3 there is a pupil of finite area S_p. Its shape is described by the pupil frame function $P(\vec{\xi})$ equal to one in the pupil and zero elsewhere; $\vec{\xi}$ is the transverse coordinate in the input and output planes. The introduction of a pupil of finite size is necessary for evaluating the noise properties of our system. We choose all optical intervals in the scheme to be equal to the focal length f of the identical lenses L_1 and L_2.

For simplicity we restrict our analysis to monochromatic images. However, our scheme can easily be generalized to include polychromatic images. Clearly, the spectral bandwidth of such images should be within the bandwidth of the cavity employed in the scheme. Hence, in general, filters to make light quasimonochromatic before amplification are necessary.

The reason for combining the OPA with input and output lenses is as follows. It will be clear from below that without lenses the OPA would amplify the plane waves with a narrow bandwidth of transverse vectors $\vec{q}$ that satisfy the resonance condition (Oppo, Brambilla, and Lugiato, 1994). Therefore, without lenses, the system would essentially behave as a narrow-band filter that selectively amplifies a narrow region in the spatial Fourier plane of vectors $\vec{q}$. Lenses L_1 and L_2 located as shown in Fig. 19(b) perform the spatial Fourier transform, thus converting the $\vec{q}$ plane into the $\vec{\rho}$ plane.

We shall assume that the amplified image is detected by a CCD camera. To be more precise, we shall take into account the fact that each pixel has a finite area S_d and that the photocurrent from each pixel is collected during the observation time T_d. Thus the quantity of interest for us is the number of photoelectrons $N_I(\vec{\rho},t)$ registered by the pixel centered at point $\vec{\rho}$ in the image plane in the time window from $t-T_d/2$ to $t+T_d/2$,

$$N_I(\vec{\rho},t)=\int_{S_d} d\vec{\rho}' \int_{T_d} dt'\, i(\vec{\rho}',t'). \tag{7.1}$$

This kind of observation was discussed in Sec. III, Eqs. (3.12)–(3.14). We shall consider the mean number $\langle N_I(\vec{\rho},t)\rangle$ of registered electrons as the amplified signal of our scheme. Its variance, $\langle \Delta N_I^2(\vec{\rho},t)\rangle$, characterizes the noise properties of the amplified image, and the power signal-to-noise ratio R_I of the amplified image is given by[7]

$$R_I=\langle N_I(\vec{\rho},t)\rangle^2/\langle \Delta N_I^2(\vec{\rho},t)\rangle. \tag{7.2}$$

The equivalent quantities $\langle N_O(\vec{\rho},t)\rangle$, $\langle \Delta N_O^2(\vec{\rho},t)\rangle$, and R_O, measured in the object plane, describe the signal and noise of the input image. For a stationary signal none of these quantities depends on time. Our goal is to compare R_I and R_O and to show that under certain conditions they can be equal. We refer to this situation as a noiseless amplification.

We denote by $a(\vec{\rho},t)$ and $a^\dagger(\vec{\rho},t)$ the photon annihilation and creation operators in the object plane P_1 and by $e(\vec{\rho},t)$ and $e^\dagger(\vec{\rho},t)$ the corresponding operators in the image plane P_4. Using Eqs. (3.12) and (3.13) together with the photodetection formulas (3.3) and (3.4), we can express $\langle N_I(\vec{\rho},t)\rangle$ and $\langle \Delta N_I^2(\vec{\rho},t)\rangle$ through the mean irradiance $\langle e^\dagger(\vec{\rho},t)e(\vec{\rho},t)\rangle$ and the intensity correlation function $\langle e^\dagger(\vec{\rho},t)e^\dagger(\vec{\rho}',t')e(\vec{\rho}',t')e(\vec{\rho},t)\rangle$ of the field in the image plane. To evaluate these observable quantities in terms of the input signal and the gain of our amplifier we need the relation between the field operators $e(\vec{\rho},t)$ in the image plane and $a(\vec{\rho},t)$ in the object plane.

For the moment we assume that there is no *pupil* in plane P_3. In the next subsection we shall see that this assumption gives divergent results for the inherent noise of the scheme. Then we shall generalize the results of this subsection to include the pupil.

Let us denote the field operators in the input and the output planes of the OPA as $b_{\rm in}(\vec{\xi},t)$ and $b_{\rm out}(\vec{\xi},t)$, re-

[7]In this section we consider the power signal-to-noise ratio (Thomas, 1969) instead of the one defined by Eq. (3.14); with the power signal-to-noise ratio the final results look simpler.

spectively [Fig. 19(b)]. These operators obey the free-field commutation relations equivalent to Eq. (3.2). The operator $b_{\rm in}(\vec{\xi},t)$ is expressed through the operator $a(\vec{\rho},t)$ in the object plane by the following transformation performed by the lens L_1:

$$b_{\rm in}(\vec{\xi},t)=\frac{1}{\lambda f}\int d\vec{\rho}\,\exp\left[-i\frac{2\pi}{\lambda f}\vec{\xi}\cdot\vec{\rho}\right]a(\vec{\rho},t), \tag{7.3}$$

where f is the focal length of the lens and λ is the wavelength of the light.

We use a paraxial approximation and consider only one longitudinal cavity mode closest to resonance with the input signal. The behavior of the slowly varying field operator $b(\vec{\xi},t)$ of this mode inside the cavity is described by the following equation:

$$\frac{\partial}{\partial t}b(\vec{\xi},t)-i\frac{c}{2k}\nabla_\perp^2 b(\vec{\xi},t)$$
$$=-(\kappa+i\Delta)b(\vec{\xi},t)+\sigma b^\dagger(\vec{\xi},t)+\sqrt{2\kappa}b_{\rm in}(\vec{\xi},t). \tag{7.4}$$

Here κ is the cavity decay constant equal to

$$\kappa=cT/2L, \tag{7.5}$$

where T is the intensity transmission coefficient of the cavity outcoupling mirror, L is the perimeter of the cavity, and c is the light velocity in a vacuum; the detuning parameter Δ is defined as

$$\Delta=\omega_c-\omega_s, \tag{7.6}$$

where ω_c is the longitudinal cavity frequency closest to the frequency ω_s of the signal field. Because the optical parametric oscillator is below threshold we can neglect pump depletion and consider the amplitude of the pump field as a fixed c-number; σ is the constant of parametric interaction proportional to this amplitude; $\nabla_\perp^2$ denotes the transverse Laplacian; and k is the wave number of the traveling wave inside the cavity, $k=2\pi/\lambda$.

The output field operator $b_{\rm out}(\vec{\xi},t)$ is the sum of two waves, one of which is reflected from and another transmitted through the outcoupling mirror of the cavity:

$$b_{\rm out}(\vec{\xi},t)=\sqrt{2\kappa}b(\vec{\xi},t)-b_{\rm in}(\vec{\xi},t). \tag{7.7}$$

To express the output field operators through the input operators we take the spatio-temporal Fourier transform of $b(\vec{\xi},t)$,

$$\tilde{b}(\vec{q},\Omega)=\int d\vec{\xi}\,dt\,b(\vec{\xi},t)\exp[i(\Omega t-\vec{q}\cdot\vec{\xi})], \tag{7.8}$$

and solve the linear system for $\tilde{b}(\vec{q},\Omega)$ and $\tilde{b}^\dagger(-\vec{q},-\Omega)$ obtained from Eq. (7.4). After some algebra we arrive at the following relation between the corresponding Fourier amplitudes $\tilde{b}_{\rm in}(\vec{q},\Omega)$ and $\tilde{b}_{\rm out}(\vec{q},\Omega)$ on the input and the output of the OPA:

$$\tilde{b}_{\rm out}(\vec{q},\Omega)=U(\vec{q},\Omega)\tilde{b}_{\rm in}(\vec{q},\Omega)+V(\vec{q},\Omega)\tilde{b}_{\rm in}^\dagger(-\vec{q},-\Omega), \tag{7.9}$$

with the coefficients $U(\vec{q},\Omega)$ and $V(\vec{q},\Omega)$ given by

$$U(\vec{q},\Omega)=\frac{[\kappa-i\Delta(\vec{q},\Omega)][\kappa-i\Delta(\vec{q},-\Omega)]+|\sigma|^2}{[\kappa+i\Delta(\vec{q},\Omega)][\kappa-i\Delta(\vec{q},-\Omega)]-|\sigma|^2},$$
$$V(\vec{q},\Omega)=\frac{2\kappa\sigma}{[\kappa+i\Delta(\vec{q},\Omega)][\kappa-i\Delta(\vec{q},-\Omega)]-|\sigma|^2}, \tag{7.10}$$

where $\Delta(\vec{q},\Omega)=\Delta-\Omega+cq^2/2k$. Since both $b_{\rm in}(\vec{\xi},\Omega)$ and $b_{\rm out}(\vec{\xi},\Omega)$ satisfy the free-field commutation relation (4.6), the transformation (7.9) must be unitary. The necessary condition for unitarity of (7.9) is $|U(\vec{q},\Omega)|^2-|V(\vec{q},\Omega)|^2=1$. It is easy to check that this condition is satisfied by $U(\vec{q},\Omega)$ and $V(\vec{q},\Omega)$ from Eq. (7.10).

The transformation of the field amplitude from the object plane P_1 to the input plane P_2 given by Eq. (7.3) is equivalent to the following relation between the Fourier amplitudes $\tilde{b}_{\rm in}(\vec{q},\Omega)$ and $\tilde{a}(\vec{q},\Omega)$:

$$\tilde{b}_{\rm in}(\vec{q},\Omega)=\lambda f\tilde{a}\left(-\frac{\lambda f}{2\pi}\vec{q},\Omega\right). \tag{7.11}$$

Since the lens L_2 has the same focal length as L_1, we have an identical relationship between the Fourier amplitudes $\tilde{b}_{\rm out}(\vec{q},\Omega)$ and $\tilde{e}(\vec{q},\Omega)$ in the output plane P_3 and in the image plane P_4:

$$\tilde{e}(\vec{q},\Omega)=\lambda f\tilde{b}_{\rm out}\left(-\frac{\lambda f}{2\pi}\vec{q},\Omega\right). \tag{7.12}$$

Using Eqs. (7.11) and (7.12) together with Eq. (7.9) and performing the inverse Fourier transform with respect to the spatial argument, we obtain the desired relationship between the field amplitudes in the object and the image planes:

$$e(\vec{\rho},\Omega)=u(\vec{\rho},\Omega)a(\vec{\rho},\Omega)+v(\vec{\rho},\Omega)a^\dagger(-\vec{\rho},-\Omega), \tag{7.13}$$

with $u(\vec{\rho},\Omega)$, and $v(\vec{\rho},\Omega)$ given by

$$u(\vec{\rho},\Omega)=\frac{[1-i\delta(\vec{\rho},\Omega)][1-i\delta(\vec{\rho},-\Omega)]+|g|^2}{[1+i\delta(\vec{\rho},\Omega)][1-i\delta(\vec{\rho},-\Omega)]-|g|^2},$$
$$v(\vec{\rho},\Omega)=\frac{2g}{[1+i\delta(\vec{\rho},\Omega)][1-i\delta(\vec{\rho},-\Omega)]-|g|^2}. \tag{7.14}$$

Here we have introduced the dimensionless coupling strength g of the parametric interaction,

$$g=\sigma/\kappa, \tag{7.15}$$

and the dimensionless mismatch function $\delta(\vec{\rho},\Omega)$,

$$\delta(\vec{\rho},\Omega)=\Delta/\kappa-\Omega/\kappa+(\rho/\rho_0)^2, \tag{7.16}$$

with ρ_0 defined as

$$\rho_0=f\sqrt{\frac{\lambda T}{2\pi L}}. \tag{7.17}$$

As shown by Oppo, Brambilla, and Lugiato (1994), for $\Delta>0$ the threshold of the optical parametric oscillator corresponds to $|g|^2=1+(\Delta/\kappa)^2$; for $\Delta\leq 0$ the threshold value is $|g|=1$. In the analysis below we shall consider the situation of exact resonance, $\Delta=0$, or negative detuning, $\Delta<0$. Therefore, to ensure a linear amplification regime, the coupling strength g must be $|g|<1$. For simplicity we shall consider the case of real g.

Equations (7.13)–(7.17) give us the desired relationship between the field operators in the object and image planes, which we shall use for calculations of the quantum fluctuations of the amplified image.

B. Quantum fluctuations of the amplified image

In our analysis we shall restrict ourselves to stationary images. We shall assume that the field in the object plane P_1 is in a coherent state with the complex amplitude $s(\vec{\rho})$ modulated in space. This spatial modulation of the complex amplitude represents the input signal of the scheme or the "image" that is to be amplified.

We should like to stress here that this modulation can be so faint that it is insufficient for recording a real "physical" image in the form of a transparency or a hologram. Of course, having such a transparency would enable us to "amplify" the image more easily, simply by increasing the intensity of the light illuminating it. However, we have in mind a situation in which we do not have such a possibility.

For simplicity we shall consider the situation in which $s(\vec{\rho})$ is a real and even function of $\vec{\rho}$. In practice this can be obtained by using not one optical image in the object plane, but two mirror copies separated from each other by some spatial interval $2a$, so that they do not overlap:

$$s(\vec{\rho})=s_0(\vec{\rho}-\vec{a})+s_0(-\vec{\rho}-\vec{a}), \tag{7.18}$$

where $s_0(\vec{\rho})$ is the original image of finite size smaller than the distance a. It follows from the stationarity of the input signal that

$$\langle a(\vec{\rho},\Omega)\rangle=s(\vec{\rho})2\pi\delta(\Omega). \tag{7.19}$$

Using Eqs. (7.13) and (7.19) we can evaluate any correlation function of the field operators $e(\vec{\rho},t)$ and $e^{\dagger}(\vec{\rho},t)$ in the image plane. For this we have to express this correlation function through the *normal-ordered* correlation functions of the field operators $a(\vec{\rho},t)$ and $a^{\dagger}(\vec{\rho},t)$ in the object plane and then use Eq. (7.19), taking into account that the input field is in a coherent state. There is, however, a difficulty. When doing this, for example, for the mean irradiance $\langle e^{\dagger}(\vec{\rho},t)e(\vec{\rho},t)\rangle$, we obtain

$$\langle e^{\dagger}(\vec{\rho},t)e(\vec{\rho},t)\rangle=s^2(\vec{\rho})|u(\vec{\rho},0)+v(\vec{\rho},0)|^2 + \delta(\vec{0})\frac{1}{2\pi}\int d\Omega|v(\vec{\rho},\Omega)|^2. \tag{7.20}$$

The first term in Eq. (7.20) gives the amplified signal, while the second one describes the noise added by the OPA. The physical origin of that noise is well known—it is due to spontaneous parametric radiation. Indeed, an OPA generates so-called twin photons even when there is no signal on its input, $s(\vec{\rho})=0$, and the first term in Eq. (7.20) vanishes. The irradiance of the field generated in this case is given by the second term. Unfortunately, as we can see from Eq. (7.20), it is proportional to $\delta(\vec{0})$, i.e., it diverges. The reason for this divergence lies in our approximation of an infinitely large spatial bandwidth for our system, as follows from Eq. (7.13). Therefore, to estimate the noise of our amplifier, we have to introduce a pupil of finite size into the scheme.

This, however, brings about another problem, since now part of the light gets lost in the system, and therefore the transformation of the field operators from the object plane to the image plane cannot be unitary. Indeed, in the case without a pupil, we have obtained a field operator $b_{\rm out}(\vec{\xi},t)$ in the plane P_3 that obeys commutation relations analogous to Eq. (3.2). When we insert the pupil in this plane, the contribution from $b_{\rm out}(\vec{\xi},t)$ to the field in the image plane becomes

$$e(\vec{\rho},t)=\frac{1}{\lambda f}\int d\vec{\xi}\,P(\vec{\xi})b_{\rm out}(\vec{\xi},t)\exp\left[-i\frac{2\pi}{\lambda f}\vec{\rho}\cdot\vec{\xi}\right], \tag{7.21}$$

where $P(\vec{\xi})$ is the pupil frame function defined in Sec. VII.A. From Eq. (7.21) it is easy to see that $e(\vec{\rho},t)$ no longer obeys Eq. (3.2). The reason for this is obvious. Now the integral in Eq. (7.21) is taken only over the part of the output plane in which $P(\vec{\xi})$ is equal to unity. Thus Eq. (7.21) does not take into account the contribution of the field from the part of the output plane that lies outside the pupil. This gives us an idea of how to restore unitarity of the transformation from the object to the image plane.

Let us introduce an auxiliary field operator $c(\vec{\xi},t)$ in the output plane P_3 that obeys the free-field commutation relations (3.2) and is independent of $b_{\rm out}(\vec{\xi},t)$ and $b_{\rm out}^{\dagger}(\vec{\xi},t)$, i.e., commutes with them. This auxiliary field operator will give us the necessary contribution from the part of the P_3 plane outside the pupil. The total field in the image now reads

$$e(\vec{\rho},t)=\frac{1}{\lambda f}\int d\vec{\xi}\,P(\vec{\xi})b_{\rm out}(\vec{\xi},t)\exp\left[-i\frac{2\pi}{\lambda f}\vec{\rho}\cdot\vec{\xi}\right] + \frac{1}{\lambda f}\int d\vec{\xi}[1-P(\vec{\xi})]c(\vec{\xi},t)\exp\left[-i\frac{2\pi}{\lambda f}\vec{\rho}\cdot\vec{\xi}\right]. \tag{7.22}$$

It is easy to check that $e(\vec{\rho},t)$ and $e^{\dagger}(\vec{\rho},t)$ now satisfy the commutation relations (3.2). From Eq. (7.22) we can also see the physical meaning of the introduced auxiliary operator $c(\vec{\xi},t)$. It gives the contribution to the field in the image plane P_4 from the part of P_3 that lies outside the pupil and in which the field is in the vacuum state. Since the operators $c(\vec{\xi},t)$ and $c^{\dagger}(\vec{\xi},t)$ commute with the operators $b_{\rm out}(\vec{\xi},t)$ and $b_{\rm out}^{\dagger}(\vec{\xi},t)$ and are in the vacuum state, there will be no contribution from the $c(\vec{\xi},t)$ term in Eq. (7.22) to any *normal-ordered* correlation function of the field operators $e(\vec{\rho},t)$ and $e^{\dagger}(\vec{\rho},t)$. This is why in classical theory there is no need to write the second term in Eq. (7.22).

The importance of this term in quantum theory was recognized by Yuen and Shapiro (1978) at the very beginning of the study of squeezed states of light. They developed a theory of optical communication with squeezed states of light in free space which diffraction

should be taken into account; in order to separate the two contributions in Eq. (7.22) they used the modal theory of diffraction.

Since in our case the second term in Eq. (7.22) does not contribute to the normal-ordered correlation functions in Eqs. (3.3) and (3.4), from now on we shall omit this term when writing the field operator $e(\vec{\rho},t)$ in the image plane P_4. By expressing the field operator $b_{\rm out}(\vec{\xi},t)$ through $a(\vec{\rho},t)$ and $a^\dagger(\vec{\rho},t)$ and substituting this expression into Eq. (7.22), we arrive at the following result for $e(\vec{\rho},\Omega)$:

$$e(\vec{\rho},\Omega)=\frac{1}{\lambda f}\int d\vec{\rho}\,' p(\vec{\rho}-\vec{\rho}')[u(\vec{\rho}\,',\Omega)a(\vec{\rho}\,',\Omega) + v(\vec{\rho}\,',\Omega)a^\dagger(-\vec{\rho}\,',-\Omega)], \tag{7.23}$$

which generalizes Eq. (7.13) to the case with a pupil. The function $p(\vec{\rho})$ in Eq. (7.23) is related to the pupil frame function as

$$p(\vec{\rho})=\frac{1}{\lambda f}\int d\vec{\xi}\,P(\vec{\xi})\exp\left[i\frac{2\pi}{\lambda f}\vec{\rho}\cdot\vec{\xi}\right] \tag{7.24}$$

and is called the *impulse response* of the optical system. For an infinitely large pupil $p(\vec{\rho})=\lambda f\delta(\vec{\rho})$, and Eq. (7.23) recovers the previous result (7.13). Notice that the typical linear spatial scale of change of the impulse response function is $\lambda f/S_p^{1/2}$, where S_p is the pupil area. To obtain explicit analytical results we shall assume that this distance is much smaller than the typical scale over which functions $u(\vec{\rho},0)$ and $v(\vec{\rho},0)$ [which is of the order of ρ_0 from Eq. (7.17)] as well as the input signal $s(\vec{\rho})$ change. This will allow us to take the latter functions out of integral when they enter as a product with impulse response $p(\vec{\rho})$.

To check that introduction of the pupil allows us to estimate the noise of the system, let us calculate the mean irradiance $\langle e^\dagger(\vec{\rho},t)e(\vec{\rho},t)\rangle$ using the new expression for $e(\vec{\rho},t)$. From Eq. (7.23) we obtain

$$\langle e^\dagger(\vec{\rho},t)e(\vec{\rho},t)\rangle=s^2(\vec{\rho})|u(\vec{\rho},0)+v(\vec{\rho},0)|^2 + \frac{1}{S_{\rm diff}}\frac{1}{2\pi}\int d\Omega|v(\vec{\rho},\Omega)|^2, \tag{7.25}$$

where we have introduced the diffraction area $S_{\rm diff}$ as

$$S_{\rm diff}=\frac{(\lambda f)^2}{S_p}. \tag{7.26}$$

Now the noise contribution is finite. Equation (7.25) also clarifies the physical origin of $\delta(\vec{0})$ in Eq. (7.20); that is, it arises when the area S_p grows infinitely.

From Eqs. (3.3), (7.1), and (7.25) we obtain for the mean number of photoelectrons

$$\langle N_I(\vec{\rho},t)\rangle=\eta S_d T_d s^2(\vec{\rho})G_\phi(\vec{\rho}) + \eta\frac{S_d}{S_{\rm diff}}\frac{T_d}{2\pi}\int d\Omega|v(\vec{\rho},\Omega)|^2. \tag{7.27}$$

Here we have introduced the phase-sensitive gain $G_\phi(\vec{\rho})$ as

$$G_\phi(\vec{\rho})=|u(\vec{\rho},0)+v(\vec{\rho},0)|^2. \tag{7.28}$$

Though the relative phase among three interacting waves (pump, signal, and idler) is fixed so as to give amplification, this gain varies across the image plane because of diffraction.

To calculate the variance $\langle\Delta N_I^2(\vec{\rho},t)\rangle$ we use Eqs. (3.13), (3.4), and (7.23). By substituting $e(\vec{\rho},\Omega)$ from Eq. (7.23) into the intensity correlation function $\langle e^\dagger(\vec{\rho},t)e^\dagger(\vec{\rho}\,',t')e(\vec{\rho}\,',t')e(\vec{\rho},t)\rangle$ from Eq. (3.4) we obtain 16 correlation functions of operators $a(\vec{\rho},\Omega)$ and $a^\dagger(\vec{\rho},\Omega)$ of mixed order and at four different points $\vec{\rho}$ and frequencies Ω. Using the commutator (3.2), we bring them to the normal order and then use Eq. (7.19) together with the fact that the input field is in a coherent state. When doing so we get two different kinds of terms: the first arises from interference of the amplified signal with the noise from spontaneous parametric radiation, and the second from the self-interference of this noise.

To simplify the calculations we shall use the assumptions that the observation time T_d is long compared with the inverse cavity bandwidth κ^{-1} and that both the diffraction area and the pixel area are small compared to the typical spatial scales of functions $u(\vec{\rho},0)$, $v(\vec{\rho},0)$, and $s(\vec{\rho})$. Moreover, we shall assume that $S_d\geqslant S_{\rm diff}$. In this case the diffraction spread of the image is small and the impulse response function $p(\vec{\rho})$ can be approximated by the delta function $p(\vec{\rho})=\lambda f\delta(\vec{\rho})$. Using these approximations we arrive at the following result:

$$\begin{aligned}\langle\Delta N_I^2(\vec{\rho},t)\rangle=&\,\eta S_d T_d s^2(\vec{\rho})G_\phi(\vec{\rho})\\ &\times[1-\eta+\eta(\cos^2\theta(\vec{\rho})\exp[2r(\vec{\rho})]\\ &+\sin^2\theta(\vec{\rho})\exp[-2r(\vec{\rho})])]\\ &+\eta\frac{S_d}{S_{\rm diff}}\frac{T_d}{2\pi}\int d\Omega|v(\vec{\rho},\Omega)|^2\\ &+\eta^2\frac{S_d}{S_{\rm diff}}\frac{T_d}{2\pi}\int d\Omega|v(\vec{\rho},\Omega)|^2\\ &\times[1+2|v(\vec{\rho},\Omega)|^2],\end{aligned} \tag{7.29}$$

where we have introduced the squeezing parameter $r(\vec{\rho})$ and the orientation angle $\theta(\vec{\rho})$ as [cf. Eqs. (4.22) and (4.23)]

$$\exp[\pm r(\vec{\rho})]=|u(\vec{\rho},0)|\pm|v(\vec{\rho},0)|, \tag{7.30}$$

$$\theta(\vec{\rho})=\arg[u(\vec{\rho},0)+v(\vec{\rho},0)]-\tfrac{1}{2}(\arg[u(\vec{\rho},0)] + \arg[v(\vec{\rho},0)]). \tag{7.31}$$

There are two shot-noise contributions in Eq. (7.29), proportional to the mean intensity of the amplified image and that of spontaneous parametric down conversion. The term proportional to $s^2(\vec{\rho})G_\phi(\vec{\rho})$ in Eq. (7.29) stems from the interference of the amplified signal with noise and the last term from self-interference of the noise. This self-interference gives the inherent noise of the amplifier, which is present even when there is no signal on its input.

C. Spatial width of the gain and conditions for noiseless amplification

Let us consider the mean number of photoelectrons given by Eq. (7.27). It consists of two terms: the first one gives the amplified signal while the second one describes the noise added by the amplifier. Introducing the angle $\phi(\vec{\rho})$ as

$$\phi(\vec{\rho})=\tfrac{1}{2}\,(\arg[u(\vec{\rho},0)]-\arg[v(\vec{\rho},0)]), \tag{7.32}$$

we can write the phase-sensitive gain $G_\phi(\vec{\rho})$ in terms of the squeezing parameter $r(\vec{\rho})$ defined in Eq. (7.30) and $\phi(\vec{\rho})$,

$$G_\phi(\vec{\rho})=\cos^2\phi(\vec{\rho})\exp[2r(\vec{\rho})] +\sin^2\phi(\vec{\rho})\exp[-2r(\vec{\rho})]. \tag{7.33}$$

Using the explicit expressions for $u(\vec{\rho},0)$ and $v(\vec{\rho},0)$ from Eq. (7.14), we can express the gain as a function of the dimensionless coupling strength g defined in Eq. (7.15) and the dimensionless mismatch $\delta(\vec{\rho},0)$ given by Eq. (7.16); in what follows we shall call $\delta(\vec{\rho},0)$ the local mismatch. In the case of real and positive g the result reads

$$G_\phi(\vec{\rho})=\frac{[(1+g)^2-\delta^2(\vec{\rho},0)]^2+4\,\delta^2(\vec{\rho},0)}{[1+\delta^2(\vec{\rho},0)-g^2]^2}. \tag{7.34}$$

The maximum gain, $G=G_\phi(\vec{R})$, is reached for such $\vec{\rho}=\vec{R}$ where the local mismatch is zero, $\delta(\vec{R},0)=\Delta/\kappa+(R/\rho_0)^2=0$, and is equal to

$$G=\left(\frac{1+g}{1-g}\right)^2. \tag{7.35}$$

Let us estimate the spatial width of the amplification region, that is, the transverse distance d at which the gain is equal to $G/2$. For this we first solve the equation $G_\phi(\vec{\rho})=G/2$ to determine the dimensionless mismatch δ_0 for which the gain is equal to one-half of its maximum value. In the interesting case of high gain, $G\gg 1$, i.e., when the dimensionless constant of parametric interaction is of the order of unity, $g\simeq 1$, we find this mismatch to be

$$\delta_0=2(\sqrt{2}-1)(1-g). \tag{7.36}$$

To estimate d we shall distinguish two different situations: zero detuning, $\Delta=0$, when the maximum amplification takes place for $\vec{R}=0$, and nonzero negative detuning, $\Delta=-|\Delta|\neq 0$, when the mismatch is nulled for some nonzero transverse distance $\vec{R}\neq 0$. In the case of zero detuning we obtain for d

$$d=\delta_0^{1/2}\rho_0, \tag{7.37}$$

with ρ_0 defined in Eq. (7.17). In the case of negative detuning the maximum gain is attained for a nonzero transverse distance R given by

$$R=\rho_0\sqrt{\frac{|\Delta|}{\kappa}}. \tag{7.38}$$

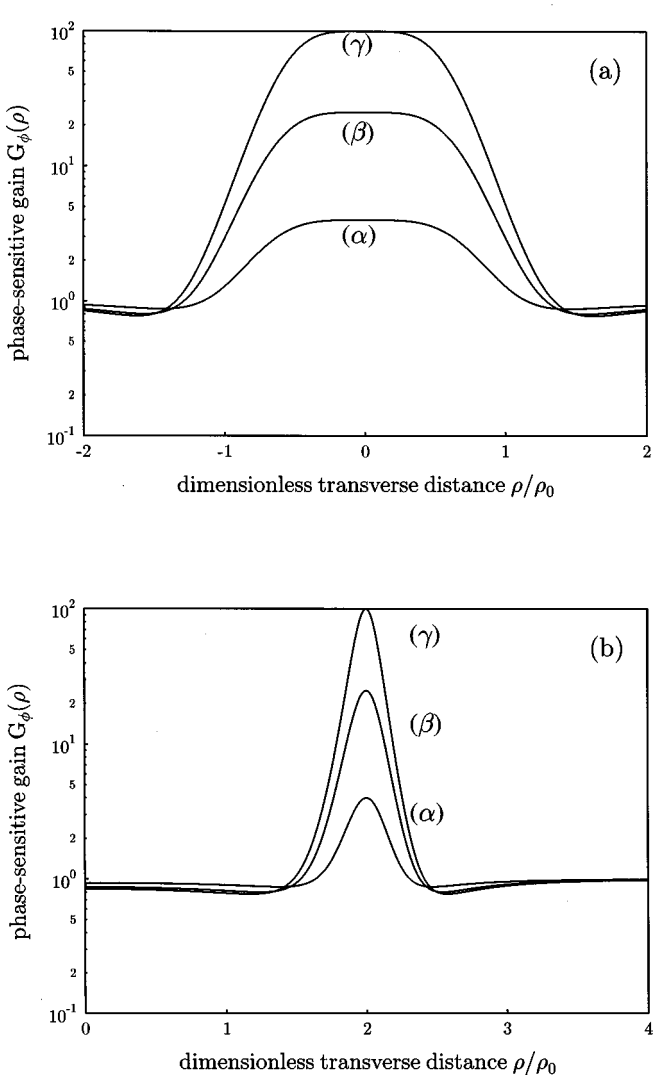

FIG. 20. Phase-sensitive gain $G_\phi(\vec{\rho})$ as a function of dimensionless transverse distance ρ/ρ_0 for exact resonance (a) and negative detuning $\Delta/\kappa=-2$ (b). Curves α, β, and γ correspond to the maximum gain of $G=4$, 25, and 100, respectively.

This means that in this case the region in which the amplification takes place has the shape of a ring with the inner radius $R-d/2$ and the outer radius $R+d/2$. From Eq. (7.36) and the definition of $\delta(\vec{\rho},0)$ given by Eq. (7.16) we obtain d as

$$d=2\,\delta_0\rho_0^2/R \tag{7.39}$$

for the case in which the ring radius is much larger than the width of its band, $R\gg d$.

Figure 20 shows the phase-sensitive gain $G_\phi(\vec{\rho})$ as a function of dimensionless distance ρ/ρ_0 for the case of exact resonance between the external signal and the cavity mode and for the case of negative detuning. Notice that in the case of zero detuning [Fig. 20(a)], there is a flat plateau in the gain curve around the point of maximum amplification, $\vec{\rho}=0$.

The two different situations of exact resonance between the external signal and the cavity mode and of negative detuning between them naturally distinguish

two possible operation regimes for the amplifier. In the case of zero detuning the amplification is performed in a "point-by-point" manner, i.e., amplifying one small region around the origin $\rho=0$ at a time. The input image can be scanned by shifting the input plane in the transverse direction. The amplification width d for this operation regime is given by Eq. (7.37). In the case of negative detuning, instead of moving the input plane one can keep it still while changing the cavity length, which controls the magnitude of the detuning $|\Delta|$. This will lead to varying of the radius R of the amplified ring [see Eq. (7.38)] and thus to the amplification of different ring-shaped stripes of the input image. The width of the stripe is given by Eq. (7.39).

As follows from Eq. (7.27), the mean number of photoelectrons, $\langle N_I(\vec{\rho},t)\rangle$, contains two contributions. The first one represents the amplified image, while the second term exists even without an input signal and comes from the inherent noise of the amplifier. Its physical origin is in the phenomenon of spontaneous parametric down conversion. This noise term determines the ultimate lower limit for the input signal $s(\vec{\rho})$ that can be amplified noiselessly. That is, the noise contribution must be small compared with the amplified signal. For a large gain, $G\gg 1$, from Eq. (7.27) we obtain the condition

$$s^2(\vec{\rho})S_{\rm diff}T_{\rm amp}\gg 1/4, \tag{7.40}$$

where we have introduced the typical temporal scale of the amplifier as $T_{\rm amp}=2\pi/\kappa$.

Another condition for noiseless amplification arises from Eq. (7.29) for dispersion of the observed number of photoelectrons. The self-interference term must be small compared with the term due to interference of the amplified signal with noise. This gives

$$s^2(\vec{\rho})S_{\rm diff}T_{\rm amp}\gg 1/8, \tag{7.41}$$

which as an order of magnitude estimate is equivalent to condition (7.40).

In the literature about amplifiers, the amount of extra noise added to the input signals is quantified by the noise figure F of the amplifier, which is defined as a ratio of the signal-to-noise ratios at its input and output (Thomas, 1969). We shall adopt this definition for our scheme of image amplification and introduce the noise figure as

$$F=\frac{R_O}{R_I}, \tag{7.42}$$

which in our case is a function of the transverse coordinate $\vec{\rho}$, $F=F(\vec{\rho})$. We shall refer to the case of $F=1$ as noiseless amplification.

It is easy to see that for an input signal in a coherent state the signal-to-noise ratio R_O in the object plane is

$$R_O=\eta S_d T_d s^2(\vec{\rho}). \tag{7.43}$$

Hence, if we assume that conditions (7.40) and (7.41) are met so that we can discard the noise terms in Eqs. (7.27) and (7.29), the noise figure at point $\vec{\rho}$ in the image plane is

$$F(\vec{\rho})=\frac{1-\eta+\eta(\cos^2\theta(\vec{\rho})\exp[2r(\vec{\rho})]+\sin^2\theta(\vec{\rho})\exp[-2r(\vec{\rho})])}{\cos^2\phi(\vec{\rho})\exp[2r(\vec{\rho})]+\sin^2\phi(\vec{\rho})\exp[-2r(\vec{\rho})]}. \tag{7.44}$$

From Eq. (7.44) one can see that if the angles $\theta(\vec{\rho})$ and $\phi(\vec{\rho})$ were equal, then for $\eta=1$ one would always have a unity noise figure, i.e., noiseless amplification for all $\vec{\rho}$. But this is not the case due to diffraction. Fortunately, as follows from the definitions of $u(\vec{\rho},0)$ and $v(\vec{\rho},0)$ [see Eq. (7.14)], they become real for $\delta(\vec{\rho},0)=0$, i.e., at the point of maximum amplification. Consequently our amplifier is noiseless at this point and in some region around it.

Figure 21 shows the noise figure $F(\vec{\rho})$ for ideal photodetection, $\eta=1$, and the same operative conditions as in Fig. 20. One can see from these figures that, indeed, the minimum of the noise figure, $F=1$, is reached at the point of maximum amplification. For zero detuning [Fig. 21(a)], the curve $F(\vec{\rho})$ has a flat plateau around the point of its minimum at $\vec{\rho}=0$. This corresponds to the plateau in the gain curve $G_\phi(\vec{\rho})$ [Fig. 20(a)]. This area is most favorable for noiseless amplification. The corresponding area in the case of nonzero detuning [Fig. 21(b)] is much smaller. This will require a smaller photodetection pixel and correspondingly more steps in scanning through the whole image.

From Eq. (7.44) we can also learn how rapidly the noise figure increases for nonideal photodetection, i.e., when $\eta<1$. For this we can fix the spatial point $\vec{\rho}=\vec{R}$, which gives the minimum noise figure, $F_{\rm min}=F(\vec{R})$, and investigate it as a function of quantum efficiency η. It follows from Eq. (7.44) that

$$F_{\rm min}=\frac{1-\eta+\eta G}{G}=\eta+\frac{1-\eta}{G}. \tag{7.45}$$

Equation (7.45) says that for a large gain, $G\gg 1$, the minimum noise figure is equal to η, i.e., can become less than unity for nonideal photodetection, $\eta<1$. Does this mean that we can improve the signal-to-noise ratio by linear amplification?

To answer this question we have to look at our definitions of F and R_O given by Eqs. (7.42) and (7.43). When defining the signal-to-noise ratio in the object plane, we assumed that the input image is detected by a nonideal array of pixels with $\eta<1$. Therefore the R_O in the input is deteriorated from the value achieved for ideal photodetection. A noiseless amplifier can compen-

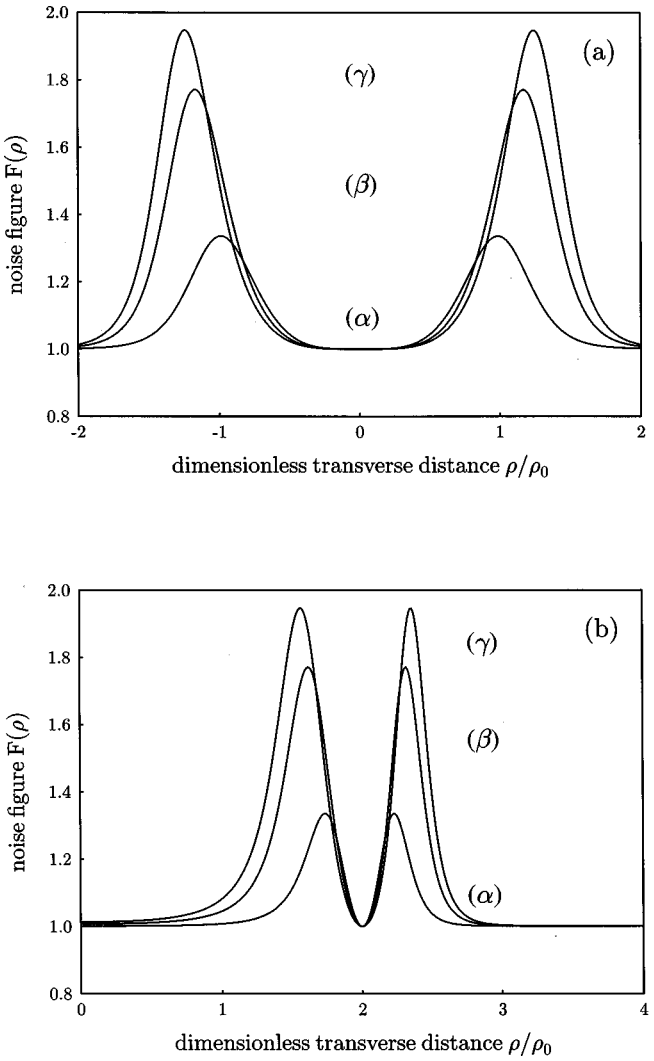

FIG. 21. Noise figure $F(\vec{\rho})$ for ideal photodetection, $\eta=1$, as a function of dimensionless transverse distance ρ/ρ_0: (a) exact resonance; (b) negative detuning $\Delta/\kappa=-2$. Curves α, β, and γ correspond to the maximum gain of $G=4$, 25, and 100, respectively.

sate for this deterioration and bring the R_I back to the value of R_O for $\eta=1$ (Levenson *et al.*, 1993a; 1993b).

Since the noise figure is intended to characterize only the noise added by the amplifier, it is more natural to use another definition of F, namely,

$$F'=\frac{R_O(\eta=1)}{R_I}. \tag{7.46}$$

This definition returns to R_O its "true" value, not deteriorated by nonideal photodetection. The new $F'(\vec{\rho})$ is given by Eq. (7.44) with an additional factor η in the denominator, and the corresponding $F'_{\min}$ is equal to

$$F'_{\min}=1+\frac{1-\eta}{\eta}\frac{1}{G}, \tag{7.47}$$

i.e., is always larger than unity.

Figure 22 shows $F'_{\min}(\eta)$ for three different gains, $G=4$, 25, and 100. We can see that for $G>25$ the minimum noise figure is almost insensitive to the quantum efficiency and stays very close to unity if η is larger than 10%.

To conclude this subsection we should like to summarize the results of our analysis. We have demonstrated two different ways of operating a noiseless image amplifier:

(1) "Point-by-point" operation, when a small area of size $\delta_0\rho_0^2$ of the image around the origin, $\vec{\rho}=0$, is amplified and the image is scanned by lateral shifting of the input plane.

(2) "Annular" operation, i.e., amplification of an annular region of width $2\delta_0\rho_0^2/R$, where R is the radius of the annulus; in this case the image is scanned by varying the cavity length that controls R.

In both kinds of operation the image is scanned. In this way the system might find applications, for example, in scanning microscopy (Wilson and Sheppard, 1984). In many other applications it would be advantageous to be able to amplify the whole image at once. For this one would have to abandon cavity-based geometry and use a traveling-wave configuration.

In Sec. VII.A we mentioned astronomy as a potential candidate (but by no means the only one) for application of a noiseless image amplifier. However, it appears that our scheme as it stands in the paper is not suited for astronomical imaging. The reason for this is the internal noise of the amplifier, which imposes severe limitations. Incidentally, such a conclusion about our scheme agrees with more general assessments of the noise limitations on image amplification in astronomy, made recently by Prasad (1994).

D. Experimental observation of quantum noise correlations in parametric image amplification

Parametric image amplification has been studied recently by several experimental groups.[8] In the experiments performed by Lantz's group, parametric image amplification was achieved for a monochromatic near-infrared image with a resolution of 60×80 points in the amplified image with a mean gain of 15 dB (Devaux *et al.*, 1995). Then the process of parametric amplification was applied for low-pass and bandpass spatial filtering of amplified images using the filtering properties of the transfer function of the amplifier (Devaux and Lantz, 1995a) and for ultrahigh-speed imaging (Devaux and Lantz, 1995b). Parametric amplification has also been employed in time-gated image recovery (Gavrielides, Peterson, and Gardimona, 1987; Wetterer, Schelonka, and Kramer, 1989) and in biomedical imaging (Cameron, Bliss, and Kimmel, 1996). Quantum fluctua-

[8]See, for example, Gavrielides, Peterson, and Gardimona, 1987; Wetterer, Schelonka, and Kramer, 1989; Guthals and Sox, 1990; Devaux *et al.*, 1995; Devaux and Lantz, 1995a, 1995b, 1995c; Cameron, Bliss, and Kimmel, 1996; Choi, Marable, and Kumar, 1997; Choi, Vasilyev, and Kumar, 1998; Marable, Choi, and Kumar, 1998.

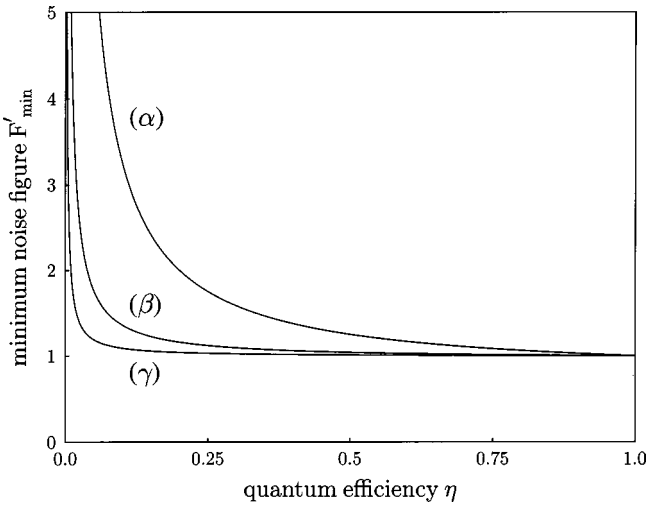

FIG. 22. Minimum noise figure $F'_{\min}$ as a function of quantum efficiency η for different gains. Curves α, β and γ correspond to the maximum gains of $G=4$, 25, and 100, respectively.

tions in parametric image amplification were studied by Guthals and Sox (1990) and in recent experiments by the group of Kumar (Choi, Marable, and Kumar, 1997; Choi, Vasilyev, and Kumar, 1998; Marable, Choi, and Kumar, 1998). In this subsection we shall describe the experiment by Kumar and collaborators (Marable, Choi, and Kumar, 1998), which, to our knowledge, gives the first experimental observation of quantum noise correlations in parametric image amplification. Recently this group has also reported the first experimental demonstration of noiseless image amplification (Choi, Vasilyev, and Kumar, 1998).

The layout of the experiment is depicted in Fig. 23. A 5.21-mm-long KTP crystal (the OPA) is pumped by a Q-switched, mode-locked, and frequency-doubled Nd:YAG laser. The IR (1064 nm) signal input and the green (532 nm) pump are each p polarized (parallel to the crystal z axis) for type-II phase matching in the crystal. The object is placed in the signal-beam path in front of the OPA. A real image of this object is formed in the center of the KTP crystal by a $\times 1$ telescope consisting of two 10-cm focal-length lenses. The spatial frequencies of this image are amplified by the pump beam, which is made coincident with the signal beam using a dichroic beamsplitter. The green pump is blocked after the crystal by using a filter that passes only the IR. CCD cameras are placed in the output image as well as the Fourier planes of a 20-cm focal-length lens that is placed after the filter. The generated idler is orthogonally polarized relative to the amplified signal because of type-II phase matching. Therefore a half-wave plate followed by a polarizing beamsplitter placed after the 20-cm lens allows us to observe either the signal or the idler output in the image as well as the Fourier planes by simply rotating the half-wave plate.

Typically, the phase-matching condition for the degenerate case, $q=0$, is fulfilled when the phase mismatch is $\Delta k \equiv k_p - k_s - k_i = 0$, where k_p is the wave number of the pump wave, and k_s and k_i are those of signal and

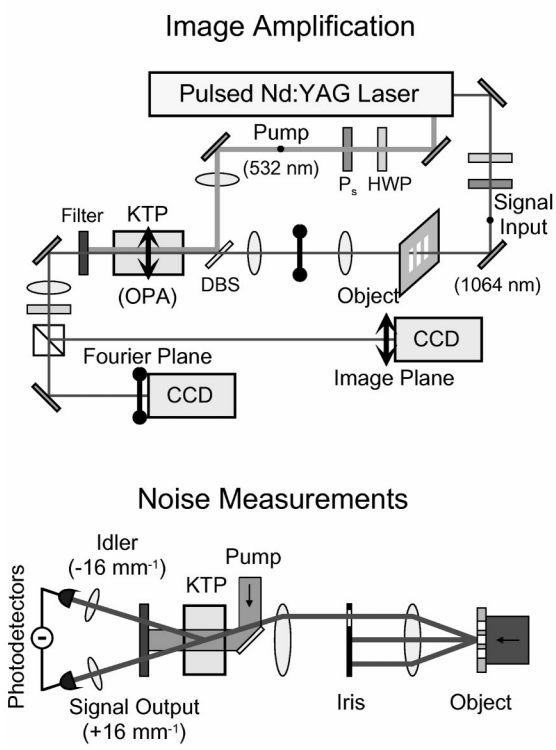

FIG. 23. Experimental layout for parametric image amplification (top) and measurement of quantum-noise correlations (bottom). (From Marable, Choi, and Kumar, 1998.)

idler waves. However, the effective phase mismatch for a spatial frequency $\vec{q}$ in a paraxial approximation is equal to [cf. Eqs. (4.28) and (4.29)]

$$\Delta k_{\text{eff}}(q) = \Delta k + \frac{q^2}{k_s} \tag{7.48}$$

for $k_i = k_s$. Therefore, by making Δk progressively more and more negative, one can bring increasingly higher spatial frequencies into the phase-matching condition, i.e., into the amplification region. In practice, Δk is adjusted by the rotation of the KTP crystal of the OPA with respect to the incident signal and pump field such that $\Delta k_{\text{eff}}(q_0)=0$. In this case, the OPA acts as a bandpass amplifier, amplifying a range of spatial frequencies around the spatial frequency q_0. In such a way one can maximize phase matching, and hence the quantum correlations, for a given value of the spatial frequency q_0.

For parametric image amplification, Marable *et al.* used a negative test pattern of three vertical lines with a uniform spacing of 62.5 μm (16 lines/mm). The horizontal Fourier transform of this object consists of three main peaks at $\xi = 0, \pm 16$ mm^{-1} ($\xi = q/2\pi$) with two smaller peaks in between at $\xi = \pm 8$ mm^{-1}. As recorded in the output image plane, real images of the bare signal (i.e., with the pump turned off), the amplified signal, and the generated idler are shown in Fig. 24(a) for an OPA gain of $\simeq 1.2$. The transverse pattern of the bare signal as recorded in the output Fourier plane is shown in Fig. 24(b). Figure 24(c) shows the transverse pattern of the

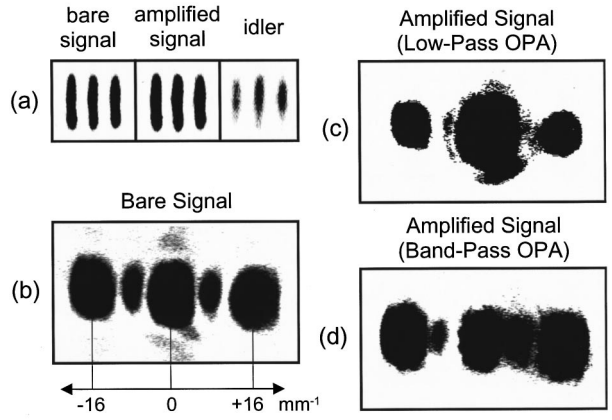

FIG. 24. Parametric amplification of a test pattern: (a) Bare signal, amplified signal, and idler patterns in the output image plane; (b) bare signal pattern in the output Fourier plane; (c) amplified signal pattern in the output Fourier plane with the OPA aligned for low-pass amplification; (d) same as in (c) but with the OPA aligned for bandpass amplification. (From Marable, Choi, and Kumar, 1998.)

amplified signal in the output Fourier plane when the OPA was aligned in the low-pass configuration ($\Delta k = 0$), and the pump power was adjusted for a gain of $\simeq 4$. As shown, the central peak ($\xi = 0$) was strongly amplified with little amplification occurring at the side peaks ($\xi = \pm 16\,\mathrm{mm}^{-1}$). The transverse pattern in the output Fourier plane for bandpass amplification with $\Delta k = -0.95$ rad/mm is shown in Fig. 24(d). Here, the pump power was the same as in Fig. 24(c) and the OPA was aligned for maximum amplification of the two side peaks at $\pm 16\,\mathrm{mm}^{-1}$.

For the measurement of quantum correlations, the goal of Marable, Choi, and Kumar was to observe noise reduction at a single spatial frequency. The OPA was first optimized for maximum gain by aligning the signal and idler patterns to be simultaneously coincident in both the real-image and the Fourier planes. By placing an iris in the Fourier plane, that is, in front of the OPA (halfway between the two lenses of the $\times 1$ telescope), they blocked all spatial frequency components of the input signal pattern except the peak centered at $\xi = +16\,\mathrm{mm}^{-1}$. Thus the input signal had a well-defined spatial frequency. The OPA was adjusted for maximum gain at $\pm 16\,\mathrm{mm}^{-1}$, corresponding to an azimuthal rotation of the KTP crystal of about 0.85° from the angle for phase matching at $\xi = 0$. In this way the input signal Fourier component was bandpass amplified, and a conjugate Fourier component at $\xi = -16\,\mathrm{mm}^{-1}$ of the idler beam was generated. Since the amplified signal Fourier component at $+16\,\mathrm{mm}^{-1}$ exited the OPA at an angle of $2 \times 17 = 34$ mrad with respect to the idler Fourier component at $-16\,\mathrm{mm}^{-1}$, it was easy to separate the two with the use of plane mirrors. The mirror that sent the beams to the CCD cameras was removed, and each beam was focused onto a separate photodetector located in the far field (i.e., in the Fourier plane). Therefore one detector saw the amplified signal Fourier component at $+16$ mm^{-1}, while the other detected the idler component at -16 mm^{-1}. Twin-beam-type noise measurements were made using direct difference detection, similar to the measurements described by Aytür and Kumar (1990). The noise power of the photocurrent difference was measured at 27 MHz with a 3-MHz resolution bandwidth.

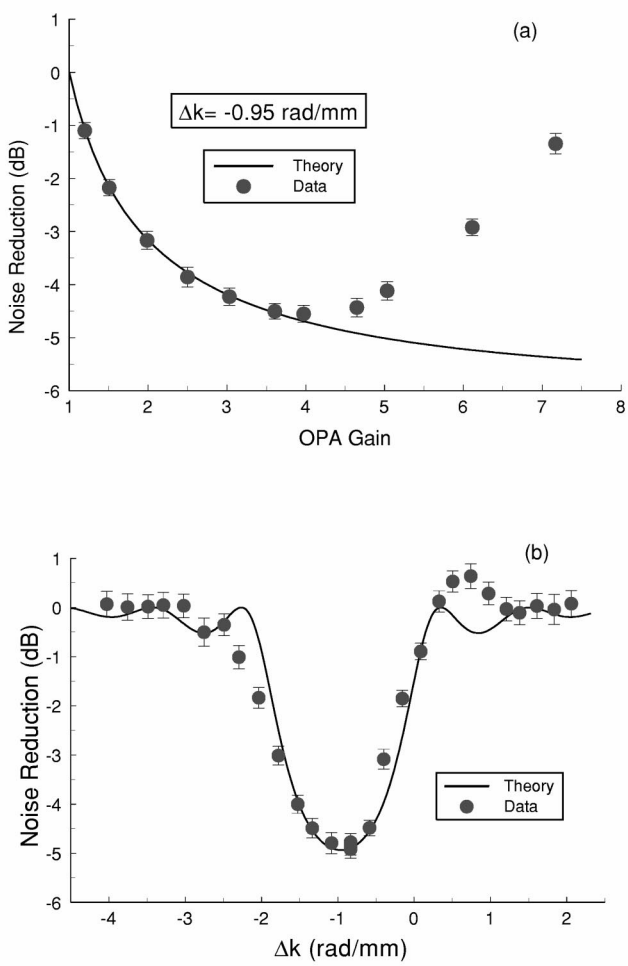

FIG. 25. Noise reduction as a function of (a) OPA gain and (b) phase mismatch Δk. (From Marable, Choi, and Kumar, 1998.)

Figure 25(a) shows the quantum-noise reduction below the shot-noise level for the detected signal and idler Fourier components as a function of the signal gain. For OPA gains below $\simeq 4$, the data are in good agreement with the theory (solid curve; Gavrielides, Peterson, and Gardimona, 1987) once a detection quantum efficiency of 0.76 is taken into account. Marable, Choi, and Kumar also measured the quantum-noise reduction as a function of the phase mismatch Δk for various values of the OPA gain. Results from one set of data for an OPA gain of $\simeq 3.9$ are shown in Fig. 25(b). As pointed out previously, Δk was varied by rotating the azimuthal angle of the KTP crystal in the OPA. The micrometer readings on the KTP rotation stage were calibrated and converted into units of Δk for comparison with the theory. As one can see, the experimental data are once again in good agreement with the theory (solid curve), once the detection quantum efficiency is taken into account.

VIII. OPTICAL IMAGING WITH MULTIMODE SQUEEZED LIGHT

A. Description of the optical scheme and observables

The question of noise limitations in optical imaging and image processing has been addressed by many authors. In particular, it has been repeatedly pointed out that incoherent imaging is preferable to coherent with respect to noise (Chavel and Lowenthal, 1978; Yu, 1985). Incoherent or partially coherent imaging is performed using either a spatially coherent point source with a broad linewidth (temporal incoherence) or a monochromatic light source of a finite size (spatial incoherence). Here we shall consider the latter situation, called *spatially partially coherent* (SPC) illumination.

Under SPC illumination each point of the extended light source, called a *channel*, produces an object image at the image plane. The coherent illumination corresponds to a point source, i.e., one channel. A large source with infinitely many channels gives another extreme, namely, spatially incoherent illumination. A typical SPC light source corresponds to a finite but large number of channels.

As shown by Chavel and Lowenthal (1978), the noise performance of an optical system employing SPC illumination depends on the nature of the noise. If the noise is present in the input, then all channels carry the same noise and there is no gain in using several channels. If the noise does not depend on the input, but is inherent to each channel, then the gain is equal to the square root of the number of channels. Chavel and Lowenthal analyzed two different kinds of technical noise in the scheme: the setup noise concentrated in the pupil of the system and the input noise such as impulse noise or granularity noise of the object.

The noise limitations of optical SPC systems due to quantum fluctuations of light were investigated by Kolobov (1995). Quantum fluctuations of light give an ultimate noise performance in optical imaging and image processing. One has to take quantum fluctuations into account in the case of photon-limited or low-light-level images. Such images arise in many different areas, for example, astronomy or low-light-level spectroscopy. In optical computing, processing information at a low light level will increase the speed of computation. In addition to these naturally quantum-limited situations, one can encounter photon-limited processing even if there is an abundance of light. Often only a sparse sampling (i.e., a small number of detected photons) of the input image is needed for processing (Morris, 1989).

An example is real-time machine vision. In this case one digitizes the input image using a two-dimensional photodetection array such as a CCD camera. For an array with dimensions, say, 1000×1000 elements, one has to process the information from a million pixels. This is too much information for processing in real time even for large computers. Therefore one usually tries to reduce the amount of information by using, for example, edge-enhanced images. An alternative approach would be to process low-light-level images. In this case one would collect photoelectrons with the maximal counting rate allowed by the system until there was enough information about the input image to achieve an acceptable signal-to-noise level.

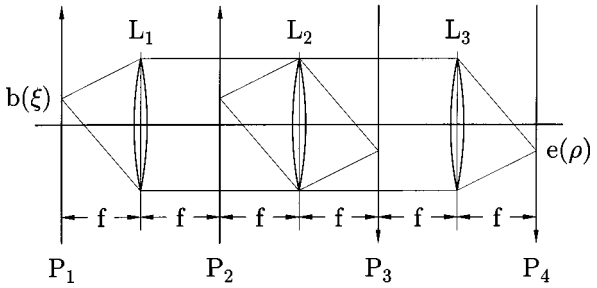

FIG. 26. Schematic diagram of an optical processor with a spatially partially coherent source of light. Object transparency located in the object plane P_2 is imaged in the image plane P_4 by lenses L_2 and L_3. The source plane P_1 is the output plane of a traveling-wave optical parametric amplifier (OPA) or another source of spatially squeezed light. This source is imaged in the Fourier plane P_3 by lenses L_1 and L_2.

In this section we shall give the standard quantum limit for SPC imaging with coherent light. Then we shall demonstrate that by employing multimode squeezed light for SPC illumination one can go beyond this limit. As the source of multimode squeezed light we shall consider the traveling-wave OPA, investigated in Sec. IV. We already know that in homodyne detection of multimode squeezed light by a CCD camera with a properly chosen size of pixels we can obtain simultaneously many sub-Poissonian photocurrents from individual pixels. Using the aforementioned terminology with channels, we can say that such a source has several ''quantum'' channels and each channel produces an object image with fluctuations below the shot-noise level. Since these quantum channels are independent, we may expect an improvement in noise performance employing a source with many channels. We shall see from the calculations that this physical picture is indeed correct.

Let us consider the schematic setup of an optical processor with an SPC source of squeezed light (Fig. 26). In the object plane P_2 there is an object transparency with the amplitude transmission $\tau(\vec{\rho})$; $\vec{\rho}$ is a transverse coordinate in the object and the image planes. This transparency is imaged in the image plane P_4 by lenses L_2 and L_3. All optical intervals in the scheme are chosen to be the same and equal to the focal length of the lenses. Therefore, with suitable axis orientation (see Fig. 26), the illuminating and imaging magnifications are $M=+1$.

We assume that the source plane P_1 is the output plane of a traveling-wave OPA. To have the possibility of changing the spatial coherence of the source we shall assume that there is an aperture of a variable area S_s in the source plane P_1. The shape of the aperture is determined by the source frame function $S(\vec{\xi})$ equal to one in the aperture and zero elsewhere; $\vec{\xi}$ is a transverse coordinate in the source and the Fourier planes. The source

is imaged in the Fourier plane P_3 by lenses L_1 and L_2.

In the Fourier plane P_3 we place a pupil of area S_p. Its form is defined by the pupil frame function $P(\vec{\xi})$ equal to one in the pupil and zero elsewhere.

In the literature about optical image processing (Chavel and Lowenthal, 1978; Yu, 1985), a typical quantity of interest is the image irradiance $I_i(\vec{\rho},t)$ in the image plane P_4, equal to the photon flux density. Its quantum-mechanical counterpart is the corresponding quantity for describing the quantum noise properties of the system. The quantum-mechanical mean value $\langle I_i(\vec{\rho},t)\rangle$ of the image irradiance is a signal of the scheme. Its variance, $\sigma_i^2(\vec{\rho},t)=\langle \Delta I_i^2(\vec{\rho},t)\rangle$, characterizes the noise properties of the processor, and a signal-to-noise ratio is given by $R_i(\vec{\rho},t)=\langle I_i(\vec{\rho},t)\rangle/\sigma_i(\vec{\rho},t)$ (Goodman, 1985; Yu, 1985). Below we shall express the signal-to-noise ratio for the image irradiance as a function of the illuminating and imaging aperture areas S_s and S_p for a given source of spatially multimode squeezed light.

For simplicity we shall explicitly consider only the spatial dependence of the fields. Let $b(\vec{\xi})$ and $b^\dagger(\vec{\xi})$ be the photon annihilation and creation operators in the source plane normalized so that $\langle I_s(\vec{\xi})\rangle=\langle b^\dagger(\vec{\xi})b(\vec{\xi})\rangle$ is the mean value of the source irradiance at point $\vec{\xi}$ in the source plane. The mean value of the image irradiance is given by the theory of partial coherence (Born and Wolf, 1964),

$$\langle I_i(\vec{\rho})\rangle=\frac{1}{\lambda f}\int d\vec{\xi}\, S(\vec{\xi})|h(\vec{\rho},\vec{\xi})|^2\langle I_s(\vec{\xi})\rangle, \tag{8.1}$$

where f is the focal length of the lenses, λ is the wavelength of the light, and $S(\vec{\xi})$ is the source frame function introduced above. The function

$$h(\vec{\rho},\vec{\xi})=\frac{1}{\lambda f}\int d\vec{\rho}\,'\,\tau(\vec{\rho}\,')p(\vec{\rho}-\vec{\rho}\,')\exp\left[-i\,\frac{2\pi}{\lambda f}\,\vec{\xi}\cdot\vec{\rho}\,'\right] \tag{8.2}$$

is the normalized complex amplitude at point $\vec{\rho}$ in the image plane due to point $\vec{\xi}$ in the source plane. The function $p(\vec{\rho})$ in Eq. (8.2) is the Fourier transform of the pupil frame function $P(\vec{\xi})$,

$$p(\vec{\rho})=\frac{1}{\lambda f}\int d\vec{\xi}\,P(\vec{\xi})\exp\left[-i\,\frac{2\pi}{\lambda f}\,\vec{\rho}\cdot\vec{\xi}\right], \tag{8.3}$$

and is called the *coherent impulse response* of the imaging system (Goodman, 1985; Yu, 1985).

The variance of the image irradiance can be obtained using Eq. (8.1) together with a formula similar to Eq. (3.4) for the correlation function of the photocurrent density:

$$\begin{aligned}\langle \Delta I_i^2(\vec{\rho})\rangle=\frac{1}{(\lambda f)^2}\int d\vec{\xi}\int d\vec{\xi}\,' S(\vec{\xi})S(\vec{\xi}\,')|h(\vec{\rho},\vec{\xi})|^2\\ \times|h(\vec{\rho},\vec{\xi}\,')|^2(\langle I_s(\vec{\xi})\rangle\delta(\vec{\xi}-\vec{\xi}\,')\\ +[\langle{:}I_s(\vec{\xi})I_s(\vec{\xi}\,'){:}\rangle-\langle I_s(\vec{\xi})\rangle\langle I_s(\vec{\xi}\,')\rangle]).\end{aligned} \tag{8.4}$$

From Eq. (8.4) we can see that there are two contributions to the variance of the image irradiance. In the first one we recognize the shot noise, and in the second (in square brackets) the contribution from the spatial intensity correlation function. From Eq. (8.4) it is easy to see that the standard quantum limit for the image irradiance is given by [cf. Eq. (3.15)]

$$R_{\mathrm{SQL}}=\langle I_i(\vec{\rho})\rangle^{1/2}. \tag{8.5}$$

This limit is expected for a coherent state of light. Any other classical light will result in a positive contribution from the intensity correlation term. However, if the light emitted by the source is in a nonclassical, for instance, squeezed state, the contribution from the intensity correlation term can be negative and can partially or even completely compensate for the shot-noise term.

B. Quantum fluctuations in optical imaging with multimode squeezed light

Let us consider the situation when the source field operator $b(\vec{\xi})$ has the form

$$b(\vec{\xi})=\alpha+\delta b(\vec{\xi}), \tag{8.6}$$

where α is the c-number complex amplitude of a strong plane wave (local oscillator) and $\delta b(\vec{\xi})$ is a "small" operator-valued fluctuation in the source plane. The assumption that the source plane P_1 is the output plane of the traveling-wave OPA allows us to use the results from Sec. IV. As shown there, the spatial Fourier amplitudes,

$$\delta b(\vec{q})=\int d\vec{\xi}\,e^{-i\vec{q}\cdot\vec{\xi}}\delta b(\vec{\xi}), \tag{8.7}$$

on the output of the OPA are expressed through the corresponding Fourier amplitudes $\delta a(\vec{q})$ on its input surface as

$$\delta b(\vec{q})=U(\vec{q})\,\delta a(\vec{q})+V(\vec{q})\,\delta a^\dagger(-\vec{q}), \tag{8.8}$$

with coefficients $U(\vec{q})$ and $V(\vec{q})$ given by Eq. (4.3) for $\Omega=0$.

Using Eqs. (8.6)–(8.8), we can write the correlation function of the intensity fluctuations from Eq. (8.4) as

$$\langle{:}I_s(\vec{\xi})I_s(\vec{\xi}\,'){:}\rangle-\langle I_s(\vec{\xi})\rangle\langle I_s(\vec{\xi}\,')\rangle=|\alpha|^2\Gamma_\theta(\vec{\xi}-\vec{\xi}\,'), \tag{8.9}$$

with $\Gamma_\theta(\vec{\xi}-\vec{\xi}\,')$ given by

$$\Gamma_\theta(\vec{\xi}-\vec{\xi}\,')=\frac{1}{(2\pi)^2}\int d\vec{q}\,\exp[i\vec{q}\cdot(\vec{\xi}-\vec{\xi}\,')]\Gamma_\theta(\vec{q}), \tag{8.10}$$

$$\begin{aligned}\Gamma_\theta(\vec{q})=-1+(\exp[2r(\vec{q})]\cos^2\theta(\vec{q})\\ +\exp[-2r(\vec{q})]\sin^2\theta(\vec{q})),\end{aligned} \tag{8.11}$$

$$\exp[\pm r(\vec{q})]=|U(\vec{q})|\pm|V(\vec{q})|,$$

$$\theta(\vec{q})=\tfrac{1}{2}\arg[U(\vec{q})V(-\vec{q})]-\varphi, \tag{8.12}$$

where $\varphi=\arg\alpha$. The function $\Gamma_\theta(\vec{q})$ in Eq. (8.11) is the squeezing spectrum for multimode squeezed light ex-

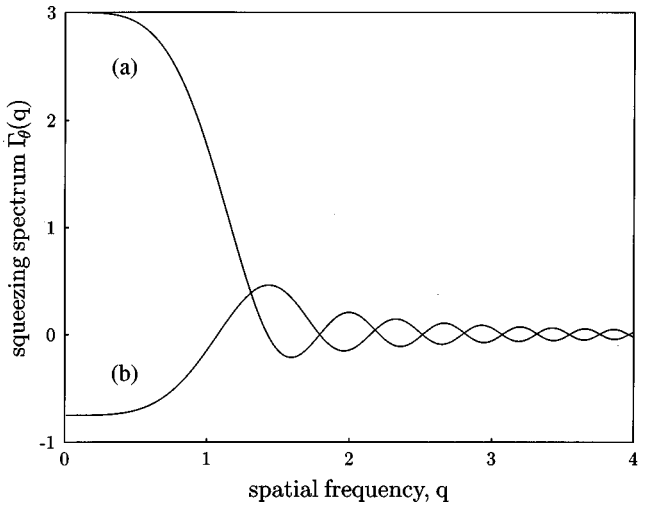

FIG. 27. Normalized spatial-frequency squeezing spectrum $\Gamma_\theta(q)$ for a traveling-wave OPA. Curve (a) gives the stretching spectrum, $\Gamma_+(q)$: curve (b) is for the squeezing spectrum, $\Gamma_-(q)$. The OPA phase-sensitive gain is $\exp(2r_m)=4$. The spectrum is normalized so that $\Gamma_\theta(q)=0$ for a coherent state and $\Gamma_\theta(q)=-1$ for a perfectly squeezed state. The spatial frequency q is in units of $(S_m)^{-1/2}$.

pressed as a function of the spatial frequency $\vec{q}$ and normalized so that $\Gamma_\theta(\vec{q})=0$ for a coherent state and $\Gamma_\theta(\vec{q})=-1$ for a perfectly squeezed state [cf. Eq. (4.25)]. The functions $r(\vec{q})$ and $\theta(\vec{q})$ defined by Eq. (8.12) are the squeezing parameter and the orientation angle of the squeezing ellipse relative to the complex amplitude α.

Maximum squeezing occurs at the spatial frequency q_m for which the phase mismatch is zero and the squeezing parameter $r(q)$ reaches its maximum value r_m (see Sec. IV.C). Choosing $\theta(q_m)=\pm\pi/2$ gives the noise spectrum $\Gamma_-(q)$ (squeezing spectrum), and $\theta(q_m)=0,\pi$ gives the noise spectrum $\Gamma_+(q)$ (stretching spectrum). At the spatial frequency q_m, we have

$$\Gamma_-(q_m)=-1+\exp[-2r_m],\quad \Gamma_+(q_m)=-1+\exp[2r_m], \tag{8.13}$$

i.e., reduction or increase of the noise compared with a coherent state of light. For $q_m=0$, which corresponds to degenerate matching, the spectra $\Gamma_\pm(q)$ are shown in Fig. 27.

For simplicity, we shall assume that the amplitude transmission of the object transparency $\tau(\vec{\rho})$ is a slowly varying function in space compared with the impulse response $p(\vec{\rho})$ from Eq. (8.3). In this case, as follows from Eqs. (8.2) and (8.3), the normalized complex amplitude $h(\vec{\rho},\vec{\xi})$ is

$$h(\vec{\rho},\vec{\xi})=\tau(\vec{\rho})P(\vec{\xi})\exp\left[-i\frac{2\pi}{\lambda f}\vec{\rho}\cdot\vec{\xi}\right], \tag{8.14}$$

i.e., it represents a replica of the object amplitude transmittance $\tau(\vec{\rho})$ multiplied by the pupil frame function $P(\vec{\xi})$ and phase shifted by the skew illumination. From Eqs. (8.1), (8.4), (8.9), and (8.14) the mean irradiance $\langle I_i(\vec{\rho})\rangle$ and its variance $\langle\Delta I_i^2(\vec{\rho})\rangle$ read

$$\langle I_i(\vec{\rho})\rangle=\frac{|\tau(\vec{\rho})|^2|\alpha|^2}{\lambda f}\int d\vec{\xi}\,S_{\min}(\vec{\xi})=\frac{|\tau(\vec{\rho})|^2|\alpha|^2}{\lambda f}S_{\min}, \tag{8.15}$$

$$\langle\Delta I_i^2(\vec{\rho})\rangle=\frac{|\tau(\vec{\rho})|^4|\alpha|^2}{(\lambda f)^2}\left[\int d\vec{\xi}\,S_{\min}(\vec{\xi})+\int d\vec{\xi}\int d\vec{\xi}\,'S_{\min}(\vec{\xi})S_{\min}(\vec{\xi}\,')\Gamma_\theta(\vec{\xi}-\vec{\xi}\,')\right], \tag{8.16}$$

where $S_{\min}(\vec{\xi})=S(\vec{\xi})P(\vec{\xi})$ and $S_{\min}=\min(S_s,S_p)$ is the smallest of the source and pupil apertures. Let us introduce the dimensionless spatial coordinate $\vec{x}$ as $\vec{\xi}=(S_{\min})^{1/2}\vec{x}$, and the dimensionless spatial frequency $\vec{\kappa}$ as $\vec{q}=(S_m)^{-1/2}\vec{\kappa}$, where S_m is the minimum photodetection area introduced in Sec. IV.C. As discussed there, this area gives the size of the smallest photodetector from which one can collect photocurrent with the subshot-noise fluctuations. In terms of the dimensionless variables $\vec{x}$ and $\vec{\kappa}$, Eq. (8.16) can be written as

$$\langle\Delta I_i^2(\vec{\rho})\rangle=\frac{|\tau(\vec{\rho})|^4|\alpha|^2}{(\lambda f)^2}S_{\min}[1+F_\theta(\mu)], \tag{8.17}$$

where $\mu=(S_{\min}/S_m)^{1/2}$ and the function $F_\theta(\mu)$ is

$$F_\theta(\mu)=\frac{1}{(2\pi)^2}\int d\vec{\kappa}\,\Gamma_\theta(\vec{\kappa}/\mu)|S_{\min}(\vec{\kappa})|^2,$$

$$S_{\min}(\vec{\kappa})=\int d\vec{x}\,e^{i\vec{\kappa}\cdot\vec{x}}S_{\min}(\vec{x}). \tag{8.18}$$

Equations. (8.17) and (8.18) express the variance $\langle\Delta I_i^2(\vec{\rho})\rangle$ as a function of the source and pupil aperture areas, S_s and S_p, and the area S_m.

The function $F_\theta(\mu)$ in general can be computed numerically for a given geometry of the source and pupil apertures and for a given light source. Two limiting cases can be evaluated analytically. When $\mu\gg1$, i.e., $S_{\min}\gg S_m$, the function $F_-(\mu)$, which is equal to

$$F_-(\mu)|_{\mu\gg1}=-1+e^{-2r_m}, \tag{8.19}$$

can be very close to -1 for $\exp[-2r_s]\ll1$. As follows from Eq. (8.17), in this case the contribution from $F_-(\mu)$ to $\langle\Delta I_i^2(\vec{\rho})\rangle$ almost compensates for the shot-noise fluctuations and brings an improvement in the signal-to-noise ratio.

In the opposite limit, $\mu\ll1$ ($S_{\min}\ll S_m$),

$$F_\theta(\mu)|_{\mu\ll1}=\mu^2\frac{1}{(2\pi)^2}\int d\vec{\kappa}\,\Gamma_\theta(\vec{\kappa})\ll1. \tag{8.20}$$

Therefore, when the area S_m is very large compared to the area of illuminating and imaging apertures, the contribution from $F_\theta(\mu)$ into $\langle\Delta I_i^2(\vec{\rho})\rangle$ is negligible compared with the shot noise and there is no advantage of using squeezed light for the signal-to-noise ratio.

For the circular illuminating and imaging apertures, $F_\theta(\mu)$ has the form

$$F_\theta(\mu)=2\int_0^\infty\frac{dx}{x}J_1^2(x\mu/\sqrt{\pi})\Gamma_\theta(x), \tag{8.21}$$

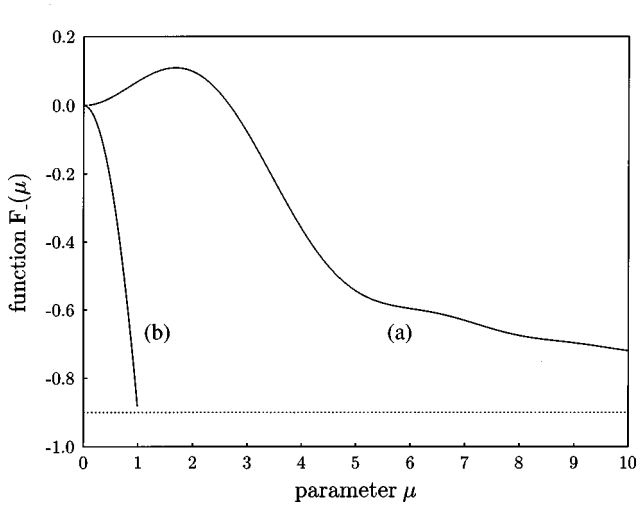

FIG. 28. The function $F_\theta(\mu)$ defined by Eq. (8.18) for multimode and single-mode squeezed light: (a) $F_-(\mu)$ for circular illuminating and imaging apertures [see Eq. (8.21)] and for a traveling-wave OPA with the phase-sensitive gain $\exp(2r_m)=10$; (b) $F_-(\mu)$ for a traveling-wave OPA with the same gain but only one transverse spatial mode, $\vec{q}=0$. The dotted line shows the minimum of $F_-(\mu)$ that can be reached for these two sources with such a gain. It is realized for $\mu\to\infty$ in case (a) and $\mu=1$ in case (b).

where J_1 is a first-order Bessel function of the first kind. Figure 28(a) shows the result of computation of $F_-(\mu)$ for a traveling-wave OPA. In this case the parameter μ is

$$\mu=2\pi r/\sqrt{\lambda l}, \tag{8.22}$$

where r is the radius of the smallest of the illuminating and imaging apertures and l is the length of the crystal used in the OPA.

C. Noise performance of an optical image processor with single-mode and multimode squeezed light

It is interesting to compare the variance $\langle\Delta I_i^2(\vec{\rho})\rangle$ for multimode squeezed light given by Eq. (8.17) with the result that can be obtained using single-mode squeezed light. Such light can be generated, for example, by a cavity OPA with a single transverse spatial mode, $\vec{q}=0$. In this case the cavity plays the role of a narrow-band spatial filter that selects one single mode from a continuum of spatial modes of the traveling-wave OPA. Assuming that the spectrum of this filter is $H(\vec{q})=(2\pi)^2\delta(\vec{q})/S_s$ and substituting it into the integrand in Eq. (8.10), we obtain the correlation function $\Gamma_-(\vec{\xi}-\vec{\xi}')$ for single-mode squeezed light,

$$\Gamma_-(\vec{\xi}-\vec{\xi}')=(-1+\exp[-2r_m])/S_s. \tag{8.23}$$

It is easy to see that the variance $\langle\Delta I_i^2(\vec{\rho})\rangle$ for such a source is still given by Eq. (8.17) with $F_-(\mu)$ equal to

$$F_-(\mu)=\mu^2(-1+\exp[-2r_m]), \tag{8.24}$$

with the following parameter μ:

$$\mu=(S_{\min}/S_s)^{1/2}=\begin{cases}(S_p/S_s)^{1/2}, & \text{if } S_p<S_s,\\ 1, & \text{if } S_p>S_s.\end{cases} \tag{8.25}$$

Therefore in this case the parameter μ is restricted to the interval $0\leqslant\mu\leqslant 1$. The optimum value of the variance $\langle\Delta I_i^2(\vec{\rho})\rangle$ is obtained for $\mu=1$ and is equal to that obtained with multimode squeezed light for $\mu\gg 1$. For $\mu<1$ the behavior of the variance $\langle\Delta I_i^2(\vec{\rho})\rangle$ for the single-mode source given by Eqs. (8.17) and (8.24) is the same as for nonideal detection of squeezed light by a detector with the quantum efficiency $\eta=\mu^2$. Figure 28(b) shows $F_-(\mu)$ for single-mode squeezed light.

Note that the discussed situation of a single spatial mode with $\vec{q}=0$ corresponds to a normal illumination of the source plane P_1 by a plane wave. In this case only one point, namely, the diffraction-limited spot, illuminates the object in the plane P_2. The whole image can be reconstructed either by scanning the object or by tilting the illuminating plane wave. This should be considered not as a practical method of realization but rather as an illustration of the difference between the single-mode and multimode cases.

Let us consider the signal-to-noise ratio for a light source of coherent and squeezed light as a function of the spatial coherence of the source. As mentioned above, under SPC illumination the image of the object is created by several channels of the source. The number of channels, or the *space bandwidth product* N_s defined by a source of area S_s and an object of area S_o, is equal to (Chavel and Lowenthal, 1978; Yu, 1985)

$$N_s=S_oS_s/\lambda^2f^2. \tag{8.26}$$

The number of channels that eventually contribute to the output image is constrained by the pupil area S_p and is given by the space bandwidth product N_p of the optical system,

$$N_p=S_oS_p/\lambda^2f^2. \tag{8.27}$$

The ratio between space bandwidth products of the source and the system,

$$c=\frac{N_s}{N_p}, \tag{8.28}$$

gives the *spatial coherence parameter* c for the optical system. A strictly coherent light source can be considered as a source with one channel, $N_s=1$. Then, from Eq. (8.28), we obtain for the spatial coherence parameter of such a source $c=N_p^{-1}$. Since N_p is usually as large as 10^6 or more, for a spatially coherent source we have $c\ll 1$. As this increases to infinity an extremely incoherent illumination results. A typical range of c for an SPC source is $0.2\leqslant c\leqslant 0.7$ (Yu, 1985).

Since we are interested in the comparison of a partially coherent to a coherent system, let us define the gain G in signal-to-noise ratio R as a ratio between R for a source with N_s channels and that for a source with one channel, $N_s=1$, in a coherent state,

$$G(c)=R(N_s)/R(N_s=1,\ \text{coherent state}). \tag{8.29}$$

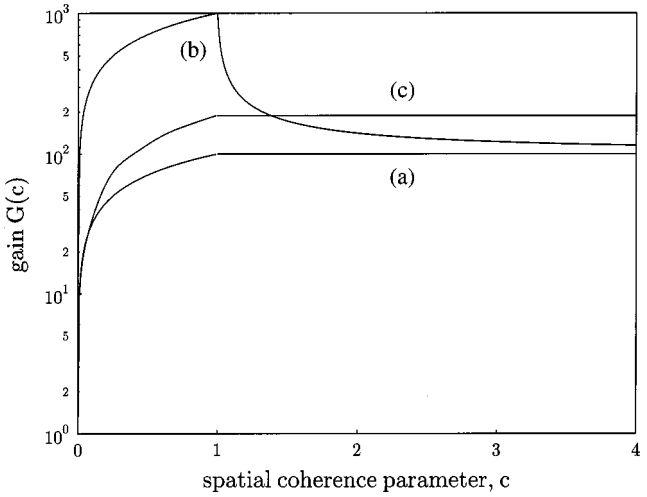

FIG. 29. The signal-to-noise ratio gain $G(c)$ between spatially partially coherent and strictly coherent illumination as a function of the spatial coherence parameter c: (a) a source in a coherent state; (b) a single-mode traveling-wave OPA; (c) a multimode traveling-wave OPA with the same gain. The space bandwidth product is $N_p=10^4$ and the phase-sensitive gain of the OPA is $\exp(2r_m)=10$. For curve (c) the ratio $S_p/S_m=10^2$.

It is interesting to compare this gain as a function of c for an SPC source in a coherent state, a single-mode squeezed state, and a multimode squeezed state.

From Eqs. (8.15) and (8.17) with only the shot-noise contribution we obtain $G(c)$ for the SPC source in a coherent state

$$G(c)=\begin{cases}\sqrt{cN_p}, & \text{if } N_p^{-1}\leqslant c\leqslant 1,\\ \sqrt{N_p}, & \text{if } c>1.\end{cases} \tag{8.30}$$

Figure 29(a) shows a plot of the gain $G(c)$ given by Eq. (8.30). For $c<1$, when the size of the illuminating aperture is smaller than the size of the imaging aperture, the gain is growing as a square root of the space bandwidth product N_s of the source. However, when the source size becomes larger than the pupil size, $c>1$, the system no longer supports the additional channels and the gain stays at the constant level $\sqrt{N_p}$ given by the space bandwidth product of the optical system. Note that the same behavior for $G(c)$ was found by Chavel and Lowenthal (1978) with respect to the technical noise concentrated in the Fourier plane of the system.

For an SPC source with single-mode squeezed light, $G(c)$ is obtained from Eqs. (8.15), (8.17), (8.24), and (8.25) as

$$G(c)=\begin{cases}\sqrt{cN_p}\exp[r_m], & \text{if } N_p^{-1}\leqslant c\leqslant 1,\\ \sqrt{N_p}/\sqrt{1+(-1+\exp[-2r_m])/c}, & \text{if } c>1.\end{cases} \tag{8.31}$$

Its plot is shown in Fig. 29(b). Again, for $c<1$ the gain is growing as the square root of N_s but now with an additional factor $\exp[r_m]$ because of squeezing. This factor improves $G(c)$ compared with the coherent-state case. The maximum of $G(c)$ is reached at $c=1$. For $c>1$, when the source size becomes larger than the pupil size, part of the light gets lost in the optical scheme. For a single-mode source of squeezed light this loss is equivalent to a degradation in the quantum efficiency of photodetection and causes the squeezing to deteriorate. When c grows to infinity the gain $G(c)$ becomes equal to that obtained with an SPC source in a coherent state.

The gain $G(c)$ for an SPC source of multimode squeezed light is obtained from Eqs. (8.15), (8.17), and (8.18) as

$$G(c)=\begin{cases}\sqrt{cN_p}/\sqrt{1+F_-[(cS_p/S_m)^{1/2}]}, & \text{if } N_p^{-1}\leqslant c\leqslant 1\\ \sqrt{N_p}/\sqrt{1+F_-[(S_p/S_m)^{1/2}]}, & \text{if } c>1.\end{cases} \tag{8.32}$$

The gain also depends on the ratio of the pupil area S_p to the area S_m. A plot of this ratio is given in Fig. 29(c) for a circular pupil aperture and a traveling-wave OPA as the source of multimode squeezed light for $S_p/S_m=10^2$. For the same squeezing parameter r_m as in Fig. 29(b) we can see that for $c<1$ the gain $G(c)$ is growing with increasing c and is somewhat smaller than in the case of a single-mode source. But upon reaching its maximum at $c=1$ it stays constant for all $c>1$ in contrast to the case of the single-mode source.

We can conclude that partially coherent illumination is preferable to coherent illumination for the quantum noise performance of the scheme. Employing a source of squeezed light instead of a source in a coherent state allows us to improve the signal-to-noise ratio beyond the standard quantum limit. A multimode light source has better noise performance than a single-mode source for incoherent illumination with a spatial coherence parameter much larger than unity.

IX. CONCLUSIONS AND OUTLOOK

We have shown in this article that multimode squeezed states of light come about as a natural generalization of single-mode squeezed states. Moreover, they can be easily produced in squeezing experiments when no special care is taken to cut out just one spatial mode of the field by means of a high-Q optical cavity. Traveling-wave configurations are most natural for the generation of multimode squeezed states. To observe multimode squeezed states, one has to employ a dense array of photodetectors, instead of just one photodetector, as in the case of single-mode squeezing.

In spite of the deceptive simplicity of the idea of generalizing from single-mode squeezing to multimode squeezing, this idea brings about a wealth of new physical phenomena. We have tried to illustrate the potential of multimode squeezing by considering here just a few applications, including optical imaging with sub-shot-noise sensitivity, sub-shot-noise microscopy, and noiseless amplification of optical images. This is, however, by no means a complete list of the applications of multimode squeezed states. In conclusion we should like to mention some other phenomena related to multimode squeezing that are still awaiting investigation.

We mentioned in Sec. IV that homodyne detection of multimode squeezed states is very similar to the scheme of optical holography. The interference of a strong coherent plane wave from a local oscillator with parametric down-conversion waves with different transverse components $\vec{q}$ is nothing else but the writing of an optical hologram. Here the local oscillator wave plays the role of the reference wave while the down-conversion waves act as the subject waves. The result of writing such a hologram is paradoxical from the semiclassical point of view: along with classical intensity modulation in the cross section of the light beam due to interference, one obtains regularization of the photon statistics in this cross section.

Another possible application of multimode squeezed states is in the area of optical image recognition with photon-limited images (Morris, 1989). We noted in Sec. VIII that in several applications it is advantageous to work with low-light-level or photon-limited images. In this case, apparently, the ultimate performance limit of the scheme is set by random quantum fluctuations of the light intensity in the cross section of the light beam. This can be clearly seen from Fig. 30, which shows the role of quantum fluctuations of light in low-light-level optical imaging. Multimode squeezed light would allow us to obtain a better performance from a prototype scheme while providing the possibility of effectively suppressing such randomness.

One other interesting subject that we did not discuss in this review but that might be related to multimode squeezed states is the question of a quantum limit in optical resolution and the possibilities for improving it using nonclassical light. The classical resolution criterion of Rayleigh was formulated having in mind a simple observation procedure. Rayleigh's choice of resolution limit, which seems at first sight rather arbitrary, is based on the presumed resolving capabilities of the human visual system. Rayleigh himself said about his criterion: ''This rule is convenient on account of its simplicity and it is sufficiently accurate in view of the necessary uncertainty as to what exactly is meant by resolution'' (Rayleigh, 1899).

Since Rayleigh's day, technical progress has created many refined tools and methods that allow us to obtain better and better resolution. For example, while Rayleigh's criterion puts a limit of about 0.2 μm for the determination of spacing between two points under an optical microscope, by processing microscopic images a precision of $\sim$1 nm has been achieved (Kamamura, 1987).

A detailed discussion of resolution is outside the scope of this review and can be found, for example, in a recent survey (den Dekker and van den Bos, 1997). We should like to point out that the ability to resolve two point sources depends fundamentally on the signal-to-noise ratio associated with the detected image intensity pattern. (Note that Rayleigh's resolution criterion does not consider the noise associated with the observation procedure.) It is therefore natural to expect an analog of the standard quantum limit of resolution and the possibility of improving the resolution beyond this limit with multimode squeezed light.

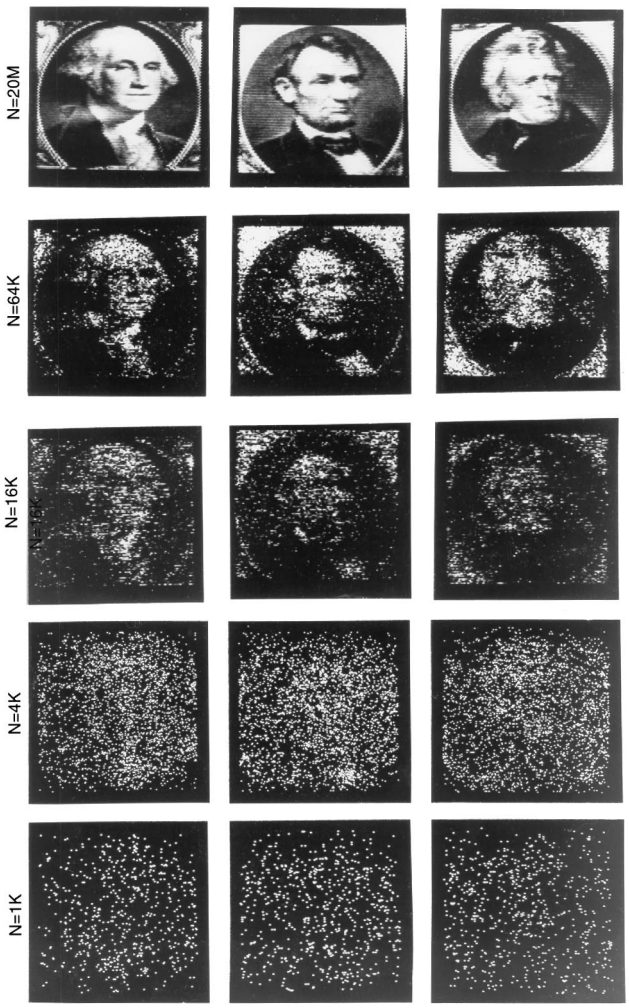

FIG. 30. Images of engraved portraits obtained using a two-dimensional, photon-counting detection system. First column, portrait of George Washington; second column, Abraham Lincoln; third column, Andrew Jackson. N is the number of detected photoevents over the entire image. The spatial coordinates of each detected photoevent are digitized to eight-bit accuracy. (From Morris, 1989.)

Last but not least, we should like to mention a quite different field in which multimode squeezed states and quantum spatial fluctuations occur. This is the field of optical pattern formation, which studies the spatial and spatio-temporal phenomena that arise in the structure of the electromagnetic field in the plane orthogonal to the direction of propagation. The latest development in this area shows that there are many situations in which quantum fluctuations of light in the transverse plane of the light beam have to be taken into account. For example, a recent study by the group of Boyd investigated filamentation of a laser beam initiated by quantum fluctuations of light in its transverse area (Nagasako, Boyd, and Agarwal, 1997). For details we refer to the reader a review article on spatial pattern formation by Lugiato, Brambilla, and Gatti (1999).

ACKNOWLEDGMENTS

I am highly indebted to my thesis advisor Ivan Sokolov, with whom I started to work on the subject of spatial squeezing. His clear and physically intuitive way of thinking and of tackling physical problems has been ever since a guiding example for me in my own investigations as well as in collaborations with other people. Fritz Haake is a second teacher and advisor who has helped me a great deal to enrich my knowledge and to improve my style of working. My thanks and gratitude to him. While working on this project, I have enjoyed collaborations with many good physicists and interesting people, among whom I would like to mention with gratitude Claude Fabre, Alessandra Gatti, Elisabeth Giacobino, Prem Kumar, Eric Lantz, Luigi Lugiato, and Serge Reynaud.

This work was done in the framework of the activities of the Network QSTRUCT (Quantum Structures) of the Training and Mobility of Researchers Program of the European Union.

REFERENCES

Abramowitz, M., and I. Stegun, 1965, Eds., *Handbook of Mathematical Functions* (Dover, New York), p. 771.
Agarwal, G. S., and E. Wolf, 1968, Phys. Rev. Lett. **21**, 180.
Agarwal, G. S., and E. Wolf, 1970a, Phys. Rev. D **2**, 2161.
Agarwal, G. S., and E. Wolf, 1970b, Phys. Rev. D **2**, 2187.
Agarwal, G. S., and E. Wolf, 1970c, Phys. Rev. D **2**, 2206.
Akhmanov, S. A., A. V. Belinskii, and A. S. Chirkin, 1988, Kvant. Elektron. Moscow **15**, 873 [Sov. J. Quantum Electron. **15**, 560 (1988)].
Arecchi, F. T., E. Gatti, and A. Sona, 1966, Phys. Lett. **20**, 27.
Aytür, O., and P. Kumar, 1990, Phys. Rev. Lett. **65**, 1551.
Aytür, O., and P. Kumar, 1992, Opt. Lett. **17**, 529.
Belinskii, A. V., and N. N. Rosanov, 1992, Opt. Spektrosk. **73**, 153 [Opt. Spectrosc. **73**, 89 (1992)].
Bergman, K., and H. A. Haus, 1991, Opt. Lett. **16**, 663.
Bialynicka-Birula, Z., and I. Bialynicka-Birula, 1987, J. Opt. Soc. Am. B **4**, 1621.
Bondurant, R. S., P. Kumar, J. H. Shapiro, and M. Maeda, 1984, Phys. Rev. A **30**, 343.
Bondurant, R. S., and J. H. Shapiro, 1984, Phys. Rev. D **30**, 2548.
Born, M., and E. Wolf, 1964, *Principles of Optics*, 2nd ed. (Pergamon, New York), Chap. X.
Cahill, K. E., and R. J. Glauber, 1969a, Phys. Rev. **177**, 1857.
Cahill, K. E., and R. J. Glauber, 1969b, Phys. Rev. **177**, 1882.
Cameron, S. M., D. F. Bliss, and M. W. Kimmel, 1996, Proc. SPIE **2679**, 195.
Carmichael, H. J., and D. F. Walls, 1976a, J. Phys. B **9**, L43.
Carmichael, H. J., and D. F. Walls, 1976b, J. Phys. B **9**, 1199.
Caves, C. M., 1981, Phys. Rev. D **23**, 1693.
Caves, C. M., 1982, Phys. Rev. D **26**, 1817.
Caves, C. M., and D. D. Crough, 1987, J. Opt. Soc. Am. B **4**, 1535.
Caves, C. M., and B. L. Schumaker, 1985, Phys. Rev. A **31**, 3068.
Chavel, P., and S. Lowenthal, 1978, J. Opt. Soc. Am. **68**, 721.
Choi, S.-K., M. L. Marable, and P. Kumar, 1997, in *QELS'97 Technical Digest*, *1997*, OSA Technical Digest Series, Vol. 12 (Optical Society of America, Washington, D.C.), p. 94.
Choi, S.-K., M. Vasilyev, and P. Kumar, 1998, in *CLEO'98 Technical Digest*, *1998*, OSA Technical Digest Series, Vol. 6 (Optical Society of America, Washington, D.C.), p. 470.
Cohen-Tannoudji, C., 1977, in *Frontiers in Laser Spectroscopy*, Les Houches, Session XXVII, edited by R. Balian, S. Haroche, and S. Liberman (North-Holland, Amsterdam), p. 4.
Collet, M. J., and C. W. Gardiner, 1984, Phys. Rev. A **30**, 1386.
Collet, M. J., and D. F. Walls, 1985, Phys. Rev. A **35**, 2887.
Cresser J. D., J. Häger, G. Leuchs, M. Rateike, and H. Walther, 1982, in *Dissipative Systems in Quantum Optics*, edited by R. Bonifacio (Springer-Verlag, Berlin), p. 21.
Dagenais, M., and L. Mandel, 1978, Phys. Rev. A **18**, 2217.
Davidovich, L., 1996, Rev. Mod. Phys. **68**, 127.
den Dekker, A. J., and A. van den Bos, 1997, J. Opt. Soc. Am. **14**, 547.
Devaux, F., and E. Lantz, 1995a, Opt. Commun. **114**, 295.
Devaux, F., and E. Lantz, 1995b, Opt. Commun. **118**, 25.
Devaux, F., and E. Lantz, 1995c, J. Opt. Soc. Am. B **12**, 2245.
Devaux, F., E. Lantz, A. Lacourt, D. Gindre, H. Maillotte, P. A. Doreau, and T. Laurent, 1995, Nonlinear Opt. **11**, 25.
Drummond, P. D., 1990, Phys. Rev. A **42**, 6845.
Fabre, C., and E. Giacobino, 1992, Eds., *Quantum Noise Reduction in Optical Systems/Experiments*, special issue of Appl. Phys. B **55**, 189.
Fisher, R. A., 1983, *Optical Phase Conjugation* (Academic, New York).
Gatti, A., and L. A. Lugiato, 1995, Phys. Rev. A **52**, 1675.
Gatti, A., L. A. Lugiato, L. Spinelli, G. Tissoni, M. Brambilla, P. Di Trapani, F. Prati, G. L. Oppo, and A. Berzanskis, 1999, *Nonlinear Optical Patterns: Applications to Spatial Soliton Arrays, Quantum Aspects*, Chaos Solitons Fractals **10**, 875.
Gatti, A., H. Wiedemann, L. A. Lugiato, I. Marzoli, G. L. Oppo, and S. Barnett, 1997, Phys. Rev. A **56**, 877.
Gavrielides, A., P. Peterson, and D. Gardimona, 1987, J. Appl. Phys. **62**, 2640.
Gehitz, M., G. C. Bjorklund, and E. A. Whittaker, 1985, J. Opt. Soc. Am. **132**, 1519.
Gilson, C. R., S. M. Barnett, and S. Stenholm, 1987, J. Mod. Opt. **34**, 855.
Glauber, R. J., 1963, Phys. Rev. **130**, 2529.
Glauber, R. J., 1965, *Quantum Optics and Electronics* (Les Houches Summer School of Theoretical Physics, University of Grenoble), edited by C. DeWitt, A. Blandin, and C. Cohen-Tannoudji (Gordon and Breach, New York), p. 53.
Goodman, J. W., 1968, *Introduction to Fourier Optics* (McGraw-Hill, New York), Chap. 1.
Goodman, J. W., 1985, *Statistical Optics* (Wiley, New York).
Grangier, P., G. Roger, and A. Aspect, 1986, Europhys. Lett. **1**, 173.
Grangier, P., G. Roger, A. Aspect, A. Heidmann, and S. Reynaud, 1986, Phys. Rev. Lett. **57**, 678.
Grangier, P., R. E. Slusher, B. Yurke, and A. LaPorta, 1987, Phys. Rev. Lett. **59**, 2153.
Guthals, D., and D. Sox, 1990, in *Proceedings of International Conference on Lasers '89*, edited by D. G. Harris and T. M. Shay (STS, Mclean, VA), p. 808.
Hanbury Brown, R., and R. Q. Twiss, 1956, Nature (London) **177**, 27.
Hanbury Brown, R., and R. Q. Twiss, 1957a, Proc. R. Soc. London, Ser. A **242**, 300.
Hanbury Brown, R., and R. Q. Twiss, 1957b, Proc. R. Soc. London, Ser. A **243**, 291.

Heidmann, A., S. Reynaud, and C. Cohen-Tannoudji, 1984, Opt. Commun. **52**, 235.
Henry, C. H., and R. F. Kazarinov, 1996, Rev. Mod. Phys. **68**, 801.
Ho, S.-T., P. Kumar, and J. H. Shapiro, 1986, Phys. Rev. A **34**, 293.
Ho, S.-T., P. Kumar, and J. H. Shapiro, 1987, Phys. Rev. A **35**, 3982.
Ho, S.-T., P. Kumar, and J. H. Shapiro, 1991, J. Opt. Soc. Am. B **8**, 37.
Holm, D. A., M. Sargent III, and B. A. Capron, 1986, Opt. Lett. **11**, 443.
Hong, C. K., and L. Mandel, 1986, Phys. Rev. Lett. **56**, 58.
Kamamura, S., 1987, Appl. Opt. **26**, 3425.
Khosla, R. P., 1992, Phys. Today **45**, 42.
Kilin, S. Ya., 1989, Opt. Spektrosk. **66**, 733 [Opt. Spectrosc. **66**, 429 (1989)].
Kimble, H. J., 1992, in *Fundamental Systems in Quantum Optics*, edited by J. Dalibard, J. M. Raimond, and J. Zinn-Justin (North-Holland, Amsterdam), Chap. 10.
Kimble, H. J., M. Dagenais, and L. Mandel, 1977, Phys. Rev. Lett. **39**, 691.
Kimble, H. J., M. Dagenais, and L. Mandel, 1978, Phys. Rev. A **18**, 201.
Kimble, H. J., and L. Mandel, 1976, Phys. Rev. A **13**, 2123.
Kimble, H. J., and D. F. Walls, 1987, Eds., *Squeezed States of the Electromagnetic Field*, special issue of J. Opt. Soc. Am. B **4**, 1453.
Klyshko, D. N., 1988a, *Photons and Nonlinear Optics* (Gordon and Breach, New York).
Klyshko, D. N., 1988b, Zh. Eksp. Teor. Fiz. **94**, 88 [Sov. Phys. JETP **67**, 915 (1989)].
Klyshko, D. N., 1988c, Zh. Eksp. Teor. Fiz. **94**, 82 [Sov. Phys. JETP **67**, 1131 (1989)].
Kolobov, M. I., 1991, Phys. Rev. A **44**, 1986.
Kolobov, M. I., 1995, Phys. Rev. A **51**, 1656.
Kolobov, M. I., and P. Kumar, 1993, Opt. Lett. **18**, 849.
Kolobov, M. I., and L. A. Lugiato, 1995, Phys. Rev. A **52**, 4930.
Kolobov, M. I., and I. V. Sokolov, 1986, Zh. Eksp. Teor. Fiz. **90**, 1889 [Sov. Phys. JETP **63**, 1105 (1986)].
Kolobov, M. I., and I. V. Sokolov, 1989a, Zh. Eksp. Teor. Fiz. **96**, 1945 [Sov. Phys. JETP **69**, 1097 (1989)].
Kolobov, M. I., and I. V. Sokolov, 1989b, Phys. Lett. A **140**, 101.
Kolobov, M. I., and I. V. Sokolov, 1989c, Opt. Spektrosk. **66**, 753 [Opt. Spectrosc. **66**, 440 (1989)].
Kolobov, M. I., and I. V. Sokolov, 1991, Europhys. Lett. **15**, 271.
Kumar, P., and M. I. Kolobov, 1994, Opt. Commun. **104**, 374.
Kumar, P., and J. H. Shapiro, 1984, Phys. Rev. A **30**, 1568.
Le Berre-Rousseau, M., E. Ressayre, and A. Tallet, 1979, Phys. Rev. Lett. **43**, 1314.
Levenson, J. A., I. Abram, T. Rivera, P. Fayolle, J. C. Garreau, and P. Grangier, 1993a, Phys. Rev. Lett. **70**, 267.
Levenson, J. A., I. Abram, T. Rivera, and P. Grangier, 1993b, J. Opt. Soc. Am. B **10**, 2233.
Levenson, M. D., K. M. Johnson, V. C. Hanchett, and K. Chaing, 1981, J. Opt. Soc. Am. **71**, 737.
Levenson, M. D., R. M. Shelby, A. Aspect, M. Reid, and D. F. Walls, 1985, Phys. Rev. A **32**, 1550.
Loudon, R., 1983, *The Quantum Theory of Light*, 2nd ed. (Clarendon, Oxford), Chap. 4.
Loudon, R., and P. L. Knight, 1987, Eds., *Squeezed Light*, special issue of J. Mod. Opt. **34**, 709.
Louisell, W. H., 1973, *Quantum Statistical Properties of Radiation* (Wiley, New York).
Lugiato, L. A., 1994, Ed., *Nonlinear Optical Structures, Pattern, Chaos*, special issue of Chaos, Solitons and Fractals **4**, 1251.
Lugiato, L. A., M. Brambilla, and A. Gatti, 1999, in *Advances in Atomic, Molecular, and Optical Physics*, Vol. 40, edited by B. Bederson and H. Walther (Academic, Boston), p. 229.
Lugiato, L. A., and A. Gatti, 1993, Phys. Rev. Lett. **70**, 3868.
Lugiato, L. A., A. Gatti, H. Ritsch, I. Marzoli, and G. L. Oppo, 1997, J. Mod. Opt. **44**, 1899.
Lugiato, L. A., A. Gatti, and H. Wiedemann, 1997, in *Quantum Fluctuations*, edited by S. Reynaud, E. Giacobino, and J. Zinn-Justin, Les Houches, Session LXIII (1995) (Elsevier, Amsterdam), p. 431.
Lugiato, L. A., and I. Marzoli, 1995, Phys. Rev. A **52**, 4886.
Machida, S., and Y. Yamamoto, 1986, Opt. Commun. **57**, 290.
Maeda, M. W., P. Kumar, and J. H. Shapiro, 1987, J. Opt. Soc. Am. B **4**, 1501.
Malygin, A. A., A. N. Penin, and A. V. Sergienko, 1985, Dokl. Akad. Nauk SSSR **281**, 308 [Sov. Phys. Dokl. **30**, 229 (1985)].
Mandel, L., 1979, Opt. Lett. **4**, 205.
Mandel, L., and E. Wolf, 1965, Rev. Mod. Phys. **37**, 231.
Mandel, L., and E. Wolf, 1995, *Optical Coherence and Quantum Optics* (Cambridge University Press, New York).
Mander, G. L., R. Loudon, and T. G. Shepherd, 1988, in *Photons and Quantum Fluctuations*, edited by R. E. Pike and H. Walther (Hilger, Bristol), p. 190.
Marable, M. L., S.-K. Choi, and P. Kumar, 1998, Optics Express **2**, 84.
Milburn, G. J., M. L. Steyn-Ross, and D. F. Walls, 1987, Phys. Rev. A **35**, 4443.
Morgan, B. L., and L. Mandel, 1966, Phys. Rev. Lett. **16**, 1012.
Morris, G. M., 1989, in *Optical Processing and Computing*, edited by H. H. Arsenault, T. Szoplik, and B. Macukow (Academic, New York), p. 343.
Nagasako, E. M., R. W. Boyd, and G. S. Agarwal, 1997, Phys. Rev. A **55**, 1412.
Oppo, G. L., M. Brambilla, and L. A. Lugiato, 1994, Phys. Rev. A **49**, 2028.
Peřina, J., 1985, *Coherence of Light*, 2nd ed. (Reidel, Dordrecht).
Peřina, J., 1991, *Quantum Statistics of Linear and Nonlinear Optical Phenomena*, 2nd ed. (Kluwer, Dordrecht).
Piskarskas, A., A. Stabinis, and A. Yankauskas, 1989, Opt. Spektrosk. **66**, 742 [Opt. Spectrosc. **66**, 434 (1989)].
Prasad, S., 1994, J. Opt. Soc. Am. A **11**, 2799.
Protsenko, I. E., and L. A. Lugiato, 1994, Opt. Commun. **109**, 304.
Protsenko, I. E., L. A. Lugiato, and C. Fabre, 1994, Phys. Rev. A **50**, 1627.
Rarity, J. G., P. R. Tapster, and E. Jakeman, 1987, Opt. Commun. **62**, 201.
Rayleigh Lord (John William Strutt, Third Baron Rayleigh), 1899, in *Scientific Papers by John William Strutt, Baron Rayleigh*, Vol. I, 1869–1881 (Cambridge University Press, Cambridge), p. 420.
Rebka, G. A., and R. V. Pound, 1957, Nature (London) **180**, 1035.

Reid, M. D., and D. F. Walls, 1985a, Phys. Rev. A **31**, 1622.
Reid, M. D., and D. F. Walls, 1985b, J. Opt. Soc. Am. B **2**, 1682.
Reid, M. D., and D. F. Walls, 1986, Phys. Rev. A **34**, 4929.
Reynaud, S., A. Heidmann, E. Giacobino, and C. Fabre, 1992, in *Progress in Optics*, Vol. 30, edited by E. Wolf (North-Holland, Amsterdam), p. 1.
Rosenbluh, M., and R. M. Shelby, 1991, Phys. Rev. Lett. **66**, 153.
Rubin, M. H., D. N. Klyshko, Y. H. Shih, and A. V. Sergienko, 1994, Phys. Rev. A **50**, 5122.
Saleh, B. E. A., and M. C. Teich, 1985, Opt. Commun. **52**, 429.
Savage, G. M., and D. F. Walls, 1987, J. Opt. Soc. Am. B **4**, 1514.
Scarl, D. B., 1966, Phys. Rev. Lett. **17**, 663.
Shelby, R. M., M. D. Levenson, S. H. Perlmutter, R. G. DeVoe, and D. F. Walls, 1986, Phys. Rev. Lett. **57**, 2520.
Shih, Y. H., and A. V. Sergienko, 1994, Phys. Rev. A **50**, 2564.
Short, R., and L. Mandel, 1983, Phys. Rev. Lett. **61**, 2921.
Slusher, R. E., P. Grangier, A. LaPorta, B. Yurke, and M. J. Potasek, 1987, Phys. Rev. Lett. **59**, 2566.
Smirnov, D. F., and I. V. Sokolov, 1976, Zh. Eksp. Teor. Fiz. **70**, 2098 [Sov. Phys. JETP **43**, 1095 (1976)].
Smirnov, D. F., and A. S. Troshin, 1987, Usp. Fiz. Nauk **153**, 233 [Sov. Phys. Usp. **30**, 851 (1987)].
Sokolov, I. V., 1977, Zh. Eksp. Teor. Fiz. **72**, 1687 [Sov. Phys. JETP **45**, 884 (1977)].
Sokolov, I. V., 1991, Zh. Eksp. Teor. Fiz. **100**, 780 [Sov. Phys. JETP **73**, 431 (1991)].
Sokolov, I. V., 1992, Opt. Spektrosk. **73**, 1158 [Opt. Spectrosc. **73**, 689 (1992)].
Sokolov, I. V., and Ya. A. Fofanov, 1993, Opt. Spektrosk. **74**, 764 [Opt. Spectrosc. **74**, 454 (1993)].
Stoler, D., 1970, Phys. Rev. D **1**, 3217.
Stoler, D., 1971, Phys. Rev. D **4**, 1925.
Strekalov, D. V., A. V. Sergienko, D. N. Klyshko, and Y. H. Shih, 1995, Phys. Rev. Lett. **74**, 3600.
Takahashi, H., 1965, in *Advances in Communication Systems*, edited by A. V. Balakrishnan (Academic, New York), p. 277.
Teich, M. C., and B. E. A. Saleh, 1985, J. Opt. Soc. Am. B **2**, 275.
Teich, M. C., B. E. A. Saleh, and J. Peřina, 1984, J. Opt. Soc. Am. B **1**, 366.
Teich, M. C., and B. E. A. Saleh, 1989, Quantum Opt. **1**, 153.
Teich, M. C., and B. E. A. Saleh, 1990, Phys. Today **43**, 26.
Teich *et al.*, 1984.
Thomas, J. B., 1969, *An Introduction to Statistical Communication Theory* (Wiley, New York), p. 173.
Twiss, R. Q., A. G. Little, and R. Hanbury Brown, 1957, Nature (London) **180**, 324.
von Neumann, J., 1931, Math. Ann. **104**, 570.
Walker, J. G., and E. Jakeman, 1985, Opt. Acta **32**, 1303.
Walls, D. F., 1983, Nature (London) **306**, 141.
Walls, D. F., and G. J. Milburn, 1994, *Quantum Optics* (Springer-Verlag, Berlin), p. 127.
Wentzel, G., 1949, *Quantum Theory of Fields* (Wiley, New York), Chap. 1.
Wetterer, C. J., L. P. Schelonka, and M. A. Kramer, 1989, J. Appl. Phys. **65**, 3347.
Wilson, T., and C. J. R. Sheppard, 1984, *Theory and Practice of Scanning Optical Microscopy* (Academic, London).
Xiao, Min, Ling-An Wu, and H. J. Kimble, 1987, Phys. Rev. Lett. **59**, 278.
Xiao, Min, Ling-An Wu, and H. J. Kimble, 1988, Opt. Lett. **13**, 476.
Yamamoto, Y., S. Machida, S. Saito, N. Imoto, T. Yanagawa, M. Kitagawa, and G. Björk, 1990, in *Progress in Optics*, Vol. 28, edited by E. Wolf (North-Holland, Amsterdam), p. 89.
Yariv, A., 1989, *Quantum Electronics*, 3rd ed. (Wiley, New York), p. 136.
Yu, F. T. S., 1985, *White-Light Optical Signal Processing* (Wiley-Interscience, New York), Chap. 5.
Yuen, H. P., 1976, Phys. Rev. A **13**, 2226.
Yuen, H. P., and J. H. Shapiro, 1978, IEEE Trans. Inf. Theory **IT-24**, 657.
Yuen, H. P., and J. H. Shapiro, 1979, Opt. Lett. **4**, 334.
Yurke, B., 1984, Phys. Rev. A **29**, 408.
Yurke, B., 1985, Phys. Rev. A **32**, 300.
Yurke, B., and J. S. Denker, 1984, Phys. Rev. A **29**, 1419.
Yurke, B., S. L. McCall, and J. R. Klauder, 1988, Phys. Rev. A **33**, 4033.
Yurke, B., and E. A. Whittaker, 1987, Opt. Lett. **12**, 236.